INFORMATION TO USERS

This manuscript has been reproduced from the microfilm master. UMI films the text directly from the original or copy submitted. Thus, some thesis and dissertation copies are in typewriter face, while others may be from any type of computer printer.

The quality of this reproduction is dependent upon the quality of the copy submitted. Broken or indistinct print, colored or poor quality illustrations and photographs, print bleedthrough, substandard margins, and improper alignment can adversely affect reproduction.

In the unlikely event that the author did not send UMI a complete manuscript and there are missing pages, these will be noted. Also, if unauthorized copyright material had to be removed, a note will indicate the deletion.

Oversize materials (e.g., maps, drawings, charts) are reproduced by sectioning the original, beginning at the upper left-hand corner and continuing from left to right in equal sections with small overlaps.

ProQuest Information and Learning
300 North Zeeb Road, Ann Arbor, MI 48106-1346 USA
800-521-0600

Overexpression, Purification and Preliminary Characterization of Prephenate Dehydrogenase from the Hyperthermophilic Bacterium *Aquifex aeolicus*

Raphael A. Aponte

A Thesis

in

The Department

of

Chemistry and Biochemistry

Presented in Partial Fulfilment of the Requirements
For the Degree of Master of Science at
Concordia University
Montreal, Quebec, Canada

May, 2003

ABSTRACT

Overexpression, Purification and Preliminary Characterization of Prephenate Dehydrogenase from the Hyperthermophilic Bacterium *Aquifex aeolicus*

Raphael A. Aponte, M.Sc.
Concordia University, 2002

Prephenate dehydrogenase (PD) catalyzes the oxidative decarboxylation of prephenate in one of the last steps of tyrosine biosynthesis. Currently all knowledge of the catalytic mechanism of this enzyme is based on a few detailed studies of the bifunctional enzyme, chorismate mutase-prephenate dehydrogenase (CM-PD), from *E. coli*. So far, no one has succeeded in crystallizing the *E. coli* protein or any other PD. As a step toward obtaining structural information on PD, and to offer more insight into its catalytic mechanism, we have initiated studies on a monofunctional PD from the hyperthermophilic bacterium *Aquifex aeolicus*.

The putative gene for *A. aeolicus* PD was cloned from genomic DNA and the protein overexpressed in *E. coli* with a removable N-terminal hexahistidine tag. A crude extract of the protein exhibited PD activity even after boiling. Hence, the thermophilic protein was purified to homogeneity using a single heat-treatment step, elution from nickel affinity resin, and proteolytic cleavage of the His tag by thrombin. Proteolysis at the thrombin cleavage site also occurred either intracellularly or during cell lysis in the absence of thrombin and led to multiple forms of PD containing combinations of tagged and untagged monomers. Size exclusion chromatography and analytical ultracentrifugation suggested that native protein could associate as a dimer. The enzyme

displayed Michaelis-Menten kinetics at 55 °C. *A. aeolicus* PD was extremely thermally stable, exhibiting maximal activity at ~ 95 °C with a half-life of ~ 3 hours. Variable temperature far-UV circular dichroism and FT-infrared spectroscopies confirmed that the protein retained its secondary structure, which is mainly α-helical, even at high temperatures, although the protein appeared to "relax" into its active conformation with increasing temperature. The thermophilic PD was inhibited in an allosteric fashion by the end product of the pathway, tyrosine. However, size exclusion chromatography suggested that it did not undergo an oligomerization in the presence of this ligand under conditions that promoted such changes in the bifunctional *E. coli* enzyme. Sequence alignments with other PDs were used to identify conserved functional motifs and residues which may be important for the catalytic mechanism of the enzyme. Mutagenesis studies have been initiated at these residues, as have crystallization trials on the wild-type enzyme. Work presented in this thesis ultimately will allow comparison of the structure and enzymatic properties of the thermophilic PD to that of its mesophilic counterparts, and will contribute to the understanding of the mechanism and biochemical features of this enzyme family.

ACKNOWLEDGEMENTS

I would like to extend my deepest gratitude to my supervisor, Dr. Joanne Turnbull, for her direction, overwhelming and generous support, and her relentless persistence for perfection throughout my two years as her graduate student. My sincere thanks to Dr. Peter White for his assistance in analyzing AUC data, his patience and assistance during hours of HPLC runs, and for his professional advise during the course of my studies. I would also like to thank Dr. Dinesh Christendat for his collaboration with this project, Dr. Ashraf Ismail for his FTIR expertise, and Dr. Sébastien Robidoux for introducing me to experimental NMR techniques. I would also like to acknowledge the helpful staff from the Centre for Structural and Functional Genomics, in the department of Biology at Concordia University, in particular to Dr. Peter Ulycznyj.

Special thanks to all my fellow Turnbull lab rats - Kev, Julie "Goodwine", Sarah, Sue, Tony and John. I would like to express my appreciation for all the good friends I have made throughout my 6 years at Concordia University - Shady, Samer, Alain, Buda, Joey "I am Canadian", Phil "P-body" and Alvira "sizzle". I wish them all happiness and success in the future, even if it means opening a fish-bait store in the Caribbean.

I am indebted to my parents - Eveline and Arnaldo – for their love, support and for the sacrifices they have made throughout the course of all my studies - past, present and future. To my brothers and sisters – Arnaldo "Tutin", Carolina, Dany and Vetcy – for their truly inspiring efforts in ensuring that our home is always the loudest of the block.

God said, "Let the earth produce every kind of living creature: cattle, reptiles, and every kind of wild beast". And so it was.

(Genesis 1:24-25)

TABLE OF CONTENTS

LIST OF FIGURES

CHAPTER 1:

CHAPTER 2:

CHAPTER 3:

CHAPTER 4:

LIST OF TABLES

CHAPTER 2:

CHAPTER 2:

CHAPTER 3:

CHAPTER 4:

LIST OF ABBREVIATIONS

AMP	adenosine 5′-phosphate
AUC	analytical ultracentrifugation
CD	circular dichroism
CDH	cellobiose dehydrogenase
Clp	protease Ti
CM	chorismate mutase
CM-PD	chorismate mutase – prephenate dehydrogenase
CM-PDT	chorismate mutase – prephenate dehydratase
DEPC	diethylpyrocarbonate
DMSO	dimethyl sulfoxide
DNA	deoxyribonucleic acid
DSC	differential scanning calorimetry
DTT	dithiothreitol
EDTA	ethylenediamine tetra-acetic acid
ESI	electrospray ionization
FSD	Fourier self-deconvolution
FT	Fourier transform
G6PDH	glucose-6-phosphate dehydrogenase
Gdn-HCl	guanidinium hydrochloride
GluDH	glutamate dehydrogenase
HEPES	*N*′-2-hydroxyethylpiperazine-*N*′-ethanesulfonic acid

HPLC	high performance liquid chromatography
HPP	(4-hydroxyphenyl)pyruvate
IMAC	immobilized metal affinity chromatography
IPTG	isopropyl-β-D-thiogalactopyranoside
IR	infrared
KdsA	3-deoxy-D-*manno*-octulosonic acid 8-phosphate synthase
LB	Luria broth
Lon	protease La
MS	mass spectrometry
MW	molecular weight
NAD^+	oxidized form of nicotinamide adenine dinucleotide
NADH	reduced form of nicotinamide adenine dinucleotide
NTA	nitrolotriacetic acid
PAGE	polyacrylamide gel electrophoresis
PCR	polymerase chain reaction
PD	prephenate dehydrogenase
PMSF	phenylmethylsulfonyl fluoride
PRE	prephenate
TCEP	tri(2-carboxyethyl)phosphine hydrochloride
TFA	trifluoroacetic acid
Tris	tris(hydroxymethyl)aminomethane
$S_{20,w}$	sedimentation coefficient
SDS	sodium dodecylsulfate

U	units
UV	ultra violet
VT	variable temperature

CHAPTER 1

General Introduction

1.0 Biosythesis of Aromatic Amino Acids

The aromatic amino acid biosynthesis pathway in *E. coli* and other microorganisms and plants is well established (1-3), and known as the shikimate pathway. The shikimate pathway converts derivatives of glucose into the aromatic precursor, chorismate, which then serves as a precurser in the branch pathways for phenylalanine, tyrosine and tryptophan. Chorismate also serves as a precurser for a number of aromatic compounds including vitamin K, menaquinone, folate and enterochelin.

Regulation of the aromatic amino acid biosythesis pathway occurs at both the genetic and protein level. Many of the genes encoding the biosynthetic enzymes for aromatic amino acids are organized in operons. The operons are regulated by three regulatory genes *tyrR*, *trpR* or *pheR*. The protein products of these genes combine with the appropiate amino acid co-repressor, resulting in the formation of complexes that bind at the operator loci. Additional regulation is achieved through attenuation at the level of charged tRNA(s) (4). However, the major form of control is achieved though feed-back inhibition by phenylalanine, tyrosine and tryptophan of enzymes at the start and at the branch point in the biosynthetic pathways leading to these products.

1.1 The Pathway to Tyrosine and Phenylalanine Biosynthesis in *E. coli*

In *E. coli* the pathway for tyrosine biosynthesis involves two sequential reactions catalyzed by the enzyme chorismate mutase-prephenate dehydrogenase (CM-PD) (5, 6). CM (EC 5.4.99.5) catalyzes the Claisen rearrangment of chorismate to prephenate, while PD (EC 1.3.1.12) is responsible for the oxidative decarboxylation of prephenate to (4-

hydroxyphenyl)pyruvate (HPP) in the presence of NAD^+ (refer to Figure 1). An aromatic aminotransferase converts HPP to tyrosine (5). Tyrosine, the end product of the pathway is a feed back inhibitor of both mutase and dehydrogenase activities (5). The *E. coli* enzyme is homodimeric with a molecular weight of 42 kDa per monomer (7-9). It is considered bifunctional since both activities are associated with each of the polypeptide chains. However, the structural organization of the sites which catalyze the two activities within the enzyme has not been firmly established.

Alignment of the primary sequence of *E. coli* CM-PD with that of *E. coli* chorismate mutase-prephenate dehydratase (CM-PDT) the bifunctional enzyme involved in the conversion of chorismate to phenylalanine, indicates that the N-terminal 100 amino acid residues of the polypeptide chain may be responsible for the mutase activity, while the remaining 274 residues comprise the dehydrogenase (43). Evidence in favour of two distinct active sites or of specific residues involved in catalyzing each of the two reactions, are the observations that the two activities show markedly different rate profiles (10) and are inhibited to different degrees by tyrosine (11, 12), malonic acid derivatives and other substrate analogues (12). Furthermore, a putative transition state analogue of CM, *endo*-oxabicyclid diacid, selectively inhibits the mutase reaction without affecting dehydrogenase activity (12). More recently, the analogue *trans*-2,3-pleiadanedicarboxylic acid was identified, which specificially inhibits PD without affecting mutase activity (13). This premise also has been supported through recent site-directed mutagenesis studies in the Turnbull lab. Mutations made in the PD domain eliminate dehydrogenase activity (H197N) and prephenate

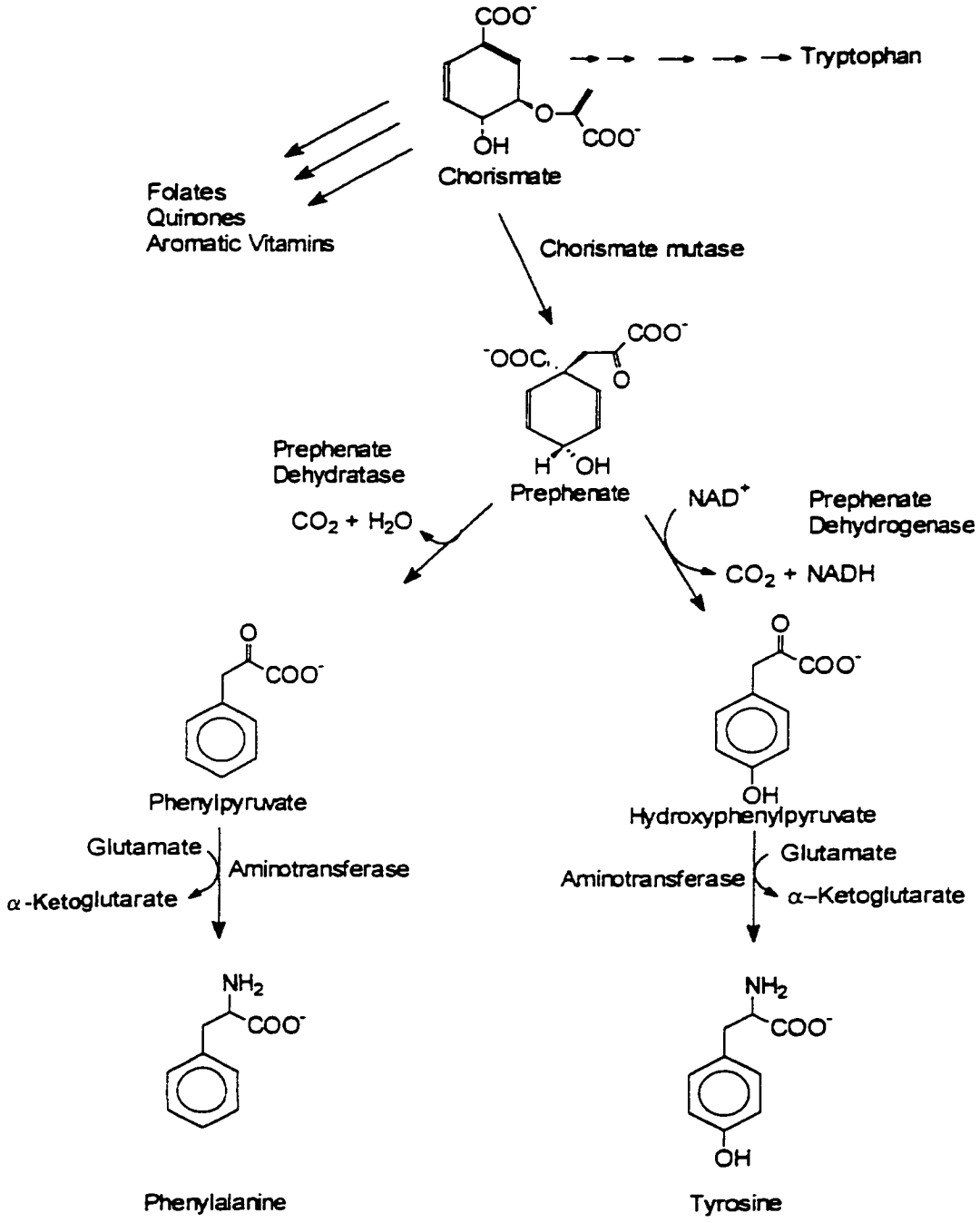

Figure 1. Aromatic Amino Acid Biosynthesis

binding (R294N) while having no affect on the mutase reaction. Similarly a mutation in the mutase domain (K37Q) has no effect on dehydrogenase activity (22).

There is compelling evidence to suggest that if there are two active sites they are in very close proximity to each other and are structurally interrelated. Some of the prephenate formed from chorismate is converted directly to HPP (14). Christopherson (42) has provided some kinetic evidence by inhibition studies with the malonic acids that the two sites are overlapping. Protein variants have been characterized which clearly affect both activities (H189N, K178R, and R286A) (16) and remarkably one mutation clearly in the dehydrogenase domain (C215A) affects the binding of chorismate (K. Mekhssian, unpublished). Moreover, time-dependent limited proteolysis analyzed by SDS-PAGE failed to resolve discrete domains (Christendat and Turnbull, unpublished) suggesting that the sites at which the two reactions occur are structurally linked.

Initial velocity, product and dead-end inhibition studies have established that PD conforms to a rapid-equilibrium random kinetic mechanism with catalysis as the rate-limiting step (17). However, the catalytic mechanism of the enzyme is still under investigation. Based on the results of pH profiles (10, 18), isotope effects (19, 20), chemical modification, peptide mapping experiments (21), and site-directed mutagenesis (16, 22), a model for the catalytic mechanism has been proposed (see Figure 2 on p. 6).

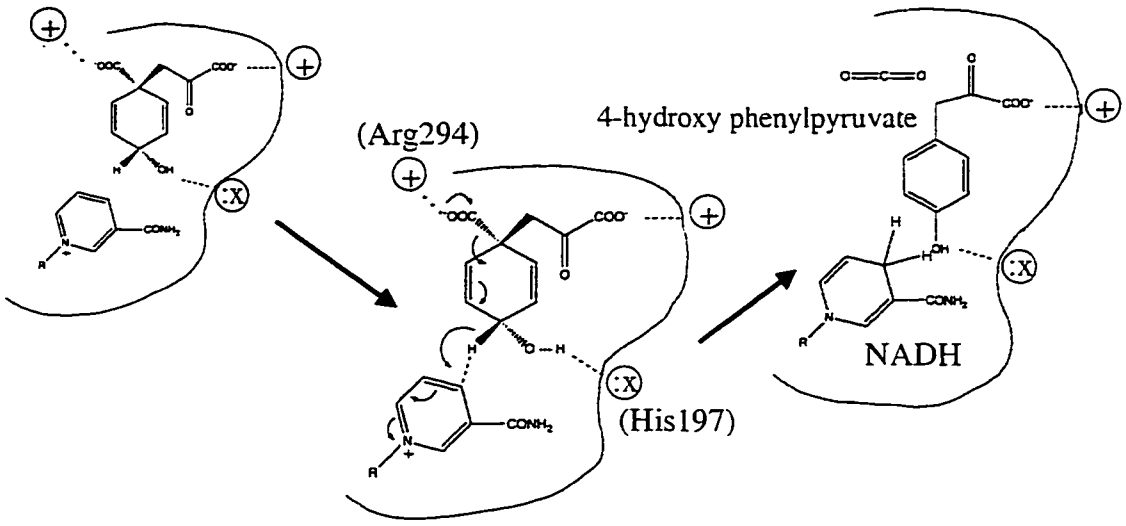

Figure 2. A possible mechanism of the PD reaction involving ionizable amino acid residues at the active site. Adapted from Christendat *et al.* (22).

It is believed that prephenate and NAD^+ bind to discrete subsites in the PD domain. A hydrogen bond acceptor facilitates hydride transfer from the 4-hydroxyl group of prephenate to NAD^+ by polarizing the hydroxyl group, lowering the activation barrier enough to bring about the concomitant hydride transfer and decarboxylation. The two chemical steps occur simultaneously, driven by the aromaticity of the product and also possibly because the ring carboxylate resides are near/in a hydrophobic pocket facilitating the removal of HPP (22). Temperature and solvent perturbation studies (18) and chemical modification of the enzyme with DEPC (21) have indicated that histidine is the catalytic residue involved. Mutagenesis studies identified this His as His197 (16). Studies examining the binding of substrate analogues to wild-type and mutant enzymes have shown that Arg294 interacts with the side chain carboxylate of prephenate (22). Other residues involved in the mechanism have not been identified, although there are

other residues conserved between PD of *E. coli* CM-PD and several monofunctional PD's.

The catalytic mechanism of chorismate mutase is better defined as there are crystal structures available for CM from *S. cerevisiae* (23), *B. subtilis* (24) and the mutase domain of the bifunctional *E. coli* CM-PDT (25) complexed to the mutase transition state analogue. While there is little sequence or structural similarity between these 3 monofunctional mutases, the active sites appear to be well conserved. The mutase domains of CM-PD and CM-PDT are highly homologouse, hence the structure of the CM portion of CM-PDT has provided valuable insights as to the residues that may participate in the mutase reaction catalyzed by CM-PD. Kinetic studies suggest that the mutase reaction catalyzed by the bifunctional enzymes and by the yeast enzyme, are mediated by enzymic acids and bases (10, 21, 25). In contrast, the monofunctional mutase from *B. subtilis* specifically binds the chair-like conformer of chorismate, which then spontaneously rearranges to prephenate (27, 28).

Tyrosine, the end product of the pathway, inhibits both dehydrogenase and mutase activities in an allosteric fashion. However, the mechanism of the inhibition is still under debate. There is evidence using analytical ultracentrifugation that tyrosine inhibits enzyme activity by promoting the formation of an inactive tetramer from the active dimer (11). In contrast, other centrifugation experiments provide no evidence for such a quaternary structural change (29, 30). Instead, it has been suggested through analysis of kinetic models that there are tertiary structural changes in the enzyme propagated through

the subunits that promote the formation of the inactive conformation of CM-PD (31). Very recent work in the Turnbull lab have identified two residues, His245 and His257 that are critical for tyrosine inhibition of both CM-PD activities (T. Lee, unpublished).

The pathway to phenylalanine is catalyzed by a similar bifunctional enzyme CM-PDT. The dehydratase is responsible for the decarboxylation and dehydration of prephenate the phenylpyuvate; no cofactor is required. An aminotransferase then catalyzes the formation of phenylalanine (see Figure 1). Unlike CM-PD, there is kinetic evidence suggesting that the two reactions are catalyzed at two independent sites and there is no channelling of prephenate from one active site to the other (32). Furthermore, recent studies by Ganem and collegues have shown that the functional portions of the protein are discrete domains. The mutase, dehydratase and the phenylalanine binding portion of the dehydratase have all been independently expressed and are being characterized (33, 44).

1.2 Strategy

Aquifex is a hyperthermophilic, hydrogen-oxidizing, microaerophilic, obligate chemolithoautotroph (35, 36). The complete genomic sequence of *A. aeolicus* was reported in 1998 from samples isolated by Karl O. Stetter from hydrothermal vents in Yellowstone National Park (15). The organism thrives at temperatures above 85 °C with $H_2/CO_2/O_2$, in environments only containing inorganic components. It does not grow on a number of organic substrates, including sugars, amino acids, yeast extract or meat extract. These growth characteristics suggests biosynthesic rather than degradative behavior (15). A putative *tyrA* gene encoding a 311 residue PD was identified in the

sequence, however no gene encoding CM or CM-PD was identified. In contrast, the *pheA* gene encoding CM-PDT was identified (15).

Based on phylogenetic analysis of small-subunit rRNA sequences, hyperthermophilic organisms proliferate in the deepest branches of the Bacterial and Archaeal domains (34, 37). The branch lengths of these hyperthermophilic lineages tend to be short, which further suggests that such organisms are the closest known extant descendants of the last common ancestor and retain many ancestral phenotypic properties (38). Figure 3 illustrates a 16S rRNA gene-based phylogenetic tree of the *Aquificales* and other Bacteria and Archaea. The branching shows that *E. coli* constitutes a separate, more deeply diverging lineage, as compared to *A. aeolicus*. Not surprisingly, pair-wise sequence alignment between *A. aeolicus* PD and the PD domain of *E. coli* CM-PD shows only 18.5% sequence identity. Multiple sequence alignments (refer to Figure 4) of 1 plant, 2 yeast and 17 bacterial PD domains, including PD from *A. aeolicus*, reveal several highly conserved residues. In addition, the conserved structural motif Gly-X-Gly-XX-Gly, associated with classical nicotinamide nucleotide-binding proteins, is reminiscent of the fingerprint region of the Rossmann fold (39), and is conserved with 19 of the 20 PDs near the N-terminus. Moreover, functional studies on *E. coli* CM-PD indicate that residues important for the catalytic mechanism and tyrosine binding are conserved in *A. aeolicus* PD (refer to Table 1). Numerous attempts to crystallize *E. coli* CM-PD for structural determination by X-ray defraction have failed. While there are crystal structures available for mutases closely related to that of *E. coli* CM-PD, there are no structures for any PD from any organism.

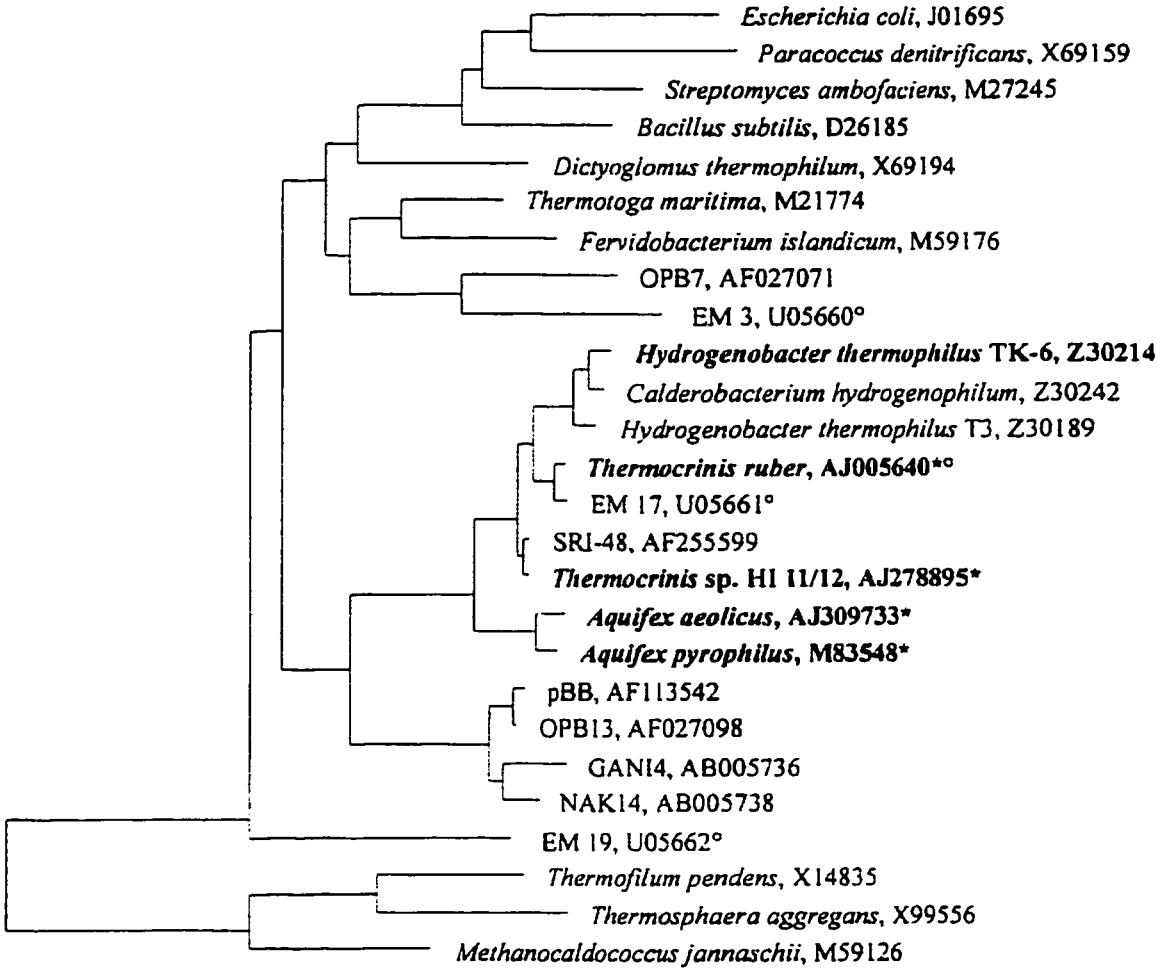

Figure 3. 16S rRNA gene-based phylogenetic tree of various Bacteria and Archaea. Adapted from Jahnke, L. L (40).

Figure 4. Multiple sequence alignment of 1 plant, 2 yeast and 17 bacterial PD domains. *A. aeolicus* PD shares 18.5% sequence identity with *E. coli* CM-PD. Conserved residues are indicated as (*). The N-terminal domain (of the 3rd, 15th, 16th and 17th sequence) have been omitted from the figure due to their length. Identical residues are highlighted in yellow, consensus sequence in light blue and residues with similar properties in dark blue. Multiple sequence alignments were performed using Vector NTI (version 8.0), by InforMax Inc.

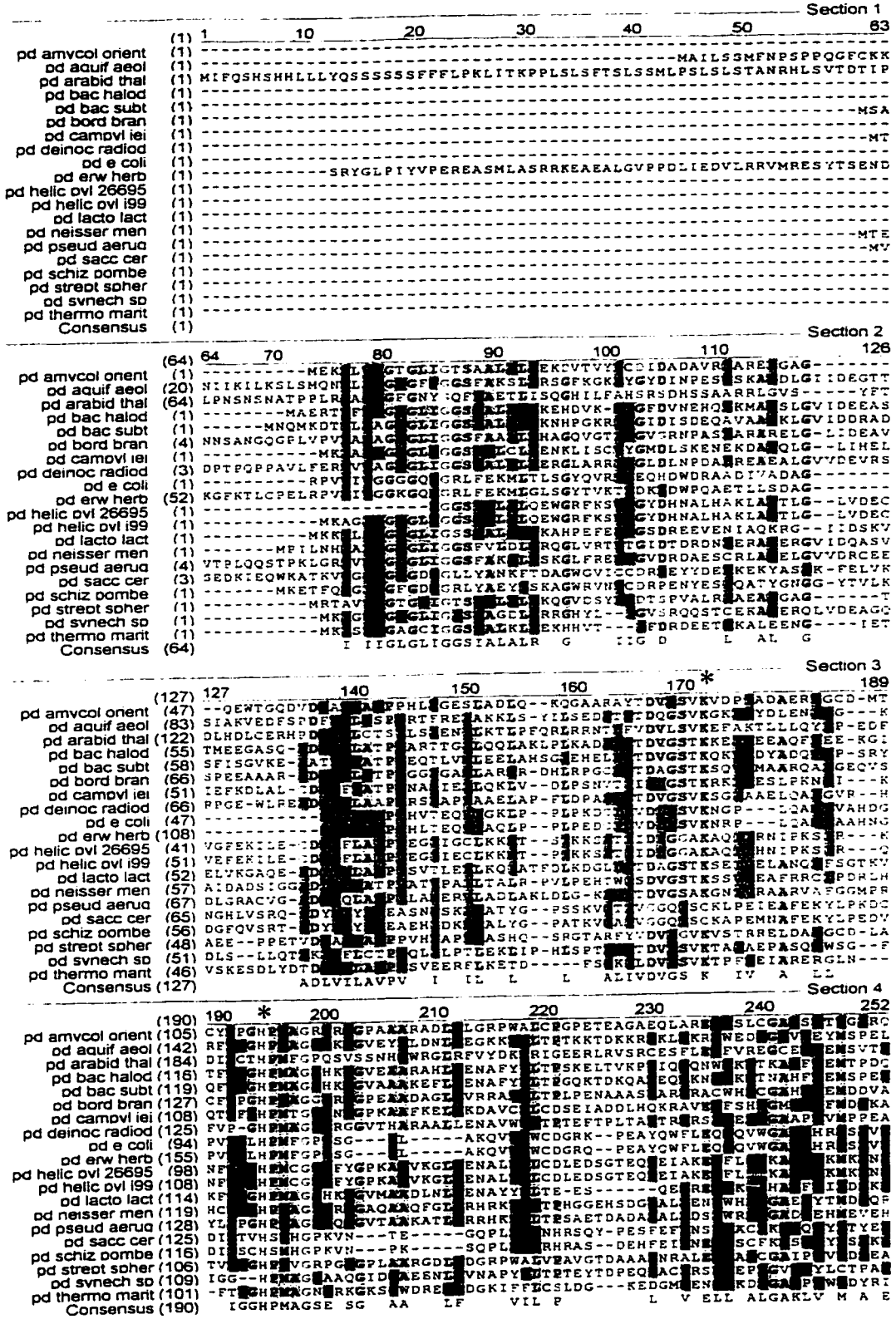
Section 1
Section 2
Section 3
Section 4
pd amycol orient
pd aquif aeol
pd arabid thal
pd bac halod
pd bac subt
pd bord bran
pd campvl iei
pd deinoc radiod
pd e coli
pd erw herb
pd helic pvl 26695
pd helic pvl i99
pd lacto lact
pd neisser men
pd pseud aeruq
pd sacc cer
pd schiz pombe
pd strept spher
pd synech sp
pd thermo marit
Consensus

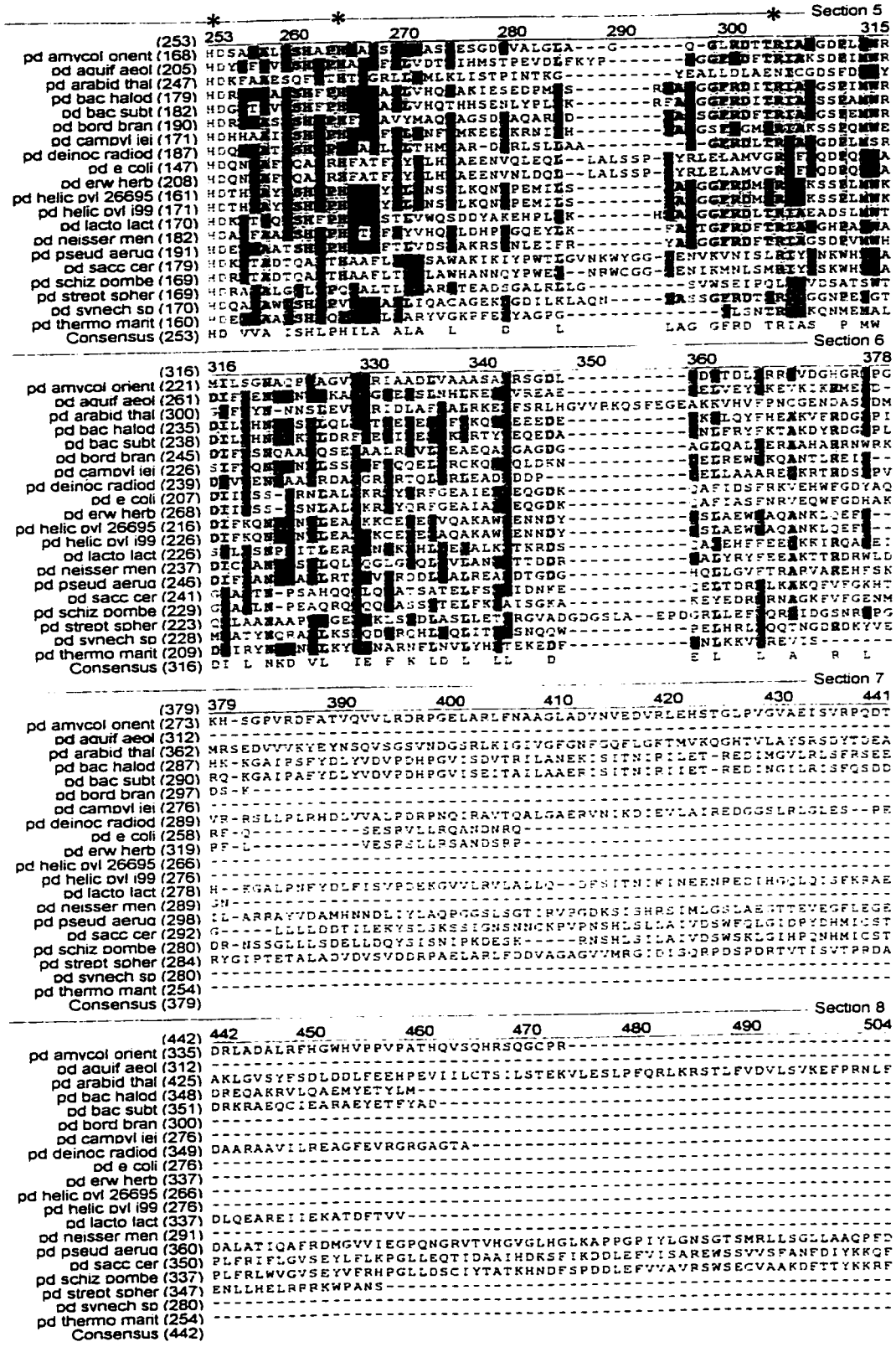
Section 5
Section 6
Section 7
Section 8

	E. coli CM-PD	*A. aeolicus* PD	Possible involvement in mechanism
Prephenate binding	Arg 294	Arg 250	electrostatic interactions with the ring carboxylate of prephenate
Catalysis	His 197	His 147	polarizes 4-OH group in prephenate
Tyrosine binding	His 245	His 205	unknown
	His 257	His 214	unknown
Active site structure	Lys 178	Lys 129	unknown

Table 1. Previously identified residues important for binding, catalysis and active site structural integrity of *E. coli* CM-PD and the corresponding conserved residues in *A. aeolicus* PD, determined by primary sequence alignment.

The results from the sequence alignments and functional studies on CM-PD suggest that *A. aeolicus* PD may be a good alternate candidate for X-ray crystallography studies. *A. aeolicus* PD also was chosen for crystallization because of the characteristics associated with proteins originating from hyperthermophilic organisms. These characteristics, which include a highly charged surface and a well packed protein core (40, 44), should facilitate the crystallization process (D. Christendat, personal communication). Moreover, there is considerable interest in the area of protein thermostability and in identifying the mechanism by which these proteins remain stable under extreme conditions. Work presented in this thesis will ultimately allow comparison of the structure and enzymatic properties of the thermophilic PD to that of its mesophilic counterparts, and to contribute to the understanding of the mechanism and biochemical features of this enzyme family.

1.3 SCOPE OF THIS THESIS

In this project, we have conducted initial kinetic and biophysical characterization of the *A. aeolicus* monofunctional enzyme, prephenate dehydrogenase. This project has been divided into four sections:

1. Overexpression, purification and preliminary structural characterization of recombinant *A. aeolicus* PD;

2. Comparison of kinetic parameters and inhibition by tyrosine between recombinant *E. coli* CM-PD and *A. aeolicus* PD;

3. Studies examining the stability and unfolding of *A. aeolicus* PD using far-UV circular dichroism, Fourier Transform infrared spectroscopies, and differential scanning calorimetry;

4. A brief summary of site-directed mutagenesis studies on *A. aeolicus* PD on residues that are conserved between *E. coli* CM-PD and *A. aeolicus* PD.

1.4 REFRENCES

1. Pittard, J. T. and Gibson, F. (1970). *Curr. Topics Cell Reg.* **2**, 29-63.
2. Umbarger, H. E. (1978). *Ann Rev. Biochem.* **47**, 533-606.
3. Somerville, R. L. (1983). *Amino Acid Biosynthesis and Genetic Regulation*, Addison, Wesley Publishing Co. pp 351-378.
4. Yanofsky, C. (1988). *J. Biol. Chem.* **263**, 609-612.
5. Koch, G.L., Shaw, D.C. and Gibson, F. (1971). *Biochim. Biophys. Acta.* **229,** 795-804.
6. Cotton, R. G. H. and Gibson, F. (1965). *Biochim. Biophys. Acta.* **100**, 76-78.
7. SampathKumar, P. and Morrison, J. F. (1982). *Biochim. Biophys. Acta.* **702**, 204-211.
8. Hudson, G. S., Wong, V. and Davidson, B. E. (1984). *Biochemistry* **23**, 6240-6249.
9. Turnbull, J., Cleland, W. W. and Morrison, J. F. (1990). *Biochemistry* **29**, 10245-10254.
10. Turnbull, J. Cleland, W. W. and Morrison, J. F. (1991). *Biochemistry* **30**, 7777-7782.
11. Hudson, G. S., Howlett G. J. and Davidson B. E. (1983). *J. Biol. Chem.* **258**, 3114-3120.
12. Turnbull, J. and Morrison, J. F. (1990). *Biochemistry* **29**, 10255-10261.
13. Vincent, S., Chen, S., Wilson, D. B. and Ganem, B. (2002). *Bioorg. Med. Chem. Lett.* **12**, 929-931.
14. Heyde, E. (1979). *Biochemistry* **18**, 2766-2775.

15. Deckert, G., Warren, P. V., Gaasterland, T., Young, W. G., Lenox, A. L., Graham, D. E., Overbeek, R., Snead, M. A., Keller, M., Aujay, M., Huber, R., Feldman, R. A., Short, J. M., Olsen, G. J. and Swanson, R. V. (1998). *Nature* 392, 353-358.

16. Christendat, D., Saridakis, V. C. and Turnbull, J. (1998). *Biochemistry* **37**, 15703-15712.

17. SampathKumar, P. and Morrison, J. F. (1982). *Biochim. Biophys. Acta.* **702**, 212-219.

18. Hermes, J. D., Tipton, P. A., Fisher, M. A., O'Leary, M. H., Morrison, J. F. and Cleland, W. W. (1984). *Biochemistry* **23**, 6263-6275.

19. Addadi, L. Jaffe, E. K. and Knowles, J. R. (1983). *Biochemistry* **22**, 4494-4501.

20. Guilford, W. J., Copley, S. D. and Knowles, J. R. (1987). *J. Am. Chem. Soc.* **109**, 5013-5019.

21. Christendat, D. and Turnbull, J. (1996). *Biochemistry* **35**, 4468-4479.

22. Christendat, D. and Turnbull, J. (1999). *Biochemistry* **38**, 4782-4793.

23. Xue, Y., Lipscomb, W. N., Graf, R., Schnappauf, G. and Braus, G. (1994). *Proc. Natl. Acad. Sci.* **91**, 10814-10818.

24. Chook, Y. M., Ke, H. and Lipscomb, W. N. (1993). *Proc. Natl. Acad. Sci.* **90**, 8600-8603.

25. Lee, A. Y., Stewart, J. D., Clardy, J. and Ganem, B. (1995). *Chem. Biol.* **2**, 195-203.

26. Hudson, G. S., Howlett, G. J. and Davidson, B. E. (1983). *J. Biol. Chem.* **258**, 3114-3120.

27. Gray, J. V. and Knowles, J. R. (1994). *Biochemistry* **33**, 9953-9959.

28. Davidson, M. M, Gould, I. R. and Hillier, I. H. (1996). *J. Chem. Soc. Perkin Trans.* **2**, 525-532.

29. Llewellyn, D. J. and Smith, G. D. (1979). *Biochemistry* **18**, 4707-4714.

30. Christopherson, R. I. and Morrison, J. F. (1985). *Biochemistry* **25**, 1116-1121.

31. Christopherson, R. I. (1985). *Arch. Biochem. Biophys.* **240**, 646-654.

32. Duggleby, R. G., Sneddon, M. K. and Morrison, J. F. (1978). *Biochemistry* **17**, 1548-1554.

33. Zhang, S. Wilson, D. B. and Ganem, B. (2000). *Biochemistry* **39**, 4722-4728.

34. Pitulle, C., Yang, Y., Marchiani, M., Moore, E. R., Siefert, J. L., Aragno, M., Jurtshuk, P. Jr. and Fox, G. E. (1994). *Int. J. Syst. Bacteriol.* **44**, 620-626.

35. Huber, R. (1992). *Arch. Microbiol.* **15**, 340-351.

36. Kawasumi, T., Igarashi, Y., Kodama, T. and Minoda, Y. (1984). *Int. J. Syst. Bacteriol.*, **34**, 5-10.

37. Jahnke, L. L., Eder, W., Huber, R., Hope, J. M., Hinrichs, K. U., Hayes, J. M., Des Marais, D. J., Cady, S. L. and Summons, R. E. (2001). *Appl. Environ. Microbiol.* **67**, 5179-5189.

38. Stetter, K. O. (1994). *Early Life on Earth.* Columbia University Press, New York, N. Y., pp. 143-151.

39. Wierenga, R. K. and Hol, W. G. J. (1983). *Nature* **302**, 842-844.

40. Jaenicke, R. (1997). BioProt Network. Institut für Biophysik und Physikalische Biochemie, Universität Regensburg, Regensburg, Germany. (http://www.protein.bio.msu.su/biokhimiya/contents/v63/full/63030370.htm)

41. Cambillau, C. and Claverie, J-M. (2000). *J. Biol. Chem.* 275, 32383-32386.

42. Christopherson, R. I., Heyde, E and Morrison, J. F. (1983). *Biochemistry* **22**, 1650-1656.

43. Hudson, G. S. and Davidson, B. E. (1984). *J. Mol. Biol.* **180**, 1023-1051.

44. Zhang, S., Pohnert, G., Kongsaeree, P., Wilson, D. B., Clardy, J. and Ganem, B. (1998). *J. Biol. Chem.* 273, 6248-6253.

CHAPTER 2

Expression, Purification and Structural Characterization of Recombinant Prephenate Dehydrogenase from *A. aeolicus*

2.0 INTRODUCTION

Affinity chromatography has been employed for decades to assist in the purification of native and recombinant proteins. Historically, this technique involves chemically coupling a small ligand onto a stationary phase and then passing an enzyme preparation over the support to select for the protein that has the greatest affinity for that ligand. The target protein can be displaced from the immobilized support by changing pH or ionic strength of the mobile phase or inclusion of other competitively binding ligands in the buffer. In fact, the purification of *E. coli* CM-PD relies on the affinity of PD's nucleotide binding site for AMP and for the dye Cibacron Blue 3GA to yield homogeneous enzyme (1).

The development of genetic engineering technology has revolutionized affinity purification of recombinant proteins by facilitating the construction of fusions between a protein of interest and tags that are small peptides (Hexa-histidine and FLAG epitopes), or full-length proteins (maltose binding protein, glutathione S-transferase and thioredoxin). The high affinity that the tag possesses for a specific immobilized ligand can be exploited to give rise to rapid and effective purification of the target protein.

Immobilized metal affinity chromatography (IMAC) is such an example. Nitrilotriacetic acid (NTA) from Qiagen is a tetradentate chelating agent that occupies four of the six ligand binding sites in the coordination sphere of Ni^{2+} leaving two sites available to interact with a hexa-His tag. Ni-NTA is coupled to Sepharose CL-6B to yield a stable solid support resin that has high binding capacity for hexa-His tagged proteins. These

proteins can be eluted from the resin by the inclusion of imidazole in the buffer (see Figure 1). This technology reportedly allows the purification of proteins from less than 1% of total cell extract to greater than 95% homogeneity in one step (2).

The hexa-His affinity tag is small and normally does not interfere with the structure or function of purified proteins. Using commercially available vectors, it can be placed at the C- or N-terminus of the target protein along with a thrombin recognition site which can facilitate removal of the affinity tag from the purified protein upon the addition of the protease (see Figure 2).

This chapter describes the expression of recombinant PD from *A. aeolicus* and its purification using IMAC. The quaternary structure of the protein is also described.

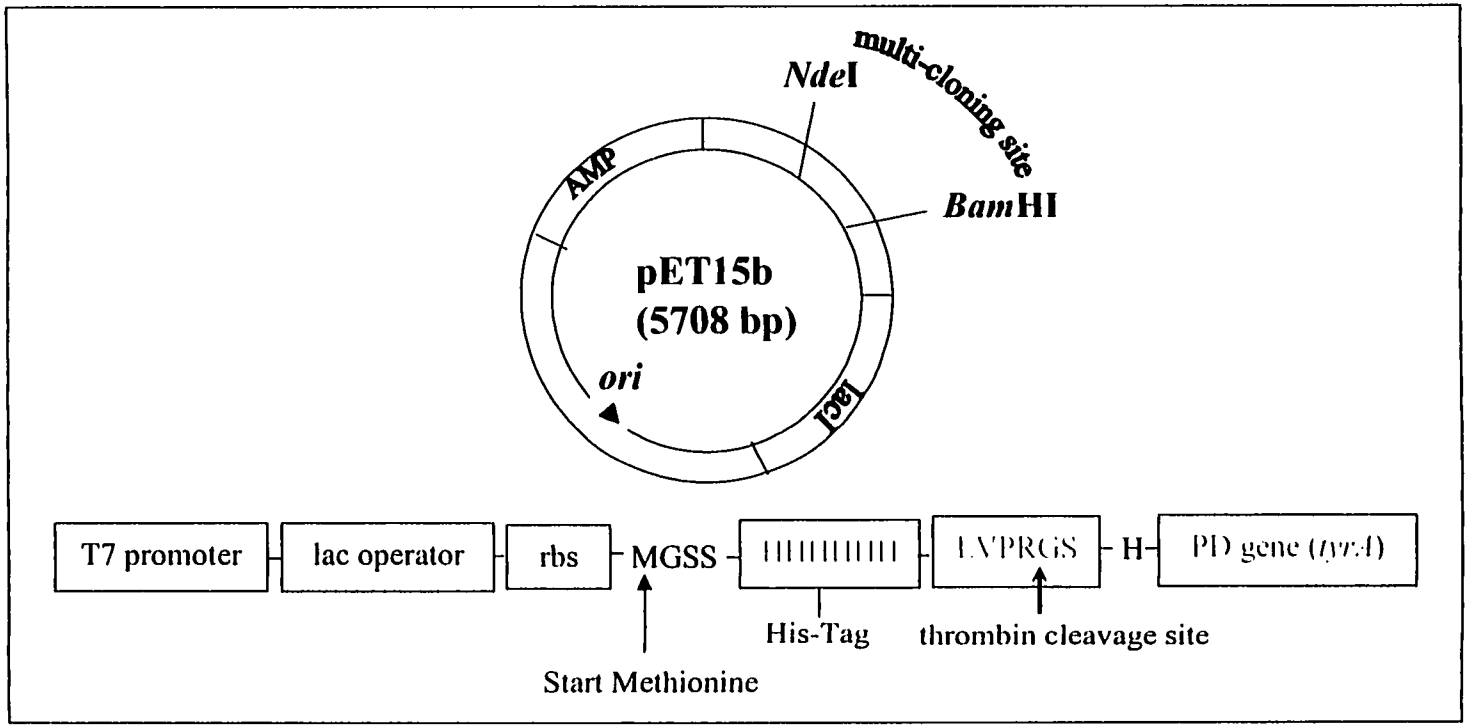

Figure 2. Novagen pET15b expression vector. The *tyrA* gene encoding *A. aeolicus* PD was cloned in-frame into the multi-cloning site at the *Nde*I and *Bam*HI restriction sites. The primary sequence of hexa-His and thrombin recognition sites at the N-terminus of PD is shown. The two arrows identify the initiating Met of the open reading frame and site of thrombin cleavage. (Adapted from the Novagen® pET Vector™ maps, Biosciences affiliate of Merck KGaA, Darmstadt, Germany. © 2001)

2.1 EXPERIMENTAL PROCEDURES

2.1.1 Materials

Kanamycin sulfate was purchased from Boehringer-Mannheim. SDS, N,N'-methylene-bis-acrylamide, ampicillin sodium salt, HEPES and yeast extract were supplied by ICN Biochemical Inc. DTT and Bio-tryptone were obtained from BioShop Canada Inc., while Bacto-agar was purchased from Difco Laboratories. Acetonitrile and TFA (HPLC grade) were purchased from Pierce. IPTG and the Wizard® Plus Miniprep DNA purification system were obtained from Promega Corporation. A protease inhibitor cocktail (400X mixture) containing pepstatin, leupeptin and antipain (each at 68 mg/ml in DMSO) with 400 mM PMSF was a generous gift from Dr. P. White at Boehringer Ingelheim Research Inc. and was stored at –20 °C until use. Ni-NTA or Superflow^{TM} chromatography resin was supplied by Qiagen; a binding capacity of 7.5 mg of hexa-His protein/ml of resin was assumed. Q-Sepharose Fast Flow anion exchange resin was from Amersham Biosciences as well as NAP-5 and NAP-10 pre-packed Sephadex G-25 size exclusion buffer exchange columns. Dialysis membrane (MW cut-off 12-14 kDa) was from Spectrapor and ultrafiltration units (MW cut-off 30 kDa) were obtained from Amicon and were washed according to manufacturers instructions. Thrombin was a generous gift from Dr. D. Christendat from the Ontario Cancer Institute, U. of Toronto, and was supplied frozen at a concentration of 0.03 mg/ml. Prephenate and chorismate were prepared as previously described (3, 4) while NAD^+ (grade I) was obtained from Boehringer-Mannheim. Stock solutions of these substrates were prepared in water or in an appropriate buffer and the pH adjusted to 7.5 before storage at –20 °C. Their exact concentrations were determined using published extinction coefficients (5) and enzymatic end-point analysis (6). (3-endo-

8-exo)-8-hydroxy-2oxa (3.3.1) non-6-ene-3,5-dicarboxylic acid bis (dicyclohexylammonium) salt, (*endo*-oxabicyclic diacid) was a generous gift from Dr. Paul Bartlett of the University of California, Berkeley, and was stored as a stock solution of 2 mM in water. All other chemical reagents were purchased from Fisher Scientific and Sigma Chemical Co. and were of the highest quality available.

2.1.2 Strains and Plasmids

The *E. coli* strains DH5α from Life Technologies Inc. [*supE*44 Δ*lacU*169 (φ80 *lacZ* ΔM15) *hsdR*17 *recA*1 *endA*1 *gyrA*96 *thi*-1 *rel*A1) and BL21(DE3) Gold from Strategene (F^- *dcm*$^+$ Hte *ompT hsdS*(r_B^- m_B^-) *gal* λ (DE3) *endA* Tet^r] were used for plasmid production and for protein expression, respectively. The plasmid pET15b (Novagen), a His-tag expression vector housing a T7 polymerase-dependent promoter for protein overexpression, was used for the construction of recombinant pRA-PD encoding the *tyrA* gene from *A. aeolicus*. Dr. A. Edwards at the Ontario Cancer Institute, U. of Toronto, donated the helper plasmid pMagik, which promotes the efficient translation of thermophilic genes in *E. coli*.

2.1.3 Construction of pRA-PD

The nucleotide sequence of the open reading frame denoted as *tyrA* was retrieved from GenBank with accession number AAC07589. Primers P1 (5'-GCGGCGGCCCATATGTTGGCTATCCTCTCCAGTAT-3') and P2 (5'-GCGCGGATCCTCAATCTATCTCCATTCTCTTTAA-3') were constructed to correspond to the 5' and 3' ends of the *tyrA* gene, respectively, and allowed the

incorporation of the flanking restriction sites *Nde*I (for P1) and *BamH*I (for P2). The restriction sites are underlined. The putative *tyrA* gene was amplified by PCR from *A. aeolicus* genomic DNA, generously provided by Drs. Robert Huber and Karl O. Stetter from the Universität Regensburg, Germany, using high fidelity *Pfu* DNA polymerase (Stratagene). This DNA fragment was cloned behind the lac promoter (for expression in *E. coli*) in plasmid pET15b to create pRA-PD which adds a sequence encoding an N-terminal hexa-His tag followed by a thrombin recognition site. Dr. D. Christendat of the Ontario Cancer Institute, U. of Toronto, graciously prepared this construct. Plasmid DNA isolated from several transformants were sent to us and were subjected to DNA sequencing (Bio S & T, Montreal, Canada) to confirm the correct sequence of the *tyrA* gene. One plasmid with the correct sequence, pRA-PD-3, was used to transform *E. coli* BL21(DE3) Gold cells.

2.1.4 Overexpression of Recombinant A. aeolicus PD

E. coli BL21(DE3) Gold was co-transformed with pRA-PD-3 and pMagik by electroporation (7) and plated on LB agar supplemented with 100 μg/ml ampicillin and 50 μg/ml kanamycin. After incubation overnight at 37 °C, a single colony was selected and used to inoculate 50 ml of LB medium containing antibiotics. The culture was shaken at 30 °C for 15 h, diluted 150-fold into the same medium (4.5 L total) and grown until an optical density of 0.5 - 0.6 at 600 nm was reached. The culture temperature was reduced to 24 °C, then protein production was induced by the addition of IPTG to a final concentration of 0.4 mM. The culture was grown for an additional 5 h and left overnight

with shaking at 18 °C. Cells were harvested by centrifugation (10,000 x g, 20 min, 4 °C) and the cell pellet was frozen at –20 °C until further processed.

2.1.5 Determination of Heat Treatment Temperature for Partial Purification

One ml aliquots of cell-free extract (section 2.1.6) were placed in a water bath set at 60°C, 65 °C, 70 °C, 75 °C, 80 °C, 85 °C or 100 °C for 1 min then transferred onto ice. Samples were then centrifuged (30,000 x g, 10 min, 4 °C) and 10 µl of each supernatant were processed as described in 2.1.9. Protein were then resolved by SDS-PSGE on a 15% polyacrylamide gel. The pellets were also analyzed electrophoretically after solubilization and vortexing in 4% SDS.

2.1.6 Standard Purification Strategy for Recombinant *A. aeolicus* PD

Cells were resuspended in ice cold **buffer A** (50 mM HEPES, 0.5 M NaCl, 5% glycerol, pH 7.5) containing 5 mM imidazole at a ratio of 15 ml buffer per litre of original culture. This buffer was supplemented with a protease inhibitor cocktail containing 5 µg/ml each of leupeptin, pepstatin and antipain and 170 µg/ml PMSF. The cell pellet was resuspended by 10-15 up-and-down strokes of a Dounce Homogenizer. Resuspended cells were disrupted by a single passage through a Thermo Spectronic French Press (pre-cooled cell) at 18,000 psi followed by centrifugation at 38,000 x g for 40 min at 4 °C. The resulting supernatant was decanted into a 50 ml plastic centrifuge tube, incubated in a 85 °C water bath for 10 min with gentle swirling, placed on ice, and again centrifuged (38,000 x g, 40 min, 4 °C). Protein was then subjected to chromatography at room temperature with flow rates adjusted by a pump. Fractions containing PD were identified

by activity assays. The soluble fraction was applied to a Q-Sepharose anion exchange column (50 ml resin pre-equilibrated with buffer A containing 5 mM imidazole), and the column was washed with 100 ml of **wash buffer** (buffer A with 30 mM imidazole) at a flow rate of 5 ml/min. PD-containing fractions that were collected from the flow-through and the column wash were loaded consecutively onto a Ni-NTA affinity column, (15 ml Superflow™ resin pre-equilibrated with buffer A and 5 mM imidazole) with a flow rate of 1 ml/min. The column was washed at 2-3 ml/min with 50 ml of wash buffer (fractions of 10 ml were collected) then with 30 ml of **elution buffer** (buffer A with 300 mM imidazole) and aliquots of 1.5 ml were collected. EDTA and DTT were added to each fraction to a final concentration of 1 mM and 0.5 mM, respectively. Fractions containing PD activity were pooled. Thrombin was added to an aliquot of this pooled fraction at a final protein:thrombin ratio of 1000:1 (w/w) then dialyzed overnight at 4 °C against 5 L of **storage buffer** (buffer A with 5 mM ß-mercaptoethanol). The thrombin-treated sample was reapplied onto the Ni^{2+} affinity column (pre-equilibrated with storage buffer) to remove any tagged protein remaining. Cleaved PD was eluted in the flow-through and wash buffers and was pooled, concentrated to ~ 10 mg/ml using a Centricon ultrafiltration unit and stored in 1 ml aliquots at 4 °C. SDS-PAGE was used to monitor the purification procedure. The sample was also monitored for several months for any loss in specific activity (section 2.1.12) or any protein degradation as judged by SDS-PAGE (section 2.1.9).

2.1.7 Purification Using Affinity Chromatography and Imidazole Step Gradient

Heat-treated cell-free extract was loaded onto Q-Sepharose followed by application onto a Ni-NTA column as previously outlined in sections 2.1.4 and 2.1.6. The Ni-NTA column was washed with buffer A containing 30, 50, 75, 100 and 200 mM imidazole (2 column volumes each) and 1.5 ml fractions were collected. The elution profile of PD was monitored by SDS-PAGE. The latter fractions from the 50 mM imidazole wash and all of the 75 mM imidazole wash were combined as the source of "heterodimeric" PD, while selected fractions from the 100-200 mM imidazole wash were pooled for treatment with thrombin. These two separate pools were dialyzed against 5 L of storage buffer and stored in 1 ml aliquots at 4 °C.

2.1.8 Affinity Chromatography Under Denaturing Conditions

Heat-treated cell-free extract, prepared as described in 2.1.4 and 2.1.6 was dialyzed for 36 h against 500 ml of 50 mM potassium phosphate, 0.3 M NaCl, 5% glycerol and 5 mM β-mercaptoethanol (pH 7.5), and an appropriate concentration of Gdn-HCl such that its final concentration in the sample was 6.0 M. The pH of the buffer was adjusted to 7.5 after adding the denaturant. Following dialysis, the sample was loaded onto a Ni-NTA column pre-equilibrated with buffer containing 6.0 M Gdn-HCl. The column was washed successively with 3 bed volumes each of this equilibration buffer containing 20 mM and 250 mM imidazole. Fractions from the latter wash containing the highest PD activity were pooled. Thrombin was added to a final protein:thrombin ratio of 1000:1 (w/w) and the sample was dialyzed against 2 changes of 5 L of storage buffer over a period of 60 h

at 4°C. The dialysate was centrifuged (16,000 x *g*, 30 min, 4 °C) to remove any precipitate and the supernatant was stored at 4 °C as 1 ml aliquots.

2.1.9 SDS-Polyacrylamide Gel Electrophoresis

Denaturing (SDS) PAGE was performed under reducing conditions and with 15% polyacrylamide gels following the method of Laemmli (8). Protein samples were diluted 1:2 (v/v) into 2X SDS sample loading buffer (1.5 M Tris-HCl, 4% SDS, 20% glycerol, 0.2 M DTT) and incubated in a boiling water bath for 2 min prior to loading on a gel. To accommodate the high concentration of salt in the protein samples, gels were electrophoresed at 50-75 V as samples migrated through the stacking gel, then the voltage was increased to 200-220 V as the samples entered the resolving gel. Electrophoresis continued until the Bromophenol Blue tracking dye migrated off the resolving gel. Bio-Rad low range molecular weight protein standards were used routinely to estimate the molecular weight of proteins in the samples. Protein was visualized by staining the gels with Coomassie Brilliant Blue R-250.

2.1.10 Visualizing His-tagged PD by Fluorescence Staining

Protein samples were resolved by SDS-PAGE as described in 2.1.9 and then the gel was treated with Pro-Q™ Sapphire 365 Oligohistidine Gel Stain (Molecular Probes), a Ni^{2+} chelating fluorescent dye synthesized with the NTA moiety, according to manufacture's instructions. The gel was then stained with Coomassie Blue R-250 to visualize all proteins.

2.1.11 Determination of Enzyme Activity and Protein Concentration

A. aeolicus PD activity was determined by continuously monitoring the formation of NADH from NAD^+ at 340 nm in the presence of prephenate using a double-beam spectrophotometer (GBC UV/VIS model 918) fitted with a thermostatically controlled (Pelletier) cuvette holder. The reaction was conducted in 1 ml quartz cuvettes (path length 1 cm) in a total volume of 1.0 ml. Reaction rates were calculated from the linear portion of progress curves using the software supplied by the spectrophotometer and an extinction coefficient of 6400 $M^{-1}cm^{-1}$ was used which takes into account the contribution of 4-hydroxyphenylpyruvate at 340 nm (9). A unit of enzyme is defined as the amount of enzyme required to produce 1 μmol of product per min at the specified temperature. Chorismate mutase (CM) activity was determined at 55 °C in **Rxn buffer** (50 mM HEPES and 150 mM NaCl, pH 7.5), containing 1 mM chorismate after initiating the reaction with 4 μl (8 μg) of purified PD. The disappearance of chorismate was followed at 274 nm as outlined in Turnbull *et al.* (1). Protein concentration was estimated using the Bio-Rad Protein Assay Kit (Bio-Rad Laboratories) with bovine serum albumin (Sigma) as a standard.

2.1.12 Activity Assays to Monitor Protein Purification

Dehydrogenase activity assays of *A. aeolicus* PD conducted at various stages of the purification procedure were performed using a **PDH mix** (100 mM Tris-HCl, (pH 7.5) 150 mM NaCl, 1 mM EDTA, 1 mM DTT, 2 mM NAD^+ and 0.5 mM prephenate). One ml of the reaction mixture was equilibrated at 55 °C for 2 min in a quartz cuvette and the reaction was initiated by the addition of 10 μl of protein.

2.1.13 Molecular Weight Determinations by Mass Spectrometry and Analytical Ultracentrifugation

Subunit molecular weight of *A. aeolicus* PD from selected stages of the purification were determined by electrospray ionization mass spectrometry (ESI-MS), by direct infusion into a Finnigan single quadrolpole instrument. Data analysis was performed using QualBrowser software. PD samples ranging from 2.5 mg/ml to 4.7 mg/ml were diluted 10-fold in 70% acetonitrile and 0.1% TFA. The calibration of the instrument was checked with bovine myoglobin standard (Pierce) prepared in the same solvent. The experimental value (16,954), determined at the beginning and the end of the analysis, agreed well with the predicted mass of 16,950 Da.

The native molecular weight of *A. aeolicus* PD from different preparations was determined using a Beckman XL-I analytical ultracentrifuge with absorbance detection set at 280 nm. PD samples (0.5 ml from 1.0-3.0 mg/ml) were buffer exchanged into 50 mM HEPES (pH 7.5), 0.3 M NaCl, 0.5 mM TCEP, 1% glycerol, using NAP-5 pre-packed gel filtration columns then diluted to give a final OD_{280} of 0.65. The samples were then centrifuged (16,000 x g, 30 min, 4 °C) and 0.39 ml of supernatant were placed in double sector cells consisting of a 1.2 cm Epon centrepiece and quartz windows along with 0.4 ml of exchange buffer as reference. The cells were mounted in an An60Ti rotor and spun at 35,000 r.p.m. at 30 °C for 10 h. Absorbance was collected in continuous mode with a step size of 0.005 cm and 5 replicative scans. The apparent sedimentation coefficient $S_{20,w}$, and an approximate molar mass were calculated from the velocity and

shape of the sedimenting boundary by fitting the time-dependent concentration profiles calculated with the Lamm equation (10) for a single species to the measured data. Calculations were performed using the program Svedberg (11) with the assistance of Dr. P. White. The buffer density and the protein partial specific volume were estimated using the program Sednterp (12).

2.2 RESULTS

2.2.1 Strategy for Expression of *A. aeolicus* PD

PCR was used to amplify the putative *tryA* gene from *A. aeolicus* genomic DNA. Cloning of this gene into pET15b allowed expression of *A. aeolicus* PD in *E. coli* BL21 (DE3) Gold cells harbouring the plasmid pRA-PD. Protein derived from this construct contained an N-terminal hexa-His tag (to facilitate protein purification by Ni-NTA affinity chromatography), and a protease recognition sequence (to allow removal of the His tag by cleavage with thrombin, after purification) (see Figure 2). To boost expression levels of *A. aeolicus* PD in *E. coli*, BL21(DE3) Gold cells were co-transformed with the helper plasmid pMagik which encodes tRNAs recognizing $AUA^{(Ile)}$, $AGA^{(Arg)}$ and $AGG^{(Arg)}$ codons, that are frequently used by archeons and eukaryotes but are rare in *E. coli* (13). This strategy is well documented by others labs that express thermophilic proteins in *E. coli* (13, 14).

2.2.2 Heat Treatment to Assist Protein Purification

A cell-free extract from a culture of *E. coli* harbouring pRA-PD was obtained as described in 2.1.4 and 2.1.6. SDS-PAGE analysis of the extract (Figure 3 lane 2) indicated that the expression strategy outlined above indeed did yield substantial levels of soluble recombinant protein as noted by bands around 37 kDa, the expected molecular weight of the PD monomer. To exploit the extreme thermal stability of *A. aeolicus* and its gene products, heat treatment of the cell-free extract was employed to remove a large portion of the host *E. coli* proteins before further purifying the dehydrogenase by column

chromatography. A denaturing gel in Figure 3 (lanes 3-9) shows clarified fractions obtained after incubating small aliquots of cell free extract for 1 min at 60 °C, 65 °C, 70 °C, 75 °C, 80 °C, 85 °C and 100 °C, respectively. There was a gradual decrease in protein levels with increasing temperature resulting from denaturation of host proteins. Two thermally stable proteins of ~ 35 kDa and 37 kDa remain soluble. There was little difference in the results of lanes 8 (85 °C) and 9 (100 °C) indicating that incubation at 85°C was sufficient to effectively remove over 50% of host proteins from the soluble fraction. Our results are in keeping with those from other studies (47, 48) which showed heat treatment of the cell-free extract improved the quality of the resulting fraction for subsequent chromatography. Moreover, this step is expected to remove *E. coli* CM-PD and facilitated the rapid screening of activity of *A. aeolicus* PD variants partially purified by heat treatment. Interestingly, the addition of a heat step is also reported to aid in the crystallization of some thermophilic proteins (L. Boju, personal communication).

Incubation of the cell-free extract at 95 °C for 1 min then cooling to room temperature, multiple times, did not appear to remove additional host protein nor did it significantly decrease the levels of heat stable protein in the soluble fraction. This is shown by SDS-PAGE analysis in Figure 4 lanes 2-5. Analysis of the particulate fractions obtained from the four incubations (lanes 6-9) indicated that most of the host *E. coli* proteins were precipitated in the first heat step.

2.2.3 Protein Purification

A summary of the purification of PD from *A. aeolicus* is presented in Table 1 and Figure 5. Experimental details are described in section 2.1. Briefly, the protocol entailed heat treatment of cell-free extract followed by chromatography on anion exchange and Ni-NTA affinity resins, and finally incubation with thrombin to remove the His tag. This procedure yielded 25 mg of thrombin-cleaved homogeneous PD per L of cell culture. This sample could be stored at 4 °C for > 4 months at 1-10 mg/ml without a decrease in specific activity or appearance of protein degradation as judged by SDS-PAGE (data not shown). The expression and purification strategy was adapted from a procedure developed by Dr. D. Christendat to facilitate high throughput purification of recombinant proteins (14, 15), but was modified to include a heat step.

SDS-PAGE analysis of fractions collected at various stages of the purification are shown in Figure 5. Lanes 2 and 3 confirmed that treatment of the cell-free extract at 85 °C for 10 min is a very effective initial purification step. Furthermore, enzymatic assays indicated very little loss in PD activity with heat treatment (Table 1). The next step, Q-Sepharose chromatography performed in a high salt buffer, allowed recovery of all of the proteins in the heat-treated extract and hence did not result in any significant purification as judged by SDS-PAGE (lane 4) or an improvement in specific activity (Table 1). The step was included however, to remove highly anionic material which often binds to proteins and impedes their crystallization (D. Christendat, personal communication). Lane 5 shows the "flow-through" after loading the sample onto Ni-NTA column; one major band was resolved and surprisingly it contained 30% of the total activity of the

Table 1. Purification Table

Purification of PD from *A. aeolicus* [a]

Step	V_{total} (ml)	Total Protein (mg)	Total Activity[b] (U)	Specific Activity[b] (U/mg)	Recovery (%)	Purification fold
Cell Extract	50.0	2075.0	2986.6	1.4	100	1.0
Heat Treated	49.0	661.5	2555.9	3.9	86	2.8
Q-Sepharose	100.0	650.0	2535.7	3.9	85	2.8
Ni-NTA						
Flow through	80.0	392.0	912.2	2.3	31	1.6
30 mM imidazole wash	50.0	52.0	88.0	1.7	3	1.2
300 mM imidazole wash	8.5	85.0	844.4	9.9	28	7.1
Thrombin treatment[c]	9.5	80.8	814.3	10.1	27	7.2

[a] Purification was achieved from a 4.5 L culture of E. coli BL21(DE3) harboring pRA-PD

[b] Determined at 55 °C

[c] values calculated from protease treatment of entire 300 mM imidazole wash

heat-treated cell extract (Table 1). Lanes 6 and 7 are representative fractions from subsequent column washes with buffer containing 30 mM then 300 mM imidazole, respectively. Finally, the protein from lane 7 was dialyzed with thrombin to cleave the His tag (lane 8) yielding a preparation over 98% pure as judged by SDS-PAGE with a specific activity of 10.1 U/mg (Table 1). Interestingly, protein samples eluting in the flow-through and imidazole washes possessed high specific activities despite their heterogeneity on SDS-PAGE, suggesting that they contained different forms of PD that were catalytically active. The purified enzyme did not possess CM activity when assayed under conditions described in 2.1.12 nor was dehydrogenase activity inhibited by the mutase transition state analogue *endo*-oxabicyclic diacid (120 μM) when assayed as described above but with 0.1 mM prephenate.

Several important observations were noted by SDS-PAGE analysis which suggested: (1) monomeric PD is present in forms that are full length (N-terminal His tagged) AND truncated (His tag removed) *prior* to thrombin treatment; and (2) under native conditions PD is dimeric but the monomers can associate using one type of subunit thus yielding either full-length or truncated homodimers, or using a mixture of the two types of subunits giving rise to a heterodimer. Accordingly, PD would have a different affinity for Ni-NTA resin depending on its subunit composition.

First, throughout the procedure for isolating His-tagged PD, two overexpressed proteins at ~ 37 kDa and ~ 35 kDa were consistently resolved by SDS-PAGE (Figure 5, lanes 2, 3, 6). Their relative migrations corresponded well to those predicted for a full-length

His-tagged subunit and one truncated at the N-terminal thrombin recognition site, respectively (see Figure 6). In the absence of protease, only the 37 kDa monomer should have been present. **Second**, when the fraction from the anion exchange column was loaded onto the Ni-NTA column, SDS-PAGE analysis of the flow-through revealed one predominant species at ~35 kDa (Figure 5, lane 5). This protein was not His-tagged since it did not bind to the affinity resin nor was it a contaminant since it displayed high PD activity (Table 1). These results suggested that the eluant contained homodimeric PD composed of catalytically active untagged monomers. Dimeric forms of PD composed of tagged monomers would have bound to the Ni-NTA resin. **Third**, both types of monomers were present at a ratio of approximately 1:1 in fractions derived from washing the Ni-NTA column with 30 mM imidazole (Figure 5, lane 6), but this ratio changed to favour the 37 kDa protein with the 300 mM imidazole wash (lane 7). These results indicated that the low imidazole wash removed heterodimeric PD (one subunit His-tagged, the other not) which possessed a moderate affinity for Ni-NTA. Increasing the step gradient to 300 mM imidazole eluted homodimeric PD (both subunits tagged) although notably contaminated with the heterodimer. **Lastly**, incubation of purified His-tagged PD with thrombin gave rise to only one subunit type of ~35 kDa (Figure 5, lane 8). This is more easily seen in the enlargement in Figure 6A for heterdomeric PD (lane 2) and thrombin-cleaved PD (lane 3). It is also apparent that the protein resolved in the lower band in lane 2 was not affected by thrombin, suggesting that the His tag on this subunit had been removed prior to adding protease. Figure 6B shows the calibration curve derived from the migration of molecular weight protein standards resolved by SDS-PAGE electrophoresis in lane 1. The relative migration of the two PD monomers within

the heterodimer are consistent with subunit molecular weights of PD with and without the His tag of 36.8 ± 1.5 and 34.9 ± 1.4 kDa, respectively. These values are close to the molecular weights predicted from the amino acid sequence for PD containing a 2.2-kDa His tag and thrombin recognition site (37,012), and for thrombin-treated PD where the His tag has been removed leaving three residues from the thrombin recognition site on the N-terminus of the protein (35,130) (see Figure 2).

The subunit molecular weight of PD from selected purification steps was determined by mass spectrometry (section 2.1.13) thereby verifying the results from the SDS-PAGE analysis shown in Figure 6. Experimentally determined values for protein derived from Ni-NTA column flow-through (35,127), the 300 mM imidazole wash (37,081), and thrombin-treated PD (35,271) were in reasonable agreement with the values predicted by the primary sequence for either a His-tagged subunit or subunit processed at the thrombin cleavage site (values listed in paragraph above). For some samples, mass accuracy was lower than expected due to the presence of high amounts of salt and non-volatile buffer in the samples. It is noteworthy that there was excellent agreement in values for the flow-through and that predicted for the purified thrombin-treated PD, thus confirming that the His-tagged PD was cleaved at only *one* site in the primary sequence of the enzyme even without adding thrombin.

The subunit composition of PD in the different purification fractions was further verified by resolving the proteins by SDS-PAGE and then treating the gel with dye containing a fluorescent NTA probe that interacts specifically with oligo-His motifs (Figure 7A).

After photographing the gel, it was then stained with Coomassie Blue R-250 to visualize all proteins (Figure 7B). The results showed that only the 37 kDa protein of the heterodimer was His-tagged (lane 4). Untagged 35 kDa subunits, as found in the Ni-NTA flow-through (lane 2), thrombin-treated PD (lane 5) and the bottom (35 kDa) band in all other fractions (lanes 3 and 4) could only be visualized by Coomassie Blue staining.

2.2.4 Preparation of Pure Heterodimeric and His-Tagged Homodimeric PD

A fraction containing purified heterodimer was prepared by Ni-NTA chromatography by replacing column washes containing 30 mM and 300 mM imidazole with several smaller step gradients of 30, 50, 75, 100 and 200 mM imidazole (see section 2.1.7). SDS-PAGE analysis of fractions from the washes (Figure 8) showed that "clean" heterodimeric PD (identified as a doublet with monomers of equal intensity) eluted at the end of the 50 mM imidazole wash (area 3) and over the entire 75 mM imidazole wash (area 4). Interestingly pure His-tagged PD was never resolved (area 5), even by modifying the chromatography conditions to include an extensive washing with 60 mM imidazole buffer followed by eluting the protein with 250 mM imidazole (data not shown).

Homogeneous His-tagged PD could be successfully isolated, however, by unfolding the heat-treated cell-free extract in phosphate buffer containing 6 M Gdn-HCl and applying this protein to the affinity column under denaturing conditions (section 2.1.8). SDS-PAGE analysis (Figure 9) shows that His-tagged subunits remained bound and were subsequently eluted in a wash of 250 mM imidazole (lane 5). The denaturant was removed by dialyzing the eluant against a large volume of storage buffer at 4 °C to

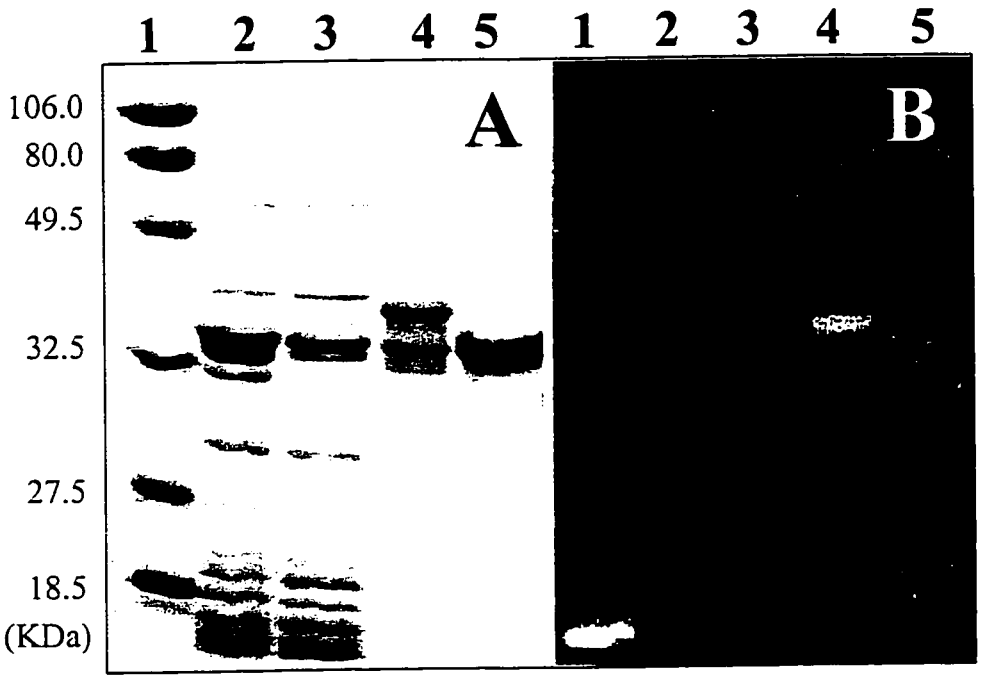

Figure 7A and 7B. SDS-PAGE analysis of protein standards (1); Ni^{2+} flow-through (2); first fraction from 30 mM imidazole wash (3); heterodimer PD (4); and homodimer PD resulting from thrombin cleavage (5). SDS-PAGE resolved with Coommassie Blue (A) and with Pro-Q™ Sapphire 365 oligo-His specific stain solution (B).

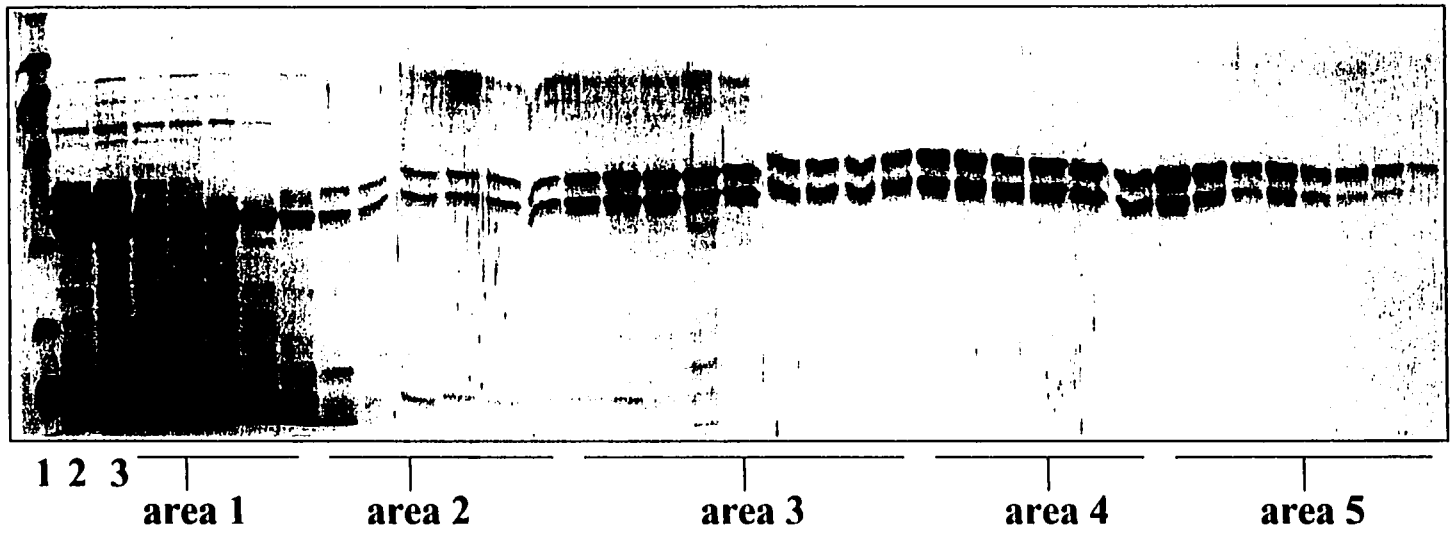

Figure 8. SDS-PAGE analysis of the purification of PD using an imidazole step gradient. Q-Sepharose treated PD was applied to the Ni-NTA column and eluted in buffer washes containing increasing concentrations of imidazole (see section 1.1.7 for details). Varying aliquots of the washes were analyzed on 15% polyacrylamide gels. Lane 1, molecular weight standards; lane 2, heat treated cell-free extract; lane 3, eluate from Q-Sepharose; area 1, flow-through from Ni-NTA; area 2, 30 mM imidazole wash; area 3, 50 mM imidazole wash; area 4, selected fractions from 75-100 mM imidazole wash; area 5, 200 mM imidazole wash.

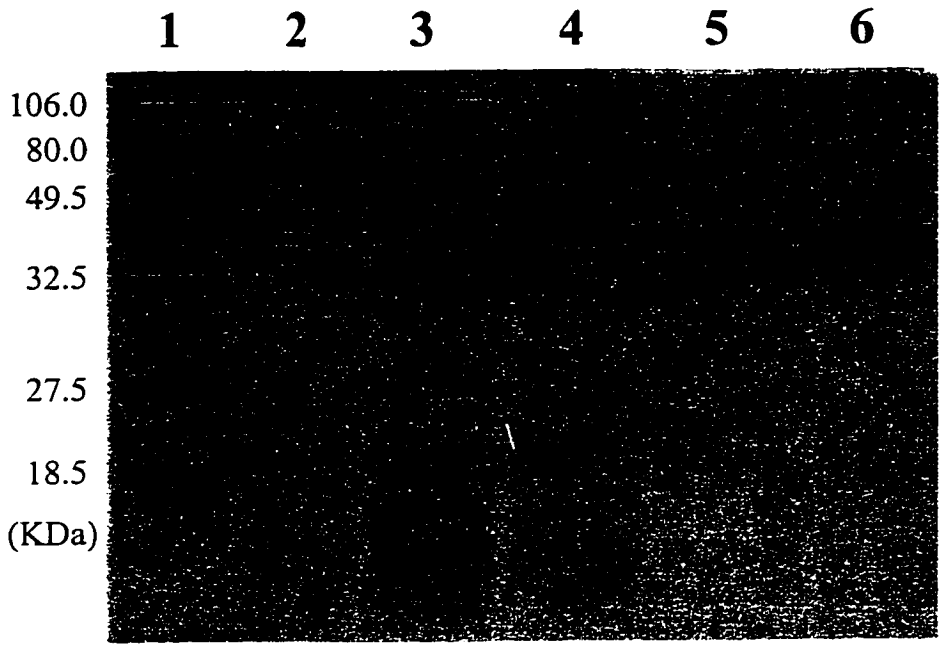

Figure 9. SDS-PAGE analysis of purification of PD by affinity chromatography under denaturing conditions. Heat treated cell-free extract, treated with 6.0 M Gdn-HCl, was applied to Ni-NTA column under denaturing conditions and PD was eluted in the same buffer containing 20 mM imidazole and 250 mM imidazole (see section 1.1.8 for details). Selected fractions were analyzed on a 15% polyacrylamide gel. Lane 1, molecular weight standards; lane 2, heat-treated cell-free extract (10 μg); lane 3, Ni-column flow-through (20 μg); lane 4, 20 mM imidazole wash (10 μg); lane 5, 250 mM imidazole wash (15 μg); lane 6, thrombin-treated PD (20 μg).

facilitate refolding of His-tagged PD. While the resulting protein had a high specific activity (7.5 U/mg), it was not effectively cleaved by thrombin under conditions previously described (lane 6). Moreover, the protein underwent a time-dependent precipitation over the course of 48 h. Regrettably, the results indicated that under these experimental conditions the protein did not refold to its native state. Pure His-tagged PD was not isolated and further characterized.

2.2.5 Quaternary Structure Determination by Analytical Ultracentrifugation

Analytical ultracentrifugation (AUC) was performed on purified thrombin-treated *A. aeolicus* PD as well as on isolated heterodimer (prepared as described above) to provide estimates of their molecular weights in solution and hence to determine if both forms of PD are dimeric under native conditions. Sedimentation velocity experiments were performed at 35,000 rpm and 30 °C. The data were best fit to a single species model for both proteins as described in section 2.1.13 to yield values for the sedimentation coefficients (s) and molecular masses shown in Table 2. Surprisingly, these experimentally determined molecular weights, while higher than a monomer, were significantly lower than theoretically calculated for a dimer. One possibility consistent with a single species fit is that at 30 °C, each protein solution contains a mixture of monomers and dimers that are rapidly interconvertible. The high quality of the absorbance data (data not shown) indicated that the proteins were suitable for further analysis by AUC. Conducting velocity runs at different protein concentrations and temperatures would verify if a monomer-dimer equilibrium was present and was temperature dependent. Sedimentation equilibrium runs would establish unequivocally

the native molecular weight of the proteins and if dimeric forms were present, the association constants for the dimers (16-19).

Table 2: Analytical Ultracentrifugation Velocity Run

	Dimeric mass from amino acid composition (kDa)	Calculated mass (kDa)	Sedimentation coefficient $S_{20,w}$
Thrombin-cleaved PD	70.26	59.47	4.854
Heterodimeric PD	74.03	56.71	5.080

2.3 DISCUSSION

Analysis of the *A. aeolicus* genome based on sequence similarities with other bacterial proteins of known function has identified an *A. aeolicus* gene showing strong similarity to *E. coli tyrA* which encodes a bifunctional PD (20). The work presented in this chapter verified that the putative *tyrA* gene of the *A. aeolicus* did in fact encode PD. The nucleotide sequence of the gene cloned into *E. coli* and the molecular weight of the purified thrombin-cleaved protein determined by mass spectrometry and SDS-PAGE analysis were consistent with that expected for the 311 amino acid polypeptide encoded by *tyrA*. Moreover, the fact that the gene product could effectively catalyze the reduction of NAD^+ in the presence of prephenate established its function as a prephenate dehydrogenase. PD was remarkably resistant to thermal denaturation (Figure 4), as expected for a protein derived from this hyperthermophilic bacterium. Unlike the *E. coli* bifunctional enzyme (21), it did not possess CM activity nor was the dehydrogenase activity inhibited by a mutase transition state analogue. Surprisingly, analysis of the *A. aeolicus* genome failed to identify a monofunctional CM, although it does contain a bifunctional mutase-dehydratase (20).

The behaviour of the protein on Ni-NTA affinity resin as analyzed by SDS-PAGE (Figure 5), together with results from the sedimentation velocity studies by AUC (Table 2), suggested that the recombinant thermophilic protein was capable of forming dimers in solution. However, the native protein exhibited a lower than predicted molecular weight by AUC at 30 °C (a temperature well below its optimum), and hence differed from *E. coli*

CM-PD where similar studies have determined an average molecular weight that is only about 5% less than that predicted for a dimer (22). Nevertheless, native *A. aeolicus* PD is referred to as "dimeric" in this thesis. Further biophysical studies are required to verify the native quaternary structure of this protein.

In the present study IMAC technology combined with a heat step was used to purify *A. aeolicus* PD to > 98% homogeneity and in quantities more than adequate for kinetic and biophysical studies. However, cloning the gene into the pET15b expression vector encoding a removable N-terminal hexa-His tag unexpectedly resulted in proteolytic cleavage of the tag from about one-half of the PD subunits present in the cell-free extract (Figure 5). Consequently, PD extracted from the cell appeared to be present in three forms wherein cleaved monomers could associate with each other or with a His-tagged monomers, all with distinct affinities for Ni-NTA resin. As the untagged homodimer would not bind to the affinity resin, regrettably ~ 30% of total active PD was lost in this purification step. To increase our yields of His-tagged PD from IMAC, the conditions for protein expression could be adjusted to minimize *in vivo* cleavage by induction at a lower temperature and/or for a shorter time period. However, omitting the overnight post-induction incubation at 18 °C did not decrease the ratio of 35 kDa to 37 kDa subunits. Moreover, overall protein yield was lower. Alternately, the protein could be engineered with a non-removable hexa-His sequence placed immediately before the N- or C-termini of the protein as has been done with recombinant type I dihydroorotase from *A. aeolicus* (23).

Mass spectrometry studies combined with SDS-PAGE (Figure 6) established with certainty the site of cleavage between the Arg-Gly bond of the 19 amino acid tag of PD (Figure 2). Thrombin is a mammalian serine protease responsible for the catalytic proteolysis of fibrinogen to fibrin in the blood clotting cascade pathway (24). Thrombin, like other serine proteases, will cleave after an arginine residue (25) in the substrate's primary sequence. However, thrombin must first bind to its peptide substrate at a specific recognition sequence (LVPRGS); the only encoded thrombin recognition site on pRA-PD is within the engineered N-terminal tag. As thrombin is not native to bacteria, and as this cleavage is observed early on in the protein purification (thrombin is only added *after* the affinity chromatography step), we concluded that the reaction must have been catalyzed by a serine protease that does not recognize specifically a thrombin binding site on the peptide substrate. Proteins from hyperthermophilic bacteria are generally more compact than their mesophilic counterparts (26, 27); the 19 residue N-terminal tail is presumably outside the protein core and being very mobile, presents itself as a likely target for non-specific cellular proteases. There are no reports in the literature describing findings similar to our study even though pET15b and comparable expression vectors have been used extensively to assist in the purification of a number of proteins from both mesophilic and thermophilic bacteria (15, 28-32). There are no reports of other *A. aeolicus* proteins expressed with cleavable tags. Furthermore, with the high throughput strategy adopted by many structural and functional genomics labs, such processing may have been overlooked since the purity of the protein is often monitored by SDS-PAGE only *after* the removal of the tag with thrombin treatment, or else the proteins are engineered with permanent oligo-His tags (23, 33).

Over forty different proteolytic enzymes have been discovered in *E. coli* (34). The majority of these enzymes are classified as serine proteases, however many of them are atypical serine proteases and are placed in distinct classes (34). The protease inhibitor cocktail (leupeptin, pepstatin, antipain and PMSF) that we added during cell lysis is effective against a broad spectrum of carboxyl- (e.g., aspartate), hydroxyl- (e.g., serine) and thiol (e.g., cysteine) proteases (35-39) and are well known as microbial antagonists (40). The presence of the 35 kDa protein in the cell-free extract suggests either that the protease inhibitor mixture was ineffective or that peptide hydrolysis occurred during expression, before the cells were broken. The lysis buffer was not supplemented with EDTA (a metalloprotease inhibitor) in order to facilitate Ni-NTA chromatography. However, metalloproteases do not hydrolyse Arg-Gly peptide bonds (24, 39, 41), the cleavage site identified in this study.

Some well characterized proteases identified in *E. coli* cells are the ATP-dependent proteases Lon (protease La) (42) and Clp (protease Ti) (43, 44), where Lon in considered to be an atypical serine protease and Clp a serine-type protease. Another example is OmpT (protease VII), an outer membrane serine protease highly specific for dibasic sties (Arg-Arg, Arg-Lys, Lys-Arg, Lys-Lys) (34, 45) which reportedly cleaves monobasic sites such as Arg-Met and Arg-Ala (46). Lon and OmpT are likely not the culprits in this study since the *E. coli* host strain BL21(DE3) Gold lacks the genes that encodes these two proteases. Reaction with Clp is also unlikely as it is a highly processive protease, degrading protein substrates to small peptides 10-20 residues long (42-44); the 35 kDa

protein isolated in the present study appears to be a stable domain. Other possible catalysts for *in vivo* thrombin-like cleavage include protease II, protease In and protease Fa, serine-type proteases found in the cytosol. These enzymes have been reported to hydrolyze N-terminal protein domains containing trypsin-like recognition sequences (34). Identification of the enzyme catalyzing the N-terminal cleavage of recombinant *A. aeolicus* PD would require considerable effort and is not important for our long term studies on this enzyme.

2.4 REFERENCES

1. Turnbull, J., Cleland, W. W. and Morrison, F. J. (1990). *Biochemistry.* **29**, 10245-10254.
2. Janknecht, R., de Martynoff, G., Lou, J., Hipskind, R. A., Nordheim, A. and Stunnenberg, H. G. (1991). *Proc. Natl. Acad. Sci.* **88,** 8972-8976.
3. Reiger, C. E. and Turnbull, J. (1996). *Prep. Biochem.* **26**, 67-76.
4. Dudzinski, P. K. and Morrison, J. F. (1976). *Prep. Biochem.* **6**, 113-121.
5. Dawson, C. M. R., Elliott, C. D., Elliott, H. W. and Jones, M. K., (1986) *Data for Biochemical Research.* 3rd edition. Oxford Science Puplications, Clarendon Press.
6. Turnbull, J., (1988). *Mechanistic Studies on a Bifunctional Enzyme.* Ph. D. Thesis. Australian National University.
7. Sambrook J. and Russell D. (2001). *Molecular Cloning*, 3rd edition. Cold Spring Harbor Laboratory Press, Cold Spring, New York. p. 16.33-16.42.
8. Laemmli, U. (1970). *Nature* **227**, 680-685.
9. Heyde, E. and Morrision, J. F. (1978). *Biochemistry.* **18**, 2766-2775.
10. Lamm, O. (1929). *Ark. Mat. Astr. Fys.* **21B**, 1-4.
11. Svedberg, T. and Peterson, K. O. (1940). *The Ultracentrifuge*, Oxford University Press, London.
12. Laue, T. M., Senear, D. F., Eaton, S. F. and Ross, J. B. A. (1992). *Analytical Ultracentrifugation in Biochemistry and Polymer Science*, Royal Society of Chemistry, Cambridge, pp. 90-125.

13. Kim, R., Sandler, J., Goldman, S., Yokota, H., Clarke, A. J. and Kim, S. H. (1998). *Biochem. J.* **330**, 295-302.

14. Christendat, D., Saridakis, V., Dharamsi, A., Bochkarev, A., Pai, F. E., Arrowsmith, H. C. and Edwards, M. A. (2000). *J. Biol. Chem.* **275**, 24608-24612.

15. Christendat, D., Yee, A., Dharamsi,A., Kluger, Y., Savchenko, A., Cort, J. R., Booth, V., Mackereth, C. D., Saridakis, V., Ekiel, I., Kozlov, G., Maxwell, K. L., Wu, N., McIntosh, L. P., Gehring, K., Kennedy, M. A., Davidson, A. R., Pai, E. F., Gerstein, M., Edwards, A. M., and Arrowsmith C. H. (2000). *Nature Structural Biology 7*, 903-909.

16. Laue, T (1995). *Meth. Enzym.* **259**, 427-452.

17. Robertson, J. G. (1995). *Biochemistry* **34**, 7533-7541.

18. Cole. J. L (1996). *Biochemistry* **35**, 15601-15610.

19. Correia, J. J., Gilbert, S. P., Moyer, M. L. and Johnson, K. A. (1995). *Biochemistry* **34**, 4898-4907.

20. Deckert, G., Warren, P. V., Gaasterland, T., Young, W. G., Lenox, A. L., Graham, D. E., Overbeek, R., Snead, M. A., Keller, M., Aujay, M., Huber, R., Feldman, R. A., Short, J. M., Olsen, G. J. and Swanson, R. V. (1998). *Nature 392*, 353-358.

21. Turnbull, J., and Morrison J.F. (1990). *Biochemistry 29*, 10255-10261.

22. Hudson, G. S, Howlett, G. J and Davidson, B. E. (1983). *J. Biol. Chem.* **258**, 3114-3120.

23. Purcarea, C., Martin, P., Vickrey, J. F., Guy, H. I., Edwards. B. F. and Evans, D. R. (2002). *Acta. Crystallogr. D. Biol. Crystallogr.* **58**, 154-156.

24. Mathews, K. C. and van Holde, E. K. (1990). Biochemistry, *First edition.* The Benjamin/Cummings Publishing Company Inc. pp. 368-399.

25. Creighton, E. T. (1993). Proteins: Structure and Molecular Properties (2nd edition). W. H. Freeman and Company, New York. p. 124.

26. Jaenicke, R. (1997). BioProt Network. Institut für Biophysik und Physikalische Biochemie, Universität Regensburg, Regensburg, Germany. (http://www.protein.bio.msu.su/biokhimiya/contents/v63/full/63030370.htm)

27. Field, P. A. and Somero, G. N. (1998). *Proc. Natl. Aca. Sci.USA* **95**, 11476-11481.

28. Parry, J. R. and Li, W. (1997) *J. Biol. Chem.* **37**, 23303-23311.

29. Krautwald, S. and Baccarini, M. (1993). *Biochem. Biophys. Res. Commun.* **192**, 720-727.

30. Patel, D., Frelinger, J., Goudsmit, J. and Kim, B. (2001). *Biotechniques.* **31**, 1194, 1196, 1198 passim.

31. Hefti, M. H., Van Vugt-Van der Toorn, C. J, Dixon, R. and Vervoort, J. (2001). *Anal. Biochem.* **295**, 180-185.

32. Manfra, D. J., Baum, C. L., Reschley, E., Lundell, D., Zavodny, P. and Dalie, B. (1995). *Protein. Expr. Purif.* **2**, 196-205.

33. Liu, D. R., Cload, S. T., Pastor, R. M., and Schultz, P. G. (1996). *J. Am. Chem. Soc. 118*, 1789-1790.

34. Neidhart, (1996). *Escherichia coli and Salmonella, Cellular and Molecular Biology, Second edition.* ASM press, Washington, DC. pp. 938-950.

35. Morty, R. E., Authie, E., Troeberg, L., Lonsdale-Eccles, J. D. and Coetzer, T. H. (1999). *Mol. Biochem. Parasitol.* **102**, 145-155.

36. Gordon, S. R. and DeMoss, J. (1999). *Exp. Cell Res.* **246**, 233-242.

37. Blankenvoorde, M. F., van't Hof, W., Walgreen-Weterings, E., van Steenbergen, T. J., Brand, H. S., Veerman, E. C. and Nieuw Amerongen, A. V. (1998). *J. Biol. Chem.* **379**, 1371-1375.

38. Sei, C., Toneff, T., Aaron, W. and Hook, V. (2002). *Peptides.* **23**, 1409.

39. Coyne, C. P., Willetto, C. and Fenwick, B. W. (1999). *Shock* **11**, 19-28.

40. Kido, H., Takeda, M., Wakabayashi, H., Tanaka, S., Nishimura, N., Takenaka, M. and Okada, M. (1993). *Gerontology.* **39**, 30-37.

41. Muszynska, A., Palka, J. and Gorodkiewicz, E. (2000). *Exp. Toxicol. Pathol.* **52**, 149-155.

42. Voellmy, R. W. and Goldberg, A. C. (1981). *Nature.* **290**, 419-421.

43. Hwang, B. J., Woo, K. M. Goldberg, A. L. and Chung C. H. (1988). *J. Biol. Chem.* **263**, 8727-8734.

44. Woo, K. M., Chung, W. J., Ha, D. B., Goldberg, A. C. and Chung, C. H. (1989). *J. Biol. Chem.* **264**, 2088-2091.

45. Donald L. J., Chernushevich, I. V., Zhou, J., Verentchikov, A., Poppe-schriemer, N., Hosfield, J. D., Westmore, B. J., Ens, W., Duckworth, W. H. and Standing G. K. (1996). *Protein Science.* **5**, 1613-1624.

46. Sugimura, K. and Nishihara, T. (1988). *J. Bacteriol.* **170**, 5625-5632.

47. Duewel, S. H., Sheflyan, G-Y. and Woodard, W., R. (1998). *Biochem. Biophys Res. Commun.* **263**, 346-351.

48. Martemyanov, A. K., Liljas A. and Gudkov T. A. (2000). *Protein Expression Purific.* **18**, 257-261.

CHAPTER 3

Steady-State Kinetics and Inhibition of *A. aeolicus* Prephenate Dehydrogenase by L-Tyrosine

3.0 INTRODUCTION

In different microorganisms a multiplicity of control patterns have been shown to exist within the branched pathway for aromatic amino acid biosynthesis (1, 2) Tyrosine, phenylalanine, and tryptophan are the important controlling effectors of the enzyme in this pathway in many species (3); in others the branch point metabolites, prephenic acid and chorismic acid, result in feedback inhibition of the activity of the first enzyme in the pathway (4, 5).

Kinetic studies on *E. coli* CM-PD have indicated that tyrosine, the end-product of this pathway, modulates both CM and PD activities (6-9). However, the dehydrogenase reaction is significantly more sensitive to the effects of tyrosine than the mutase reaction, even in the presence of NAD^+ which is reported to enhance the binding of tyrosine to the enzyme (10, 11). Previous steady-state kinetic studies on the dehydrogenase over a range of lower prephenate and NAD^+ concentrations show that the enzyme exhibits positive cooperativity in the interaction of both substrates of the active sites of dimer CM-PD (7, 8, 11). Tyrosine enhances this cooperativity. Hence PD acts as an allosteric enzyme that is subject to feedback inhibition by tyrosine. Surprisingly, no cooperative effects in the binding of chorismate or tyrosine to CM have been observed. Tyrosine has been shown to act as a linear hyperbolic non-competitive inhibitor with respect to chorismate in the mutase reaction suggesting that both chorismate and tyrosine can reside on the enzyme at same time although its reaction rate is markedly reduced when tyrosine is bound (9).

Given that tyrosine bears a close structural resemblance to both prephenate and hydroxyphenylpyruvate, it has been suggested that tyrosine competes with prephenate for binding to the active site (7, 8). However, others propose that tyrosine elicits it inhibitory effects by interacting at a separate allosteric site (9). Most inhibition studies performed on the bifunctional enzyme from *E. coli* (7, 8), *Erwinea herbicola* (12) and on the monofunctional *Bacillus subtilis* PD (13) yield kinetics consistent with tyrosine acting as a competitive inhibitor with respect to prephenate. Nevertheless, some studies on the *E. coli* enzyme have show non-competitive kinetic patterns (8, 9). Furthermore, it is reported that the tyrosine analogue aerogenate is a poor substrate for the PD reaction offering support for a separate allosteric site (9).

The mechanism of allosteric inhibition by tyrosine has received considerable attention but is still under debate. Two models have been proposed on the basis of kinetic and thermodynamic studies on the *E. coli* enzyme. Hudson *et al.* (7) have proposed that the enzyme exists in solution as an equilibrium mixture of active (dimeric) and inactive (tetrameric) forms, with L-tyrosine (and NAD^+) binding preferentially to the tetramer (9). By contrast, Christopherson (8) and Turnbull *et al.* (9) proposed that there were no quaternary structural changes but rather concluded that tyrosine, like prephenate, underwent cooperative interaction by which the binding of tyrosine on one subunit of the dimer affected the binding of tyrosine to the second subunit. The salient difference between the two models is that Christopherson suggests tyrosine competes with prephenate at its binding site whereas Turnbull *et al.* have proposed a separate allosteric site to which prephenate can also bind.

PD from *A. aeolicus* has never been characterized. The purpose of this chapter is to report the preliminary kinetic parameters of the reaction in the presence of NAD^+, prephenate and tyrosine, and to compare its kinetic behaviour with that of *E. coli* CM-PD. In addition, a rapid HPLC assay was developed to identify any structural changes associated with tyrosine binding to *E. coli* CM-PD and *A. aeolicus* PD.

3.1 EXPERIMENTAL PROCEDURES

3.1.1 Preparation of Substrates and Substrate Analogues

Prephenate and NAD^+ (Grade I) were prepared as ice cold stock solutions of 40 mM and 135 mM, respectively, in 50 mM HEPES with the pH adjusted to 7.5. Unless otherwise indicated, solutions were serially diluted in water to maintain a constant volume of 30 µl each of NAD^+ and prephenate over all substrate concentrations used in the assays. L-Tyrosine (ICN) was prepared as a stock solution of 2.22 mM in water. Grade III NAD^+ (free acid) was obtained from Fischer Scientific Inc.

3.1.2 Source of Enzymes

Purified thrombin-treated and heterodimeric PD from *A. aeolicus* were prepared as described in sections 2.1.6 and 2.1.7, respectively, and stored at 4 °C in storage buffer. Unless otherwise specified, results were obtained in this chapter using thrombin-cleaved PD. *E. coli* CM-PD (~30 U/mg) was prepared by K. Mekhssian and stored at –86 °C at a concentration > 2 mg/ml in 0.1 M N-ethylmorpholine (pH 7.5), 1 mM EDTA, 20% (v/v) glycerol, 5 mM DTT.

3.1.3 Activity Assays to Determine Kinetic Constants

Reactions in the absence of modulators were performed at 55 °C by diluting 2 X **Rxn buffer** (100 mM HEPES, 300 mM NaCl, pH 7.5) with 430 µl of water, 30 µl each of NAD^+ and prephenate at varying concentrations, and either 10 µl (19.5 µg total) of thrombin-cleaved or heterodimeric *A. aeolicus* for a total reaction volume of 1.0 ml. The assays were performed in 1 ml quartz cuvettes as follows: First, 2 X Rxn buffer and water

were equilibrated together at 55 °C for 2 min. Second, the appropriate enzyme and the fixed substrate (held at a saturating level) were added and the solution was incubated for 30 s at 55 °C. Third, the reaction was initiated with the addition of the variable substrate. At each step, components were rapidly mixed by inversion of the cuvette. Dehydrogenase activity was monitored as described in section 2.1.11. Initial velocity studies were conducted by varying one substrate at concentrations below to above its K_m value while keeping the second substrate fixed at a saturating level. Hence, reactions were performed using 9 concentrations of prephenate while holding NAD^+ constant at 2 mM. Similarly, 6-11 different concentrations of NAD^+ were used while keeping prephenate constant at 1 mM. Values of K_m and k_{cat} were obtained by fitting the data to the Michaelis-Menten equation by Grafit Software version 5.0 using non-linear least squares analysis. Turnover numbers were calculated using subunit molecular weights of 35.13 kDa for thrombin-cleaved PD, and 36.07 kDa for heterodimeric PD.

3.1.4 Activity Assays in the Presence of Modulators

The effect of L-tyrosine on the initial velocity of purified thrombin-cleaved PD was determined at 7 concentrations of tyrosine (0.01-1.0 μM) in the presence of 2 mM NAD^+ and 0.4 mM or 0.6 mM prephenate. Assays were performed at 55 °C as described in sections 3.1.2 but with tyrosine (at various concentrations) replacing water.

Kinetics were also performed at a fixed concentration of tyrosine (0.5 mM) and NAD^+ (either 1 mM, 2 mM or 4 mM), while varying prephenate from 0.10-1.0 mM. Assays were performed at 55 °C as outlined in section 3.1.2, but with 12 μg of PD. Initial

velocity data were plotted graphically in double reciprocal form using Microsoft Excel 2000 to observe any departures from linearity.

The effect of NaCl on the PD activity was monitored using 10 solutions of 2X Rxn buffer containing increasing concentrations of salt (0.1-3.0 M). The pH of each buffer was checked and adjusted to pH 7.5 with NaOH if necessary. Reactions were performed at 55 °C as described in section 3.1.2, but with both substrates added in the second step at fixed concentrations of 4 mM NAD^+ and 1 mM prephenate. The reaction was initiated with 10 μg of PD.

3.1.5 Assays to Monitor the Temperature Thermal Dependence of PD Activity

3.1.5.1 Thermal Activation

Activity of *A. aeolicus* PD was monitored between 30 °C and 95 °C. Reactions were performed as described in section 3.1.2 except in step two, 13.5 μg of enzyme and 4 mM NAD^+ were used with an equilibration of 15 s instead of 30 s prior to initiation of the reaction with 1 mM prephenate. These modifications were employed to minimize thermal decomposition of the substrates at the higher temperatures and to ensure that their levels were saturating.

3.1.5.2 Thermal Stability

Ten 1.5 ml Eppendorf tubes each containing 20 μl aliquots of PD (57 μg) were incubated at 95 °C in a water bath. At various time intervals one sample was removed, and centrifuged at 16,000 x *g* for 10 min at 4 °C. Dehydrogenase activity was

determined for 10 µl of the sample as outlined in section 3.1.2., but using fixed substrate concentrations of 2 mM NAD^+ and 1 mM prephenate. Protein concentration of the samples were also determined after centrifugation in order to calculate specific activities.

3.1.6 Determination of Native Molecular Weight in the Presence and Absence of Ligands

High performance liquid chromatography (HPLC) was used to follow quaternary structural changes in *A. aeolicus* PD (both thrombin-cleaved and heterodimeric forms) and *E. coli* CM-PD in the presence of NAD^+ and L-tyrosine at room temperature. A Waters HPLC equipped with a Waters 996 diode array detector or a Hewlett Packard (HP) 1050 HPLC with a HP 1050 autosampler, HP UV 79853 detector and a HP 35900-C interface, was used. The apparatus was fitted with a normal-phase chromatographic BioRad Bio-Silect sec 250-5 column (300 x 7.8 mm, metal free) or a Phenomenex Bio Sep-S 3000 (300 x 7.5 mm, metal free) with a guard column in series, operating at a flow rate of 1 ml/min. Samples of 0.2 mg of protein were introduced in 100 µl injections at rate of 100 µl/min through a 100 µl sample loop. Isocratic elution was employed using a mobile phase (pH 7.5) consisting of 50 mM HEPES, 150 mM NaCl, 1.0 mM NAD^+ and 0.5 mM or 1 mM tyrosine. Control experiments without NAD^+ and tyrosine in the mobile phase were also run using the same amount of protein. Protein elution was monitored at 290 nm (see below). Bio-Rad gel filtration protein standards (range of 1.35-670 kDa) were resolved in both mobile phases in order to follow changes in retention time associated with the presence of NAD^+ and tyrosine in the mobile phase. A standard

curve was generated using these proteins to correlate retention time with native molecular weight. All buffers were filtered and samples were centrifuged prior to use.

The absorption minima for NAD^+, L-tyrosine and protein were determined between 220 nm and 310 nm using a double-beam spectrophotometer (GBC UV/VIS model 918) in 1 cm quartz cuvettes. Scans were performed on filtered buffers containing 50 mM HEPES, 150 mM NaCl (pH 7.5) with either 0.5 mM Grade III NAD^+ or 1 mM L-tyrosine, or a protein solution of 0.5 mg/ml *E. coli* CM-PD in 50 mM HEPES (pH 7.5), 100 mM NaCl, 10% glycerol, 1mM DTT. Data analysis was performed using Microsoft Excel 2000. From these tracings a detection wavelength of 290 nm was chosen for the HPLC experiments.

3.2 RESULTS

3.2.1 The Effect of Salt and Temperature on *A. aeolicus* PD Activity

The effect of varying NaCl from 50 mM to 1500 mM on the specific activity of thrombin-cleaved PD is presented in Figure 1 and illustrated that enzyme activity was very dependent on the ionic strength of the medium. Maximal activity was observed between 100 mM and 200 mM NaCl but dropped off to 25% residual activity by 1500 mM NaCl. Furthermore, specific activity decreased slightly at 50 mM NaCl. At concentrations below this, the protein rapidly precipitated precluding accurate activity measurements. Hence, NaCl at a concentration of 150 mM was included in all kinetic assays. Our findings are in keeping with those of D. Christendat (personal communication) who noted that purified recombinant proteins from the thermophilic bacterium *Methanobacterium thermoautotrophicum* remained soluble only if salt was included in the storage buffer.

The specific activity of *A. aeolicus* PD is also temperature dependent. Specific activity recorded from 30 °C and 95 °C increased in a sigmoidal fashion reaching a plateau by 90-95 °C (Figure 2). This profile is in contrast to a more bell-shaped dependence as exhibited by many mesophilic proteins (14-16). The specific activity of the enzyme at 95 °C (36.6 U/mg) was 33-fold higher than the activity measured at 30 °C (1.1 U/mg). A similar temperature dependence was reported for recombinant KdsA (3-deoxy-D-*manno*-octulosonic acid 8-phosphate synthase) from *A. aeolicus*, where a 54-fold increase in specific activity was observed between 30 °C and 95 °C (17). A temperature of 55 °C was arbitrarily selected for most of our kinetic studies as at this temperature initial

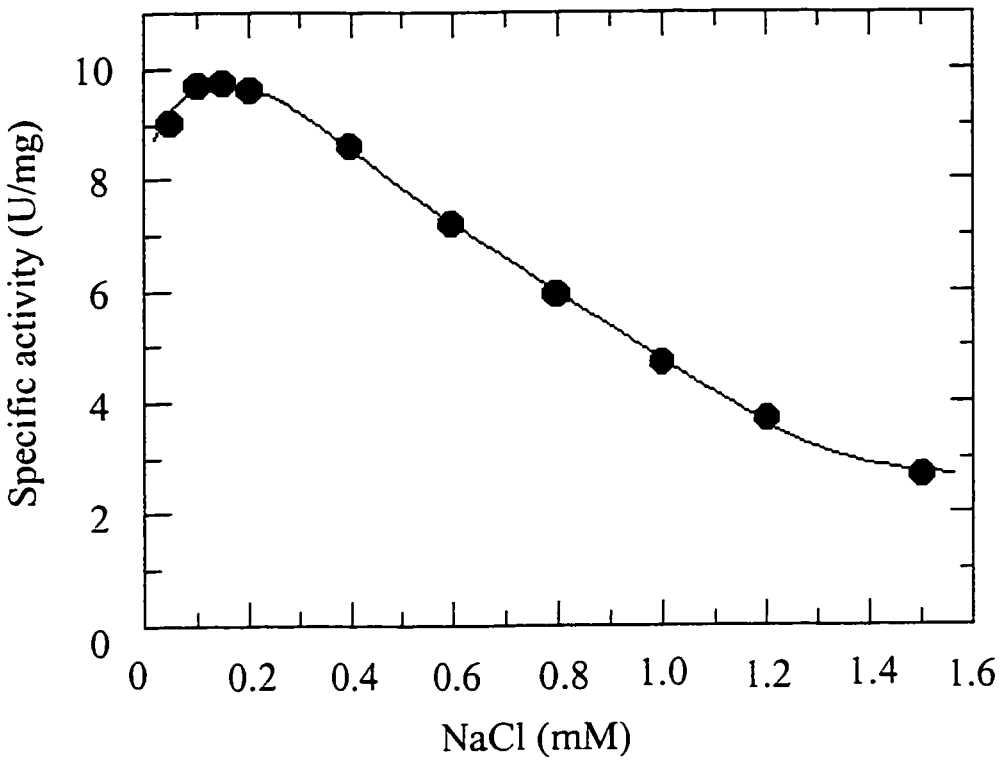

Figure 1. The effect of NaCl on dehydrogenase specific activity. Experiments were carried out at 55 °C using 9.75 μg/ml PD at increasing NaCl concentrations.

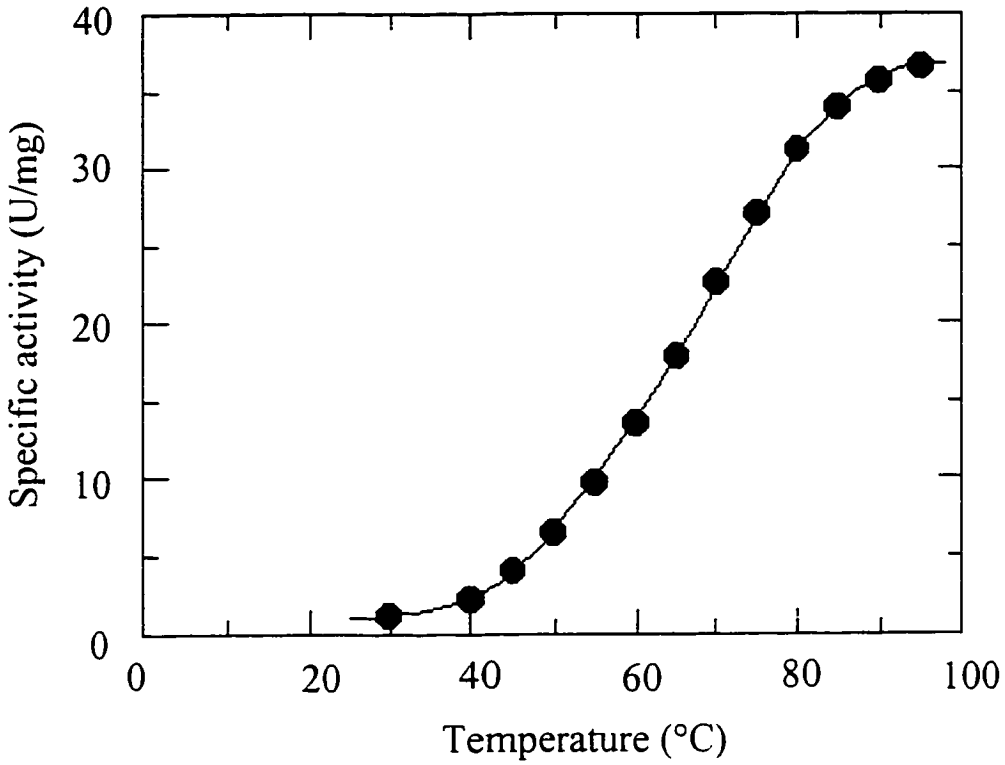

Figure 2. Determination of optimum temperature of PD activity. Assays were performed at the indicated temperatures in the presence of 1 mM prephenate and 4 mM NAD^+, using 13.5 μg/ml of enzyme.

velocities were easily recorded without requiring the addition of excessive amounts of catalyst and the thermal decomposition of substrates was minimal.

Our kinetic studies suggested that *A. aeolicus* PD is most active at or above 95°C. To investigate the stability of PD at or near its temperature optimum, the enzyme was incubated for 13 h at 95 °C while monitoring dehydrogenase activity at 55 °C and soluble protein content at various time intervals (Figure 3). Specific activity of PD decreased exponentially with time yielding a half-life ($t_{1/2}$) of ~ 3 h. This value is in the range reported for other *A. aeolicus* proteins such as KdsA, $t_{1/2}$ 1.5 h (17), and glucose-6-phosphate dehydrogenase, $t_{1/2}$ 15 h (18).

3.2.2 Kinetic Parameters of *A. aeolicus* PD

Substrate saturation curves (Figure 4) were constructed for both the thrombin-cleaved (A. B) and heterodimeric forms (C, D) of *A. aeolicus* PD at 55 °C. Initial velocities were recorded with prephenate (A, C) or NAD^+ (B, D) as the variable substrate. The fixed substrate in each reaction was maintained at or near a saturating level. The reactions catalyzed by both enzymes followed hyperbolic kinetics over this substrate concentration range. Fitting the data to the Michaelis-Menten equation yielded the kinetic parameters listed in Table 1 and are shown with the values previously reported for the dehydrogenase activity of *E. coli* CM-PD at 30 °C (19). Compared to the *E. coli* enzyme, *A. aeolicus* PD has a lower k_{cat} value and slightly higher K_m values for both prephenate and NAD^+. The differences in values between the two enzymes may, in part, be due to the temperature at which the assays were performed; 30 °C is near the temperature optimum

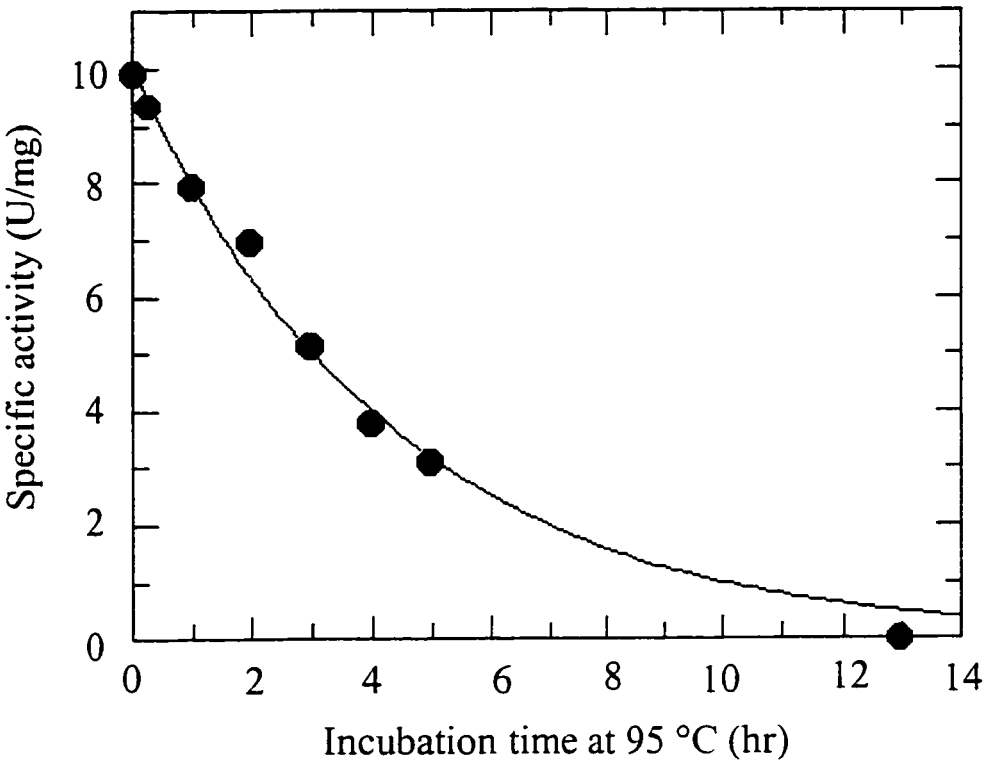

Figure 3. Thermal stability of PD activity. Ten samples of 30 µl of enzyme (2.85 mg/ml) in storage buffer (pH 7.5) were incubated at 95 °C. At various time intervals, a sample was removed and assayed for residual activity and protein concentration. The half-life was determined by fitting the data to a single exponential using Grafit 5.0.

Figures 4A-D. Variation of reaction velocity with substrate concentration for *A. aeolicus* PD at 55 °C. Curves were generated by fitting the data to the Michaelis-Menten equation using Grafit 5.0.

Figures 4A and 4B. Reactions were performed using thrombin-cleaved PD in the presence of 2 mM NAD^+ while varying prephenate (A), and in the presence of 1 mM prephenate while varying NAD^+ (B).

Figures 4C and 4D. Reactions were performed using heterodimer PD in the presence of 2 mM NAD^+ while varying prephenate (C), and in the presence of 1 mM prephenate while varying NAD^+ (D).

***A. Aeolicus* PD (thrombin-treated)**

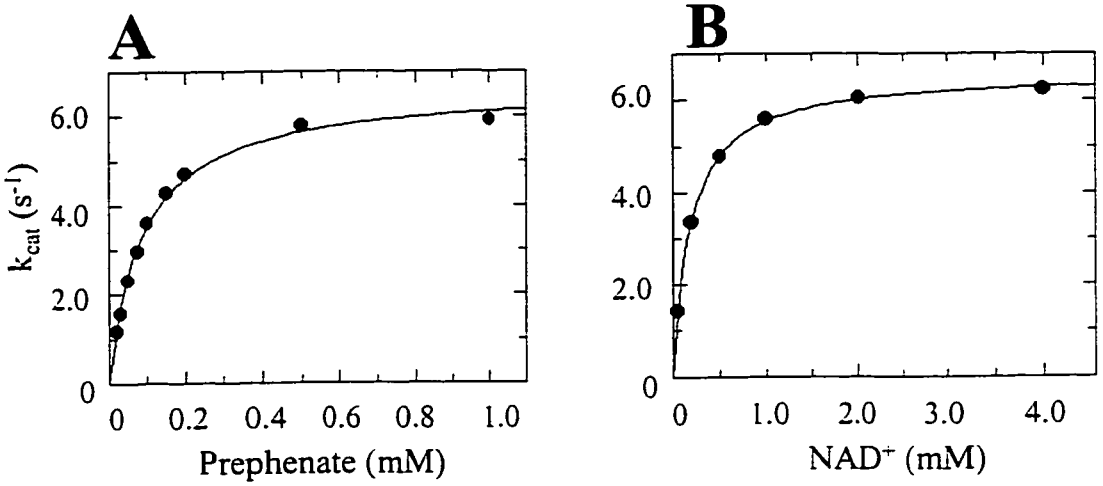

***A. Aeolicus* PD (heterodimer)**

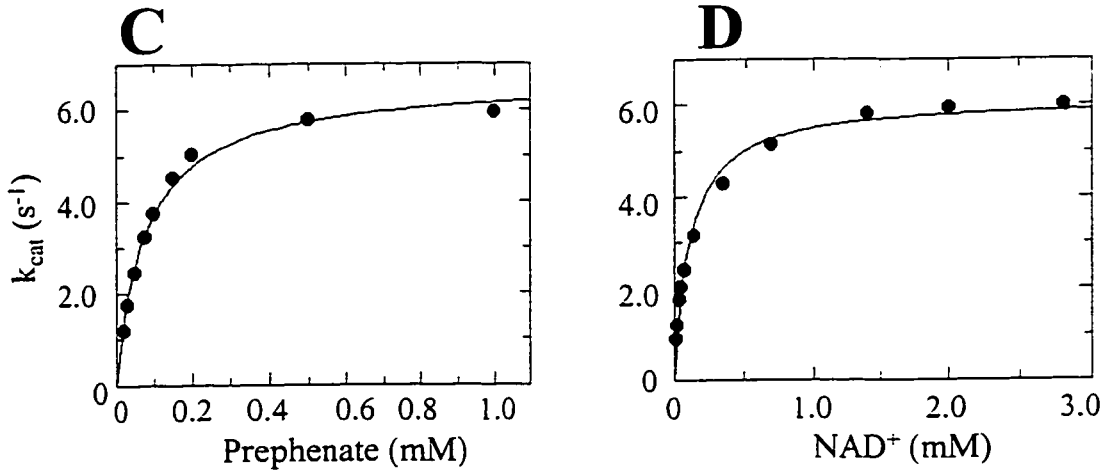

Table 1. Kinetic Parameters for *A. aeolicus* PD

	Prephenate			NAD^+		
	K_m (μM)	k_{cat} (s^{-1})	k_{cat}/K_m ($M^{-1}s^{-1}$)	K_m (μM)	k_{cat} (s^{-1})	k_{cat}/K_m ($M^{-1}s^{-1}$)
Thrombin-cleaved PD[1]	90 ± 5	6.7 ± 0.5	7.4×10^4	185 ± 4	6.6 ± 0.5	3.7×10^4
Heterodimeric PD[1]	84 ± 5	6.7 ± 0.5	7.9×10^4	112 ± 4	6.1 ± 0.5	5.4×10^4
***E. coli* CM-PD**[2,a]	44 ± 8	27 ± 1	6.2×10^5	103 ± 11	27 ± 1	2.6×10^5

[1]Kinetics performed at 55°C

[2]Kinetics performed at 30°C

[a]Christendat *et al.* (19).

of *E. coli* CM-PD (20) while 55 °C is well below optimum for *A. aeolicus* PD. Duewel *et al.* (17) reported a 5-fold increase in k_{cat} and a 2-fold decrease in the K_m for phospho*enol*pyruvate for *A. aeolicus* KdsA, when comparing the results from assays conducted at 90 °C versus 60 °C. In contrast, Subramaniam *et al.* (21) noted an average 2-fold increase in K_m for all substrates and a 3-fold increase in specific activity between 25 °C and 45 °C for the reaction catalyzed by cellobiose dehydrogenase from the thermophilic bacterium *Sporotrichum thermophile.* Kinetic studies on other proteins originating from other (hyper)thermophilic organisms (22, 23) reported similar fluctuation in K_m and k_{cat} when determined over a range of temperatures.

3.2.3 Inhibition of *A. aeolicus* PD Activity by Tyrosine

Inhibition studies were performed at 55 °C using varying amounts of L-tyrosine (0-1.0 mM) at fixed concentrations of prephenate and NAD^+ (Figure 5). In the presence of 0.4 mM prephenate (~ 4 x K_m), 2 mM NAD^+ (~10 x K_m) and 0.8 mM tyrosine, *A. aeolicus* PD was inhibited by ~50% compared to the specific activity in the absence of tyrosine. In contrast, PD activity of *E. coli* CM-PD was reportedly inhibited to > 90% when assayed at 30 °C in the presence of 0.8 mM tyrosine and similar ratios of substrate concentration to K_m (11, 24). Hudson *et al.* (7) reported that the binding of tyrosine to *E. coli* CM-PD is enhanced by NAD^+ and vice-versa. However, doubling the concentration of NAD^+ to 4 mM did not result in an increase in the percent inhibition by tyrosine (data not shown). This indicated that the marked difference in the results for *E. coli* and *A. aeolicus* PD was not due to limiting NAD^+. Figure 5 also shows that inhibition by

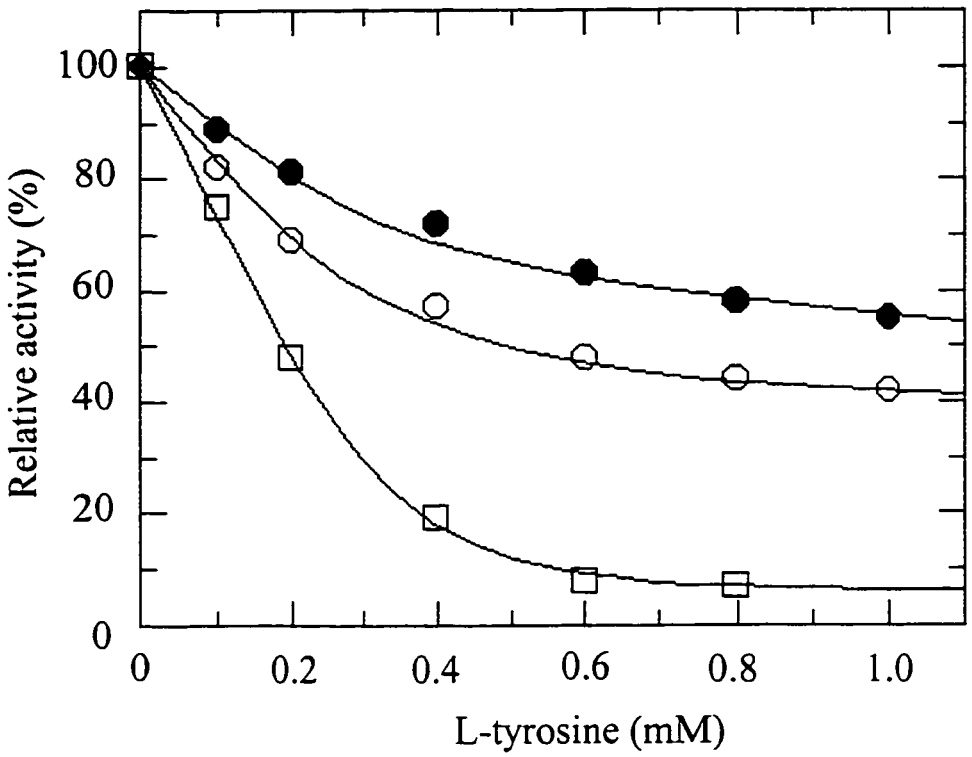

Figure 5. Inhibition of PD activity of *A. aeolicus* PD (circles) and *E. coli* CM-PD (squares) by L-tyrosine. Reactions with *A. aeolicus* PD were performed at 55 °C using 400 μM prephenate (~4X K_m^{PRE}) (filled circles) and 600 μM prephenate (empty circles). Data for *E. coli* CM-PD was taken from Turnbull *et al.* (11), from assays conducted at 30 °C in the presence of 160 μM prephenate (~4X K_m^{PRE}) (squares) and fit to a single exponential decay. NAD^+ was fixed at 2 mM in all reactions.

tyrosine is dependent on the concentration of prephenate used in the assay. Increasing prephenate from 0.4 mM to 0.6 mM reduced tyrosine inhibition by ~10%.

Inhibition of the PD reaction by tyrosine was also examined with prephenate as the variable substrate at fixed concentration of NAD^+ of 1 mM, 2 mM and 4 mM (Figure 6). In the presence of 0.5 mM L-tyrosine double reciprocal plots were concave upward. Deviations from linearity were more pronounced at the higher concentrations of NAD^+ and lowest concentrations of prephenate. Similar results have also been reported for PD of *E. coli* CM-PD by Turnbull *et al.*(9), Hudson *et al.* (7) and Christopherson (8).

3.2.4 Structural Changes Associated with Inhibition by L-Tyrosine

To determine if inhibition by tyrosine is accompanied by changes in quaternary structure, a size exclusion-based HPLC assay was developed using two different mobile phases: one where the mobile phase was free of ligands, and the other incorporated L-tyrosine and NAD^+. Aqueous buffered solvents were used to facilitate separation of native protein. This assay was performed on *E. coli* CM-PD (Figure 7) as well as the thrombin-cleaved and heterodimeric forms of *A. aeolicus* PD (Figure 8).

Figure 7A-C shows the chromatographic separation of protein standards in the absence of ligands (A) and *E. coli* CM-PD in the absence (B) and presence (C) of 0.5 mM L-tyrosine and 1 mM NAD^+. Protein standards were well separated, resulting in a linear relationship between molecular weight and retention times (inset D). An identical separation was obtained for the protein standards in the presence of NAD^+ and tyrosine (data not shown).

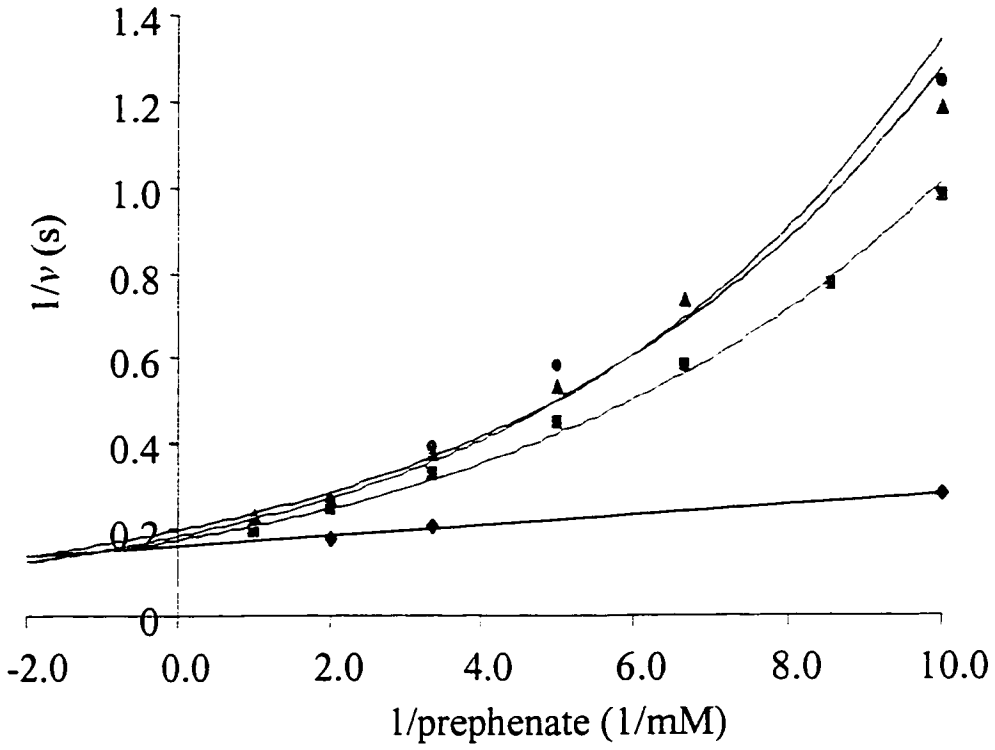

Figure 6. Double-reciprocal plots showing the inhibition of PD by L-tyrosine. 0.5 mM L-tyrosine in the presence of 1 mM NAD^+ (square), 2 mM NAD^+ (triangles) and 4 mM NAD^+ (circles) at varying prephenate concentrations. PD activity in the absence of L-tyrosine (diamonds) was also monitored in the presence of 2 mM NAD^+.

CM-PD eluted as a single peak under the two assay conditions consistent with homogeneous samples. However, the elution was faster in the presence of ligands (C) than in their absence (B). Table 2 summarizes the retention times and corresponding molecular weights calculated from the standard curve. The MW of native CM-PD predicted from its primary sequence is 84,084. Hence, the data are consistent with *E. coli* CM-PD migrating as a dimer in the absence of ligands and as a tetramer in the presence of 1 mM NAD^+ and 0.5 mM L-tyrosine.

Similarly, Figure 8A-C shows the chromatographic separation of protein standards (A) and the effect of 1 mM NAD^+ and 1 mM L-tyrosine on the elution of *A. aeolicus* thrombin-cleaved PD (C) compared to in the absence of ligands (B). The elution pattern of the heterodimer were identical to that of the thrombin-cleaved PD (data not shown). The retention times and calculated molecular weight values are tabulated in Table 2. In contrast to the *E. coli* enzyme, native *A. aeolicus* PD did not appear to migrate as a dimer since the MW of the enzyme determined experimentally did not match the predicted value of 70,260. Furthermore, *A. aeolicus* did not undergo a shift in retention time consistent with tetramerization even in the presence of a higher concentration of tyrosine (1 mM versus 0.5 mM) (data not shown). The results are more consistent with small tertiary structural changes in protein structure.

Figures 7A-D. Chromatographic separation of protein standards (A); *E. coli* CM-PD (B); and *E. coli* CM-PD in the presence of tyrosine and NAD^+ (C). Protein standard M.W. and their respective retention times were used to generate a calibration curve (D), to estimate *E. coli* CM-PD M.W.

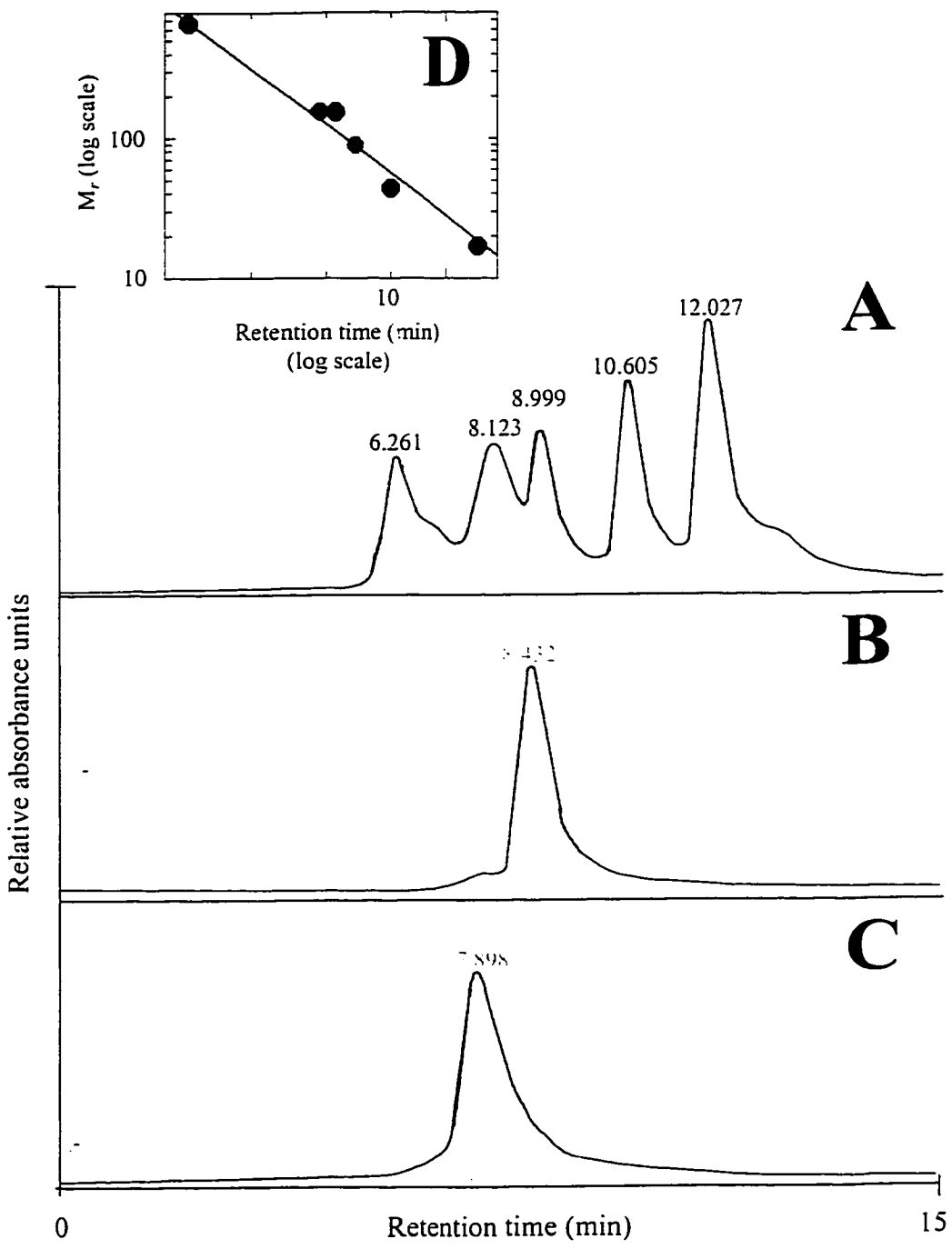
D
M_r (log scale)
100
10
10
Retention time (min)
(log scale)
A
12.027
10.605
8.999
8.123
6.261
B
C
Relative absorbance units
0
Retention time (min)
15

Figures 8A-D. Chromatographic separation of protein standards (A); *A. aeolicus* PD (B); and *A. aeolicus* PD in the presence of tyrosine and NAD^+ (C). Protein standard M.W. and their respective retention times were used to generate a calibration curve (D), to estimate *A. aeolicus* PD M.W.

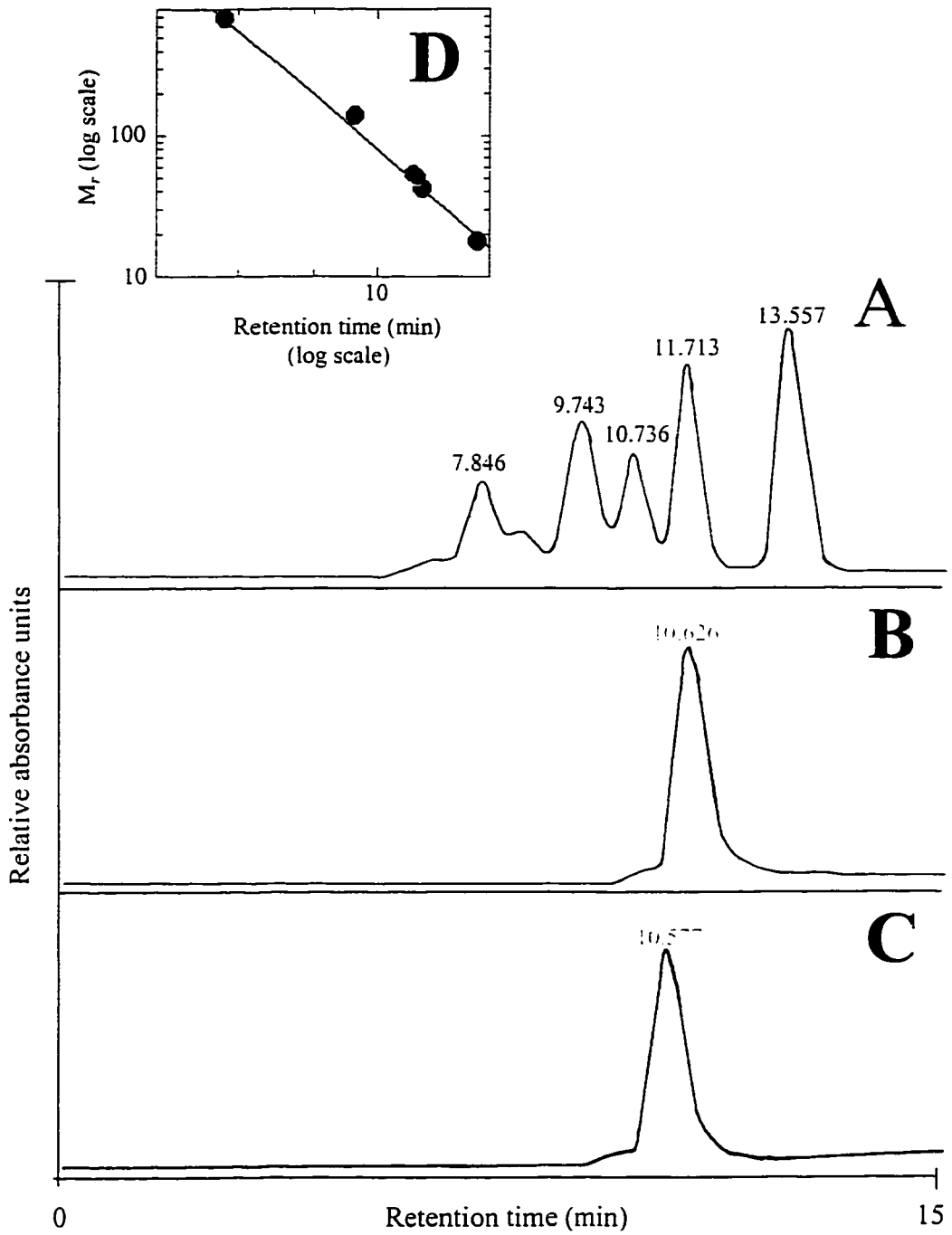
D
M_r (log scale)
100
10
10
Retention time (min)
(log scale)
A
13.557
11.713
9.743
10.736
7.846
B
C
Relative absorbance units
0
Retention time (min)
15

Table 2: Retention Time and Estimated M.W. from Gel Filtration Studies

	In the absence of ligands		In the presence of L-tyrosine and NAD^+	
	Retention time (min)	Estimated M.W. (kDa)	Retention time (min)	Estimated M.W. (kDa)
E. coli CM-PD	8.432	89.8 ± 1.9	7.898	159.0 ± 3.3
A. aeolicus PD	10.626	52.2 ± 0.7	10.577	54.7 ± 0.8

3.3 DISCUSSION

The results presented in this chapter provide further evidence that recombinant PD from *A. aeolicus* retains structural and functional features consistent with those predicted for the native hyperthermophilic prephenate dehydrogenase. Protein overexpressed and purified as described in Chapter 2 possessed exceptional thermostability enhanced specific activity at higher temperature, saturation kinetics with NAD^+ and prephenate, and sensitivity to the end product L-tyrosine. Furthermore, the kinetic parameters were not perturbed by the addition of a hexa-His tag and thrombin cleavage site at the N-terminus of the protein.

Features which distinguish thermophilic enzymes from their mesophilic counterparts are that they are more resistant to heat denaturation and exhibit low activity at ambient temperatures and higher activity at higher temperatures (22). *A. aeolicus* PD fulfills these criteria as its maximal activity is achieved at 95 °C, representing a 33-fold increase in specific activity relative to that at 30 °C (Figure 2), and its $t_{1/2}$ at 95 °C is ~ 3 h (Figure 3). These values clearly contrast with the temperature optimum of 37 °C reported for recombinant *E. coli* CM-PD (25) and partially purified monofunctional *B. subtilis* PD (13), and a $t_{1/2}$ of 8 min at 45 °C exhibited by CM-PD from *E. herbicola* (12). Unfortunately, there are very few temperature inactivation studies performed on *any* monofunctional PD's to provide an adequate comparison between thermophilic and mesophilic forms of the enzyme.

The kinetic parameters for the reaction catalyzed by *A. aeolicus* PD were determined at 55 °C by varying one substrate above and below its K_m value keeping the other substrate at a saturating level. The resulting hyperbolic saturation curves and Michaelis constants obtained for NAD^+ and prephenate compared favourable with those of PD from *E. coli* CM-PD (Table 1) assayed at 30 °C. Furthermore, extrapolation of the activity of *A. aeolicus* PD at its temperature optimum (assuming that the affinity for substrates does not vary with temperature) yields similar turnover numbers for the two enzymes. Substrate concentrations used in the present study (½ x K_m – 11 x K_m) were not low enough to observe concave upwards double reciprocal plots which has been reported for *E. coli* CM-PD in the absence of tyrosine and indicative of positive cooperativity in the binding of substrates (7, 8, 11).

End-product inhibition of PD provides major regulatory control in the pathway of tyrosine biosynthesis (11, 13). Although the transamination reaction between 4-hydroxyphenylpyruvate and L-tyrosine has not been studied in *A. aeolicus*, it is assumed that the transamination is not the limiting reaction of tyrosine biosynthesis. *A. aeolicus* PD activity was inhibited by tyrosine but only by ~50 % and under conditions that afforded > 90 % inhibition for *E. coli* CM-PD (Figure 5). The pronounced sensitivity of the *E. coli* enzyme to tyrosine paralleled those findings with other mesophilic PDs that are either monofunctional *E. herbicola*, (12), *B. subtilis* (13), *S. cerevisiae* (2), and *Neurospora crassa* (26) or bifunctional CM-PD as for *Aerobacter aerogenes* (27). It may be that tyrosine cannot bind as tightly to the hyperthermophilic PD at temperatures well below the temperature required for optimum activity. In support of this, our kinetic

analysis revealed that the interaction of NAD^+ and prephenate with *A. aeolicus* PD is somewhat weaker at 55 °C than with the *E. coli* enzyme at 30 °C (Table 1). Kinetic (9) and binding studies (7) performed on *E. coli* CM-PD have determined a K_i for tyrosine binding between 1-10 μM. Similar detailed studies must be performed on *A. aeolicus* PD to quantify the extent of tyrosine inhibition and any variations with temperature.

When assayed over a range of prephenate concentrations, tyrosine not only reduced the activity of *A. aeolicus* PD but also promoted cooperativity in the binding of prephenate to the enzyme (Figure 6). This effect was magnified by increasing the NAD^+ concentration from 1 mM to 2 mM (Figure 6), and stems from the finding that NAD^+ enhances the interaction of the enzyme with tyrosine (7, 11). Similar results have also been reported in *E. coli* CM-PD (7, 8, 11). The concave upwards double reciprocal plots suggest that tyrosine acts as an allosteric inhibitor of *A. aeolicus* PD activity. However, our data do not indicate whether the combination might be at the active site or a separate allosteric site. This would require examining the initial velocity pattern obtained by varying prephenate at different concentrations of tyrosine. These types of plots reported for both *E. coli* CM-PD (8) and *B. subtilis* PD (13) have indicated that the apparent K_m for prephenate and the Hill coefficient increased significantly with increasing tyrosine concentration. Studies as described above will be extended to *A. aeolicus* PD.

To provide further insights into the quaternary structure of the *A. aeolicus* PD and the structural basis for the mechanism by which L-tyrosine inhibits *A. aeolicus* PD and *E. coli* CM-PD, a chromatographic assay using normal-phase HPLC was developed. In

particular, size exclusion chromatography was employed, which separates molecules with respect to size and shape (28). Two different mobile phases were used for isocratic elution, with one containing L-tyrosine and NAD^+. If the mechanism for allosteric inhibition results from quaternary structural changes in either PD or CM-PD, this will be reflected as a significant decrease in retention time. Furthermore, if the allosteric inhibition involves cooperative binding of L-tyrosine resulting in tertiary structural changes, this may be reflected with either a minor increase or decrease in retention time.

Results from the present study support those finding of Hudson *et al.* (7) using sedimentation equilibrium studies by AUC which indicated that the dimeric *E. coli* enzyme undergoes tetramerization in the presence of tyrosine and NAD^+. These results were also consistent with recent gel filtration studies by Ganem and collegues who have shown that the related *E. coli* mutase-dehydratase undergoes aggregation in the presence of phenylalanine (29-31). Their elegant genetic engineering studies expressing separate domains of chorismate mutase-prephenate dehydratase (CM-PDT) also indicate that the end product brought about its effects by combining at a separate phenylalanine binding site at the C-terminus of the protein. Whether this occurs with CM-PD is presently under investigation in the Turnbull lab. Given that the intracellular concentration of tyrosine and phenylalanine are in low mM quantities and that *E. coli* CM-PD and CM-PDT are probably present at concentrations approaching those used for the studies above (7, 31), implies that the tetrameric form is physiologically relevent.

In contrast to *E. coli* CM-PD, the HPLC assay showed that *A. aeolicus* PD migrates at an apparent molecular weight of 52.2 kDa, which is significantly lower than that predicted for a globular dimer. This result supports our findings by sedimentation velocity AUC (section 2.2.5) and also is consistent with our activity assays conducted at various temperatures. It may be that at ambient temperatures a significant population of the hyperthermophilic enzyme is present in an inactive state—possibly as inactive monomers in rapid self association with the active dimer. Structural analysis of hyperthermophilic proteins indicates that these proteins are generally more compact than mesophilic proteins (32, 34) and hence would migrate on a size exclusion column as a smaller protein than predicted. This observation has also been reported by Hansen *et al.* (34), where gel filtration studies on pyrophosphatase from *Sulfolobus acidocaldarius* consistently suggested a tetramer, while AUC sedimentation equilibrium revealed a hexameric structure. Either mechanism could provide a structural basis for the temperature dependent changes in activity.

The presence of tyrosine and NAD^+ at concentrations that clearly promoted aggregation of the *E. coli* enzyme, resulted in only a minor decrease in the retention time for *A. aeolicus* PD, suggesting that the protein may have undergone tertiary structural changes. Alternately, the fact that this assay was performed at room temperature may significantly reduce PDs affinity for tyrosine and in turn affect the equilibrium between tetrameric and dimeric (or monomeric) forms such that only a small percentage of the total enzyme molecules are tetramers. Further kinetic and biophysical studies performed at different

temperatures, protein concentrations and levels of tyrosine and NAD^+ are required in order to elucidate the mechanism of tyrosine inhibition.

3.4 REFERENCES

1. Doy, C. (1968). *Rev. Pure Appl. Chem.*, **18**, 41-52.
2. Lingens, F. (1968). *Angew. Chem. Int. Ed. Engl.*, **7**, 350-357.
3. Gibson, F. and Pittard, J. (1968). *Bacteriol Rev.*, **32**, 465-492.
4. Jensen, R. A. and Nester, E. W., (1965). *J. Mol. Biol.*, **12**, 468-475.
5. Jensen, R. A., Nasser, D. S. and Nester, E. W. (1967). *J. Bacteriol.*, **95**, 1582-1593.
6. Koch, G. L. E., Shaw, D. C. and Gibson F. (1971). *Biochim Biophys. Acta.* **229**, 795-804.
7. Hudson G. S., Howlett, G. J. and Davidson, B. E. (1983). *J. Biol. Chem.* **258**, 3114-3120.
8. Christopherson, R. I. (1985). *Arch Biochem Biophys.* **240**, 646-654.
9. Turnbull, J., Morrison, J. F. and Cleland, W. W. (1991). *Biochemistry* **30**, 7783-7788.
10. Turnbull, J., Cleland, W. W. and Morrison, J. F. (1990). *Biochemistry* **29**, 10245-10254.
11. Turnbull, J. and Morrison, J. F. (1990). *Biochemistry* **29**, 10255-10261.
12. Xia, T., Zhao, G., Fischer, R. S. and Jensen, R. A. (1992). *Gen Microbiol* **138**, 1309-1316.
13. Champney S. W. and Jensen A. R. (1970). *J. Biol. Chem.* **245**, 3763-3770.
14. Segel, I. H. (1993). *Enzyme Kinetics: Behavior and Analysis of Rapid Equilibrium and Steady-State Enzyme Systems* pp. 926-941.
15. Bharadwaj, G. and Maheshwari, R. (1999). *Microbiol. Lett.* **181**, 187-193.

16. Cowan, D. A., Daniel, R. M. and Morgan, H. W. (1987). *Int. J. Biochem.* **19**, 741-743.

17. Duewel, S. H., Sheflyan, G-Y. and Woodard, W., R. (1998). *Biochem. Biophys Res. Comm.* **263**, 346-351.

18. Iyer, R. B., Wang, J. and Bachas, L. G. (2002). *Extremophiles* **6**, 283-289.

19. Christendat, D. S., Saridakis, V. C. and Turnbull, J. L. (1998). *Biochemistry* **37**, 15703-15712.

20. Campbell, N. A. (1993). *Biology, third edition.* The Benjamin/Cummings Publishing Company, Inc. Redwood City, California. pp. 104.

21. Subramaniam, S. S., Nagalla R. S. and Renganathan, V. (1999). *Arch. Biochem. Biophys.* **365**, 233-230.

22. Zuber, H. and Friedman, S. M. (1978). *Biochemistry of Thermophily.* Academic Press, New York, pp267-285.

23. Lebbink, G. H. J., Knapp, S.. van der Oost, J., Rice, D., Ladenstein, R. and de Vos M. W. (1998). *J. Mol. Biol.* **280**, 287-296.

24. Lee, T. (2002). *Examination of CM-PD Inhibition by Tyrosine* (Independent Studies Project), Concordia University, Montreal, Canada.

25. Turnbull, J. (1988). *Mechanistic Studies on a Bifunctional Enzyme,* Ph. D. Australian National University.

26. Catcheside, D. E. A., (1969). *Biochem. Biophys. Res. Commun.* **36**, 651.

27. Cotton, R. G. H. and Gibson, F. (1967). *Biochim. Biophys. Acta.* **147**, 222-237.

28. Harris, C. D. (1995). *Quantitative Chemical Analysis,* 4th edition. W. H. Freeman and Company, New York. pp. 674-679.

29. Zhang, S., Pohnert, G., Kongsaeree, P., Wilson, D. B., Clardy, J. and Ganem, B. (1998). *J. Biol. Chem.* **273**, 6248-6253.

30. Zhang, S., Wilson, D. B. and Ganem, B. (2000). *Biochemistry* **39**, 4722-4728.

31. Pohnert, G., Zhang, S., Husain, A., Wilson, D. B. and Ganem, B. (1999). *Biochemistry* **38**, 12212-12217.

32. Jaenicke, R. (2000). *Proc. Nat. Acad. Sci.* **97**, 2962-2964.

33. Hudson, G. S., Wong, V. and Davidson, B. E. (1984). *Biochemistry* **23**, 6240-6249.

34. Hansen, T., Urbanke, C., Leppanen, V. M., Goldman, A., Brandenburg, K. and Schafer, G. (1999). *Arch. Biochem. Biophys.* **363**, 135-147.

CHAPTER 4

Studies Examining the Stability and Unfolding of

A. aeolicus PD

4.0 INTRODUCTION

Fourier transform infrared (FTIR) and circular dichroism (CD) spectroscopies are sensitive and informative tools for studying the secondary structure of proteins in aqueous solutions. CD relies on the unequal absorption of left- and right-handed circularly polarized light by optically active molecules. In the far UV (170 nm–250 nm) CD bands are dominated by contributions of the peptide bonds within proteins. The electronic transitions associated with energy absorption by the peptide bond differs if the protein adopts an α-helical, β-sheet or random coil structure, the three most common secondary structures associated with proteins. The α-helix displays the strongest and most characteristic CD signal with intense negative bands at 222 and 208 nm and a positive signal at 193 nm. β-sheets yield a single minimum at 215 nm and a maximum at 195 nm. However, this signal is less intense and not as distinct as for the α-helix. The random coil structure does not yield a CD signal above 210 nm. Hence, the absorptions at 215 nm and 222 nm provide an excellent probe for monitoring secondary structural changes associated with unfolding of proteins (1). If a protein contains several types of secondary structural units then β-sheet contributions are more confidently assessed with FTIR spectroscopy.

FTIR spectroscopy is a powerful technique for detecting changes in H-bonding patterns within proteins. Absorption in the amide I region between 1700-1600 cm^{-1} arise primarily from the C=O stretching vibrations of the amide bonds. The frequency of these vibrations has been shown to be sensitive to the molecular geometry and extent of hydrogen bonding of the peptide backbone and specific conformations. The α-helix, β-

strand and β-turns as well as non-ordered structures give rise to discrete bands (see Table 1) which are resolved using mathematical methods. In order to eliminate the problem associated with the pronounced absorption of water in the amide I region, studies are typically performed in D_2O. Absorption in the amide II region is due to primarily N-H bending and can be used to monitor tertiary structure changes due to H-D exchange of amide protons (2).

Unfolding of proteins accompanies changes in enthalpy and entropy which are measured as differences in the heat capacity of the protein's folded and unfolded states. The amount of heat absorbed during unfolding can be detected by Differential Scanning Calorimetry (DSC) providing estimates of the enthalpy change and the temperature at which the protein denatures (10).

There have been no reported structural studies on PD from A. *aeolicus* and very few from *E. coli* CM-PD. The purpose of the studies in this chapter was to assess the stability of the *A. aeolicus* PD against thermal and chemical denaturation and to gain some knowledge of the protein dynamics associated with its unfolding using FTIR and CD spectroscopies. *A aeolicus* PD proved to be very thermostable. Hence, extended temperature DSC and capilliary DSC were employed to determine the T_m for this protein and for CM-PD from mesophilic *E. coli*.

Table 1: Correlation Between Protein Secondary Structure and Band Position in the Amide I' Region

Wavenumber (cm^{-1})	Assignment
1600-1614	Side-chain vibrations
1616-1620	Anti-parallel intermolecular β-sheet
1626-1629	Extended chains
1632-1637	Intramolecular β-sheet
1637-1639	3_{10} Helix
1641-1645	Random coil
1651-1655	α-Helix
1662	3_{10} Helix
1665-1673	Turns
1680-1688	Anti-parallel β-sheets or β-turns

Adapted from Creighton (11).

4.1 EXPERIMENTAL PROCEDURES

4.1.1 Materials

Gdn-HCl (99% pure) was obtained from ICN. Thrombin-cleaved *A. aeolicus* PD was prepared as described in section 2.1.6 and unless otherwise indicated was buffer exchanged into **PPS buffer** (50 mM potassium phosphate, 75 mM NaCl, pH 7.5) using a NAP-10 column, then centrifuged at 16,000 x g for 30 min and 4 °C. Buffer exchanged samples were assayed for protein content and dehydrogenase activity as previously described in sections 2.1.11 and 2.1.12, respectively. *E. coli* CM-PD was obtained as described in section 2.2.6. D_2O was a generous gift from Dr. Jack Kornblatt (Concordia University, Montreal, Canada).

4.1.2 Far-UV Circular Dichroism Spectroscopy

CD experiments in the far-UV were conducted in either a circular 0.05 cm or 0.1 cm quartz cell using a Jasco-710 spectropolarimeter interfaced to a thermostatted circulating water bath. Buffer exchanged PD was diluted to 0.75 mg/ml in PPS buffer. Spectra were obtained from 290 nm to 190 nm at temperatures of 25 °C, 55 °C, 80 °C and 95 °C by manually adjusting the setting on the water bath. Temperatures were increased to the desired value at maximum ramping speed, and the samples were allowed to equilibrate for 10 min at each temperature before recording measurements. The following parameters were used: 10 scans averaged, 50 nm/min scan rate, 0.2 nm step resolution, 0.25 s response, 1 nm bandwidth, and sensitivity of 50 mdeg. Samples were cooled from 95 °C to a desired temperature by adding ice to the circulating water bath followed by a

10 min equilibration time prior to recording spectra. Spectra were re-recorded using the same parameters listed above.

Secondary structural changes due to increasing temperature were also monitored at a single wavelength (222 nm) between 25 °C and 95 °C by using the computer controlled temperature ramping program, supplied by Jasco software, and the following parameters: ΔT °C of 20 °C/h, 0.2 °C step resolution, 1 s response, 1 nm bandwidth, sensitivity of 50 mdeg. Approximately 0.75 mg/ml of buffer exchanged PD in PPS buffer was used.

4.1.3 Fourier Transform Infrared Spectroscopy

A 1.0 ml aliquot of buffer exchanged PD (4.0 mg/ml) was lyophilized at 55°C to dryness in a vacuum-sealed oven. The resulting pellet was reconstituted in 30 μl of D_2O, (for a final concentration of ~133 mg/ml) and incubated at 55 °C for 30 min to allow for H/D exchange with buried hydrogen. An 8 μl aliquot of the sample was placed between two CaF_2 windows of a temperature controlled IR cell (Omega CN8500) equipped with 25 μm spacer. Spectra were recorded on a Nicolet 550 IR spectrometer equipped with a DTGS detector, networked to a Whatman air-purging system. Thermal stability studies were performed in two sequential cycles of heating and cooling between 40 °C and 95 °C, in increments of 5 °C, allowing for 10 min equilibration time between each temperature change. All spectra were collected by taking 516 scans at a resolution of 2 cm^{-1}. Data was corrected for water vapour and buffer contributions, and analyzed using OMNIC 6.0 software with the assistance of Dr. Ashraf Ismail (McGill University,

Montreal, Canada). Amide I′ components were assigned to different secondary structure types according to spectra-structure correlations established experimentally (3-5).

4.1.4 Differential Scanning Calorimetry

DSC measurements were performed on MicroCal VP-series DSC and capillary DSC instruments at constant heating rates of 60 °C/h and 200 °C/h, respectively. Aliquots of *A. aeolicus* PD and *E. coli* CM-PD were buffer exchanged into 100 mM potassium phosphate (pH 7.5), 0.3 M NaCl, 5% glycerol and 0.5 mM TCEP using a pre-packed Sephadex G-25 NAP-5 column. VP-DSC data acquisition was conducted at constant pressure (30 psi), using passive feedback with a 10 s filter and allowing for 10 min prescan thermostat prior to run (equilibration time). Protein concentrations used for VP-DSC analysis were 1.9 mg/ml and 2.5 mg/ml for PD and CM-PD, respectively, in a total cell volume of 0.5197 ml. VP-capillary DSC data collection was performed at the same atmospheric pressure, using medium feedback with a 2 s filter and allowing for 5 min prescan thermostat prior to run. Protein concentrations used were 6.0 mg/ml for PD and 10.0 mg/ml for CM-PD, in a total cell volume of 0.109 ml. Data analysis and thermodynamic constants were determined using Origin software equipped with two-state and multi-state models for thermal denaturation. Data acquisition and analysis was performed by MicroCal, under the supervision of Dr. Verna Frasca (Technical Services Scientist; MicroCal LLC, Northampton, MA).

4.1.5 Determination of Incubation Time for Equilibrium Unfolding by Gdn-HCl

PD (10 mg/ml) was dialyzed overnight at 4 °C against 5 L of PPS buffer. A stock solution of **Gdn buffer** (PPS buffer containing 8 M Gdn-HCl) was prepared and adjusted to pH 7.5 with NaOH and stored at 4 °C. To 30 µl of enzyme was added Gdn buffer appropriately with PPS buffer to yield a sample containing 4 M Gdn-HCl and 1.0 mg/ml enzyme as final concentrations. A control sample of dialyzed PD was also prepared at 1.0 mg/ml in PPS buffer. Spectra were recorded from 255 nm to 210 nm in a 0.05 cm quartz cuvette at room temperature after 1, 12, 24 and 36 h incubation at room temperature using the parameters listed in 4.1.2.

4.1.6 Equilibrium Denaturation by Gdn-HCl

PD (10 mg/ml) was dialyzed overnight at 4 °C against 5 L of PPS buffer. Samples (300 µl total volume) were prepared in 1.5 ml eppendorf tubes containing 30 µl enzyme mixed with appropriate amounts of Gdn buffer and PPS buffer to yield a final enzyme concentration of 1.0 mg/ml and concentrations of Gdn-HCl from 0-6 M. The final pH in samples was verified with a miniature hand held pH electrode. The samples were capped and incubated at room temperature for 24 h. Spectra were recorded as described in section 4.1.2. The change in the α-helical signal of the protein at 222 nm was reported as a function of denaturant concentration.

To verify that the denaturation was a reversible process, 1.0 mg/ml PD in 6 M Gdn-HCl (prepared as described above) was incubated for 24 h at room temperature. An aliquot of the denatured sample was then dialyzed overnight against PPS buffer at 4 °C. The

samples were allowed to equilibrate to room temperature and the degree of renaturation was monitored under conditions as described above for unfolding. Activity assays were performed as described in section 2.1.12 on samples before Gdn-HCl denaturation, after refolding and on a native sample of 1.0 mg/ml PD in PPS buffer.

4.2 RESULTS

4.2.1 Far-UV CD Spectroscopy of *A. aeolicus* PD

The far-UV CD spectrum obtained at room temperature for *A. aeolicus* PD is shown in Figure 1. Two local minima at 208 nm and 222 nm were observed and are typical for proteins containing a significant content of α-helical structure (6). CD spectra were also recorded at 55 °C, 80°C and 95 °C (Figure 2) and the signature curves were accompanied by decreases in intensity, albeit small, that were proportional to temperature. The stability of the protein was also examined at a fixed wavelength (222 nm) while temperature was increased at a rate of 1 °C every 3 min up to 95 °C (Figure 3). As noted with the previous variable temperature (VT) experiment, only a slight decrease in signal of ~10% was observed between the initial (25 °C) and final (95 °C) temperatures. The decrease in signal at 95 °C may be attributed to a slight "relaxation" of the α-helix whereby the protein adopts a functionally relevant structure (7, 8). The small changes in CD signal with increasing temperature were reversible. This is illustrated in Figure 4 which shows the changes in the CD spectra obtained by lowering the temperature from 95 °C to 25 °C through the same three temperature intervals. The protein appears to regain its structure as depicted by an increase in the signal intensity at the characteristic double minima. The ability of PD to maintain its secondary structure at 95 °C, as determined by far-UV CD is in keeping with that expected for a thermally stable protein (9). In addition, the changes observed upon heating and cooling suggest that the protein's secondary structure at room temperature is distinct from that at 95 °C, its physiological working temperature (10).

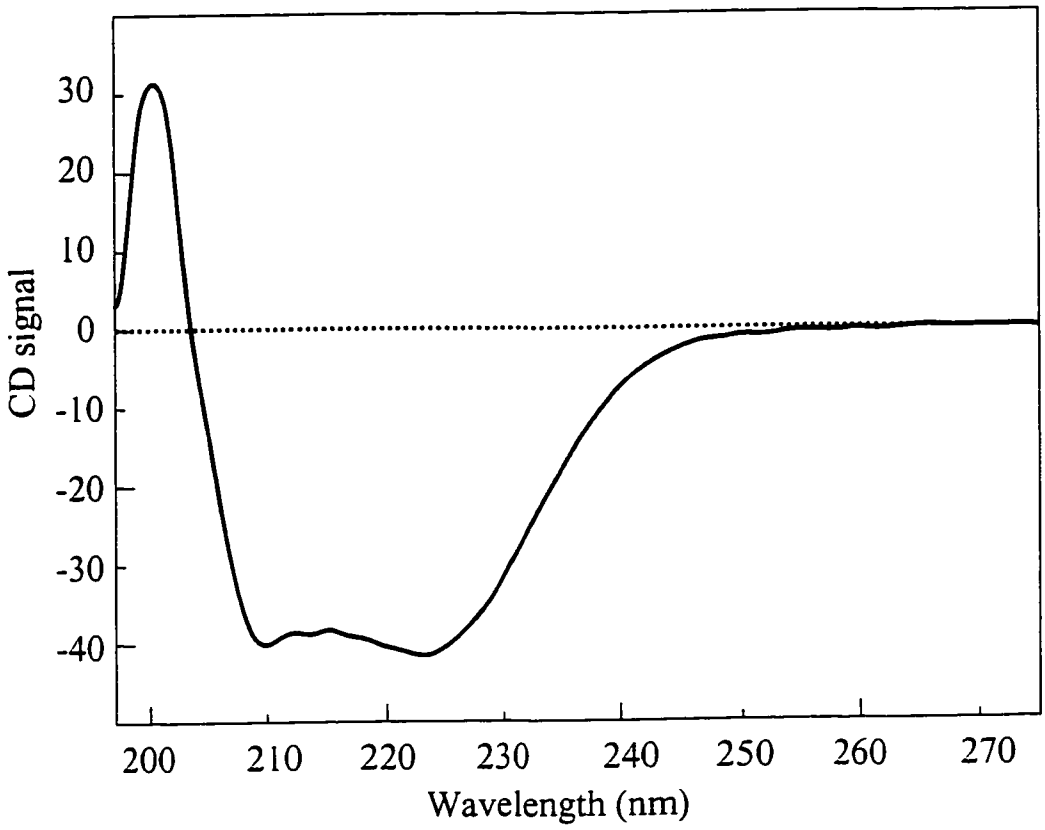

Figure 1. Far-UV CD of *A. aeolicus* PD at 25 °C

Figure 2. VT Far-UV CD of *A. aeolicus* PD at 25 °C (blue); 55 °C (dotted blue); 80 °C (dotted red); and 95 °C (red). Arrows indicate the direction of change occurring as temperature is increased.

Figure 3. VT Far-UV CD of *A. aeolicus* PD monitored at 222 nm from 30 °C to 95 °C.

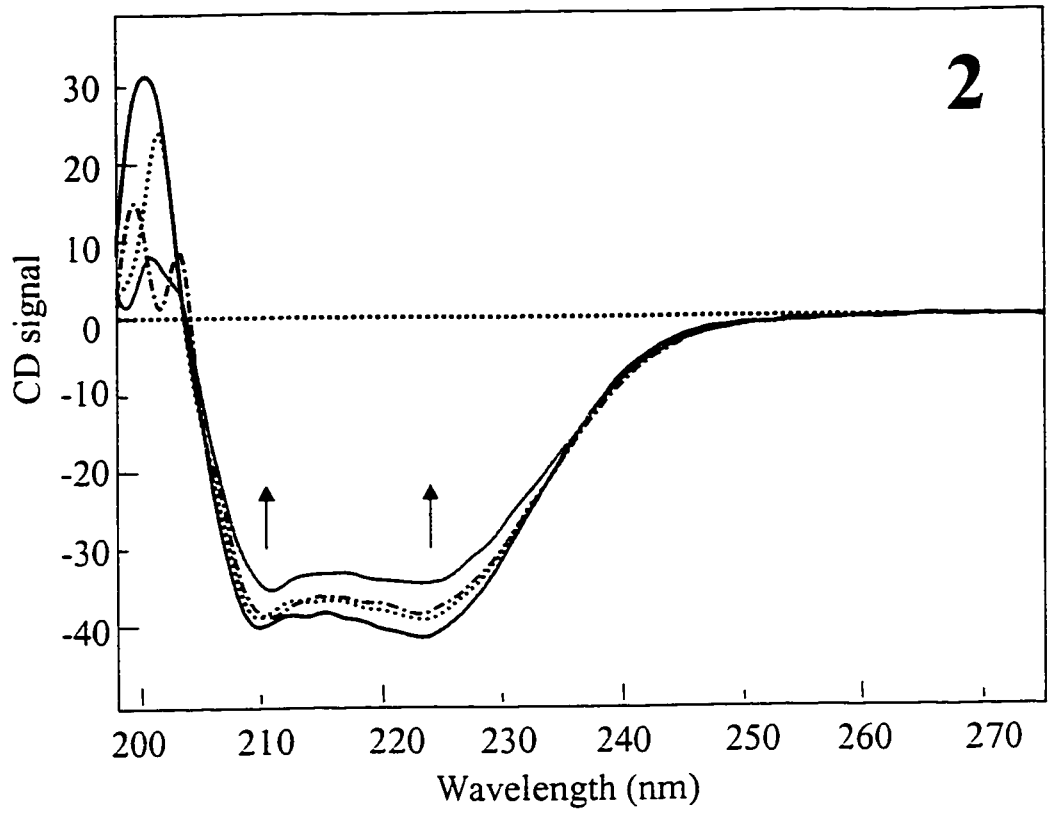
2
30
20
10
0
-10
-20
-30
-40
CD signal
200
210
220
230
240
250
260
270
Wavelength (nm)

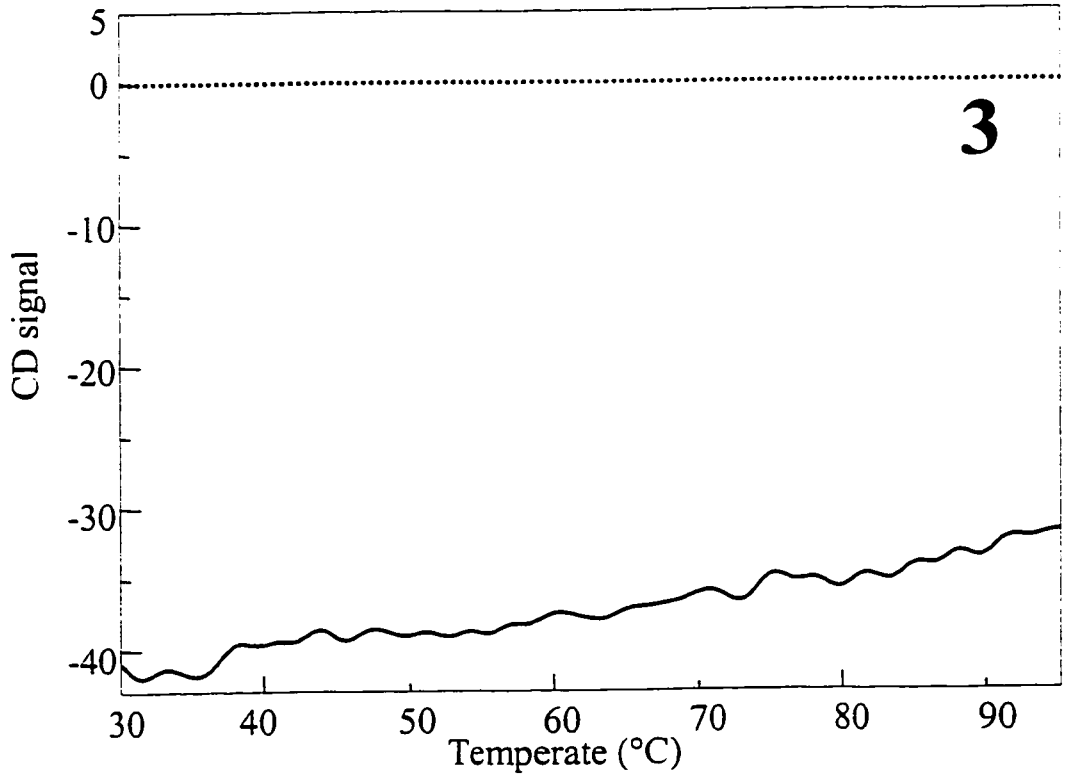
3
5
0
-10
-20
-30
-40
CD signal
30
40
50
60
70
80
90
Temperate (°C)

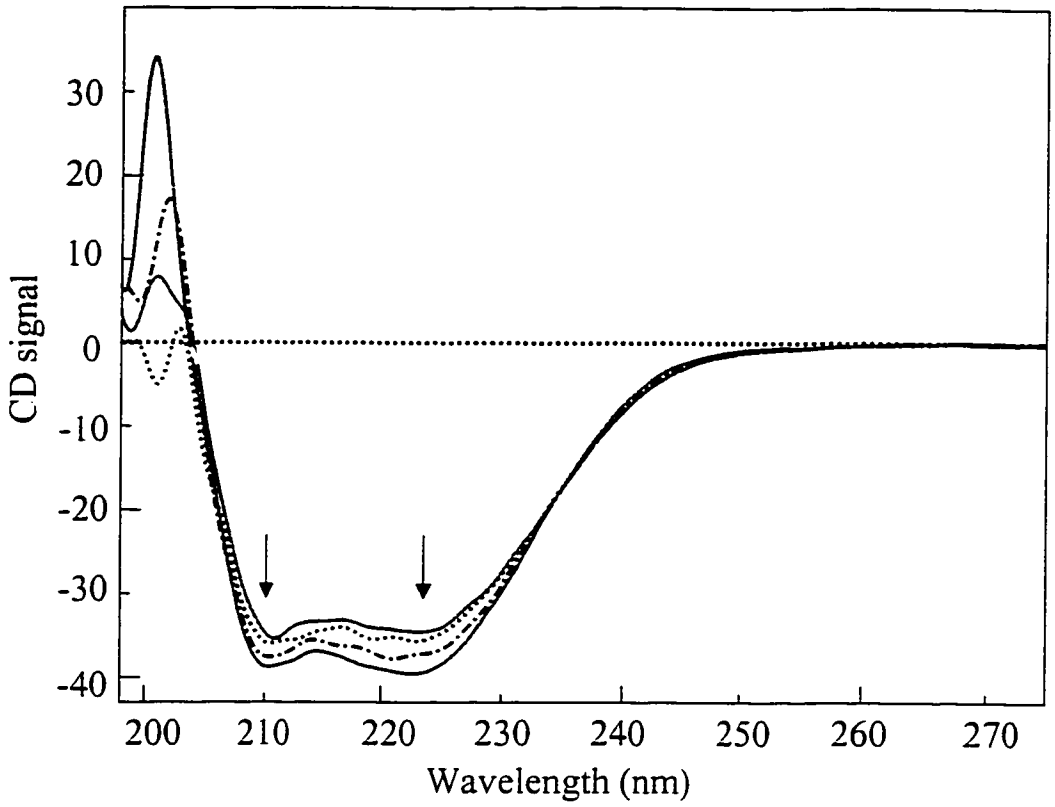

Figure 4. VT Far-UV CD of *A. aeolicus* PD at 25 °C (blue); 55 °C (dotted blue); 80 °C (dotted red); and 95 °C (red). Arrows indicate the direction of change occurring as temperature is decreased.

4.2.2 FTIR Spectroscopy of *A. aeolicus* PD

Figure 5C shows the infrared spectra in the amide I′ (1600 – 1690 cm^{-1}) and amide II′ (1480 – 1575 cm^{-1}) region of PD dissolved in D_2O. For better separation of the amide I′ and amide II′ band components, second derivative and Fourier self-deconvolution (FSD), resolution enhancement techniques were used, and are presented in Figures 5A and 5B, respectively. After FSD (Figure 5B), we can see that the amide I′ region, arising from the in-plane C=O stretching vibration weakly coupled with C-N stretching and in-plane N-H bending (4), is better resolved and four bands are observed. The strongest band at 1653 cm^{-1} is attributed to α-helix while the second most predominant band at 1634 cm^{-1} is attributed to intramolecular β-sheet structure (3, 4). These two bands are also represented in Figure 5A, as the two major negative peaks in the second derivative. The shoulder at 1665 cm^{-1} observed in Figure 5B is attributed to turns (5). Good agreement between the second derivative and FDS spectra indicate that the bands reflect structural features of the enzyme and are not artifacts derived from the mathematical methods used to resolve the individual amide I components. The results from FTIR agree well with those from far-UV CD which suggest that the α-helix is a major secondary structure component of *A. aeolicus* PD.

The weak band at 1543 cm^{-1} of the amide II′ region in Figure 5B corresponds to in-plane N-H bending strongly coupled to C-N stretching (4). The amide II′ region is the least sensitive to conformation (11) and the signal at 1543 cm^{-1} should decrease in D_2O as temperature increases due to H/D exchange (15). Finally, the strong band at 1515 cm^{-1} (Figures 5A and 5B) is assigned to the C=C of the aromatic moiety of tyrosine residues

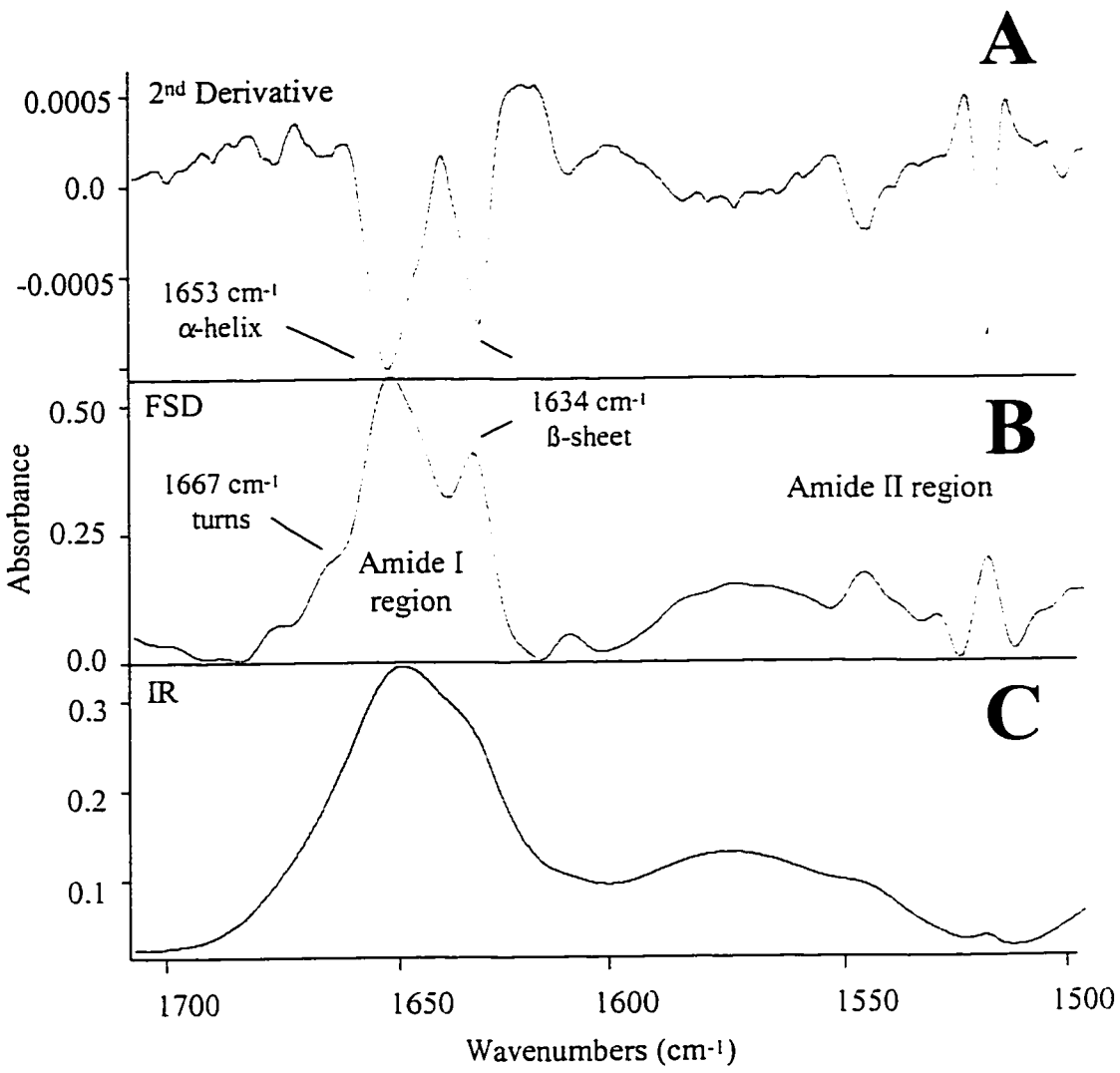

Figures 5A-C. IR spectra of *A. aeolicus* PD at 25 °C in D_2O (C); Fourier-self deconvolution of figure C (B) using enhancement factors w = 18 cm^{-1} and k = 2.3; and 2nd Derivative spectrum (A) of figure 5C.

(15). The intensity of this band should not fluctuate with changing temperature and is commonly used to verify the integrity of the sample throughout a variable temperature experiment (Dr. A. Ismail, personal communication).

4.2.3 VT-FTIR Spectra of *A. aeolicus* PD

Figure 6A-D displays the overlaid FSD spectra of VT-FTIR performed by two sequential cycles of heating and cooling from 40 °C to 95 °C (refer to section 4.1.3 for experimental details). Figure 6A shows the overlaid FSD spectra obtained by increasing temperature in the first cycle. The major bands at 1653 cm^{-1} (α-helix) and 1634 cm^{-1} (intramolecular β-sheet) slightly decreased and there is a slight broadening of the α-helix band. The decreases in intensity at 1653 cm^{-1} and 1634 cm^{-1} suggest a slight loss of helical and β-sheet structure, respectively (15). The broadening observed for the α-helix band may result from conformational changes within the protein or from a shift of the amide I band to a lower wavenumber caused by backbone carbonyl group hydrogen bonding to amide N-D rather than N-H upon H/D exchange (15). Protein aggregation results from clumping of anti-parallel β-strands between protein molecules with increasing temperature and appears as an increase in absorbance of two bands at 1616 cm^{-1} and 1684 cm^{-1} (15). No protein aggregation is observed upon heating *A. aeolicus* PD, however a small degree of aggregate is present prior to heating, represented by a small band at 1616 cm^{-1} (Figure 6A). Interestingly, the small aggregation peak at 1616 cm^{-1} decreases with increasing temperature suggesting that under these experimental conditions protein aggregation is reversible.

Figures 6A-D. Overlaid deconvolved VT-FTIR of *A. aeolicus* PD in the amide I' region for two sequential heating (A and C) and cooling (B and D) cycles of 40 °C to 95 °C. Arrows indicate the direction of changes occurring as temperature increases or decreases. Red line represents FSD at 95 °C.

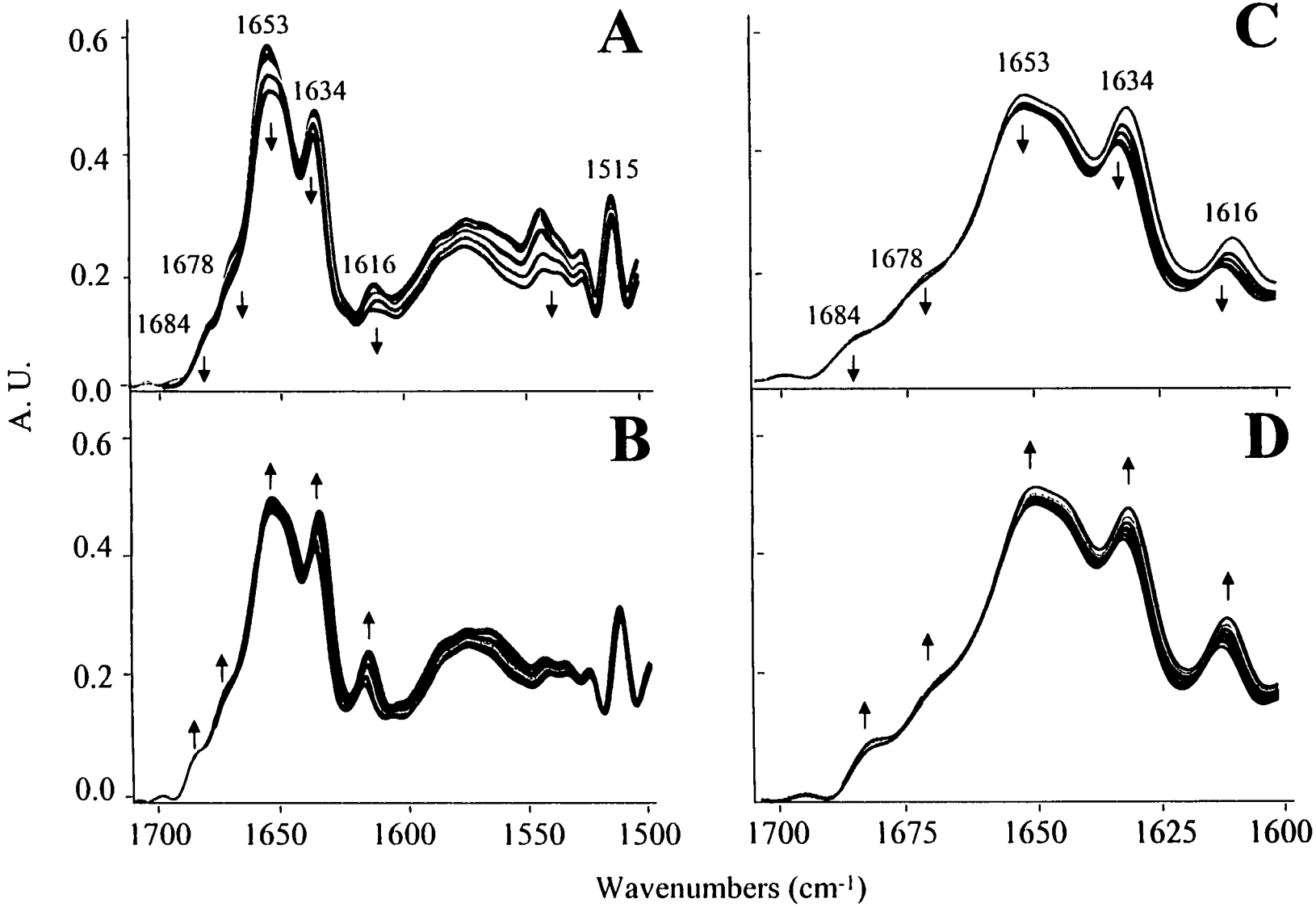
A
B
C
D
1653
1634
1515
1678
1684
1616
0.6
0.4
0.2
0.0
A. U.
1700
1650
1600
1550
1500
1675
1625
Wavenumbers (cm-1)

As expected, the band at 1543 cm^{-1} (corresponding to the amide II region) decreases with increasing temperature, indicating that the protein becomes partially relaxed allowing D_2O molecules to access the interior of the protein. The decrease at 1543 cm^{-1} continues until 95 °C, and would have likely decreased further had the temperature increased above 95 °C. This suggests that PD is well packed over the entire temperature range of 25 °C to 95 °C preventing full H/D exchange with amide groups in the interior of the protein. No significant change is observed at 1515 cm^{-1} (C=C of the aromatic moiety of tyrosine residues), indicating that the sample did not leach out of the IR cell and/or that water evaporation did not occur at the elevated temperatures.

Figure 6B shows the overlaid FSD spectra of PD for the first cooling cycle. As temperature decreased the absorbance of the bands associated with helical structure (1634 cm^{-1}) and β-sheet (1653 cm^{-1}) increased, suggesting an increase in the relative amounts of these secondary structural features within the protein. These results agreed with those from VT far-UV CD (Figure 4) which show an increase in α-helical signal at 208 nm and 222 nm as temperature was lowered. No narrowing of the α-helix band was observed as temperature decreased suggesting that the broadening previously observed in the first heating cycle was a result of H/D exchange. Both aggregation bands at 1684 cm^{-1} and 1616 cm^{-1} increased as temperature was lowered but with a more pronounced change at 1616 cm^{-1}.

Figure 6C displays the overlaid FSD spectra for the second heating cycle. Interestingly, the newly formed aggregation band at 1616 cm^{-1} decreased in intensity with elevating

temperature, indicating protein deaggregation. Furthermore, the intensity of the bands at 1634 cm^{-1} (α-helix) and 1653 cm^{-1} (β-sheet) decreased, as previously observed for the first heating cycle (Figure 6A), however the net change in absorbance intensity was not as pronounced.

The last cooling cycle is illustrated in Figure 6D and resulted in structural changes within the protein similar to those recorded during the first cooling cycle (Figure 6B). Notably, temperature decreases accompanied increases in intensity for α-helix, β-sheet, and the aggregation band at 1616 cm^{-1}.

No melting temperature was obtained with either VT far-UV CD or VT-FTIR.

4.2.4 Thermal Denaturation Monitored by DSC and Capillary DSC

The thermal unfolding of CM-PD and PD was conducted using VP-DSC and VP-Capillary DSC at pH 7.5. The DSC thermogram of CM-PD and PD are shown in Figure 7A. The tracing for CM-PD shows a very broad transition peak with a shoulder at approximately 50 °C. By contrast, a broad pre-transition baseline (between 50 °C and 90 °C) followed by a sharper transition peak is observed for PD (Figure 7A). The unusual pre-transition baseline observed for PD and the post-transition baselines for both proteins which drop sharply after unfolding, are indicative of aggregated protein (12). A melting temperature (T_m) of ~57 °C for CM-PD and ~107 °C for PD can be obtained from the peaks on each thermogram. Thermodynamic parameters associated with the unfolding

were not calculated due to the vertical drop in the post-transition baseline obtained for both proteins.

VP-capillary DSC was used in order to re-examine the thermal transition of *E. coli* CM-PD and *A. aeolicus* PD. Figure 7B shows the isothermal tracings for CM-PD and PD. Again, one broad peak for the change in the partial molar heat capacity was observed for CM-PD, while a sharper transition was observed for PD. An apparent shoulder between 95 °C and 100 °C, in the capillary DSC tracing of PD is also observed and indicative of a net loss in hydrogen bonding within the protein which may be attributed to subunit separation either preceding or follow unfolding (12). Both thermograms exhibited well-defined post-transition baselines. As a result of the broad transition peak obtained for CM-PD and the shoulder preceding the transition peak for PD, both thermograms were fitted with a two-transition model. ΔH values (changes in enthalpy upon unfolding) were calculated by integrating the area under a given transition and signifies the amount of heat absorbed during that unfolding process. Deconvolution of the single broad peak obtained for CM-PD yields a first transition (marked by subscript 1) with a rather small change in enthalpy of 32.9 ± 0.4 kcal/mol and a second more distinct transition (superscript 2) of 67.6 ± 0.3 kcal/mol. As with CM-PD, the shoulder before the sharper peak of PD broadens the transition hindering a single transition fit. Deconvolution of the peak for PD yields two transitions with enthalpy changes of 72.9 ± 1.7 and 180.2 ± 1.2 kcal/mol. The enthalpy changes as well as the T_m values derived from the two transitions for both proteins are summarized in Table 2. The thermograms show that *A. aeolicus* PD unfolds at a temperature ~51 °C higher than *E. coli* CM-PD. It is

Figure 7A and 7B: DSC (7A) and capillary DSC (7B) of *E. coli* CM-PD (blue) and *A. aeolicus* PD (red). Non-fitted T_m for each thermogram is indicated above peak.

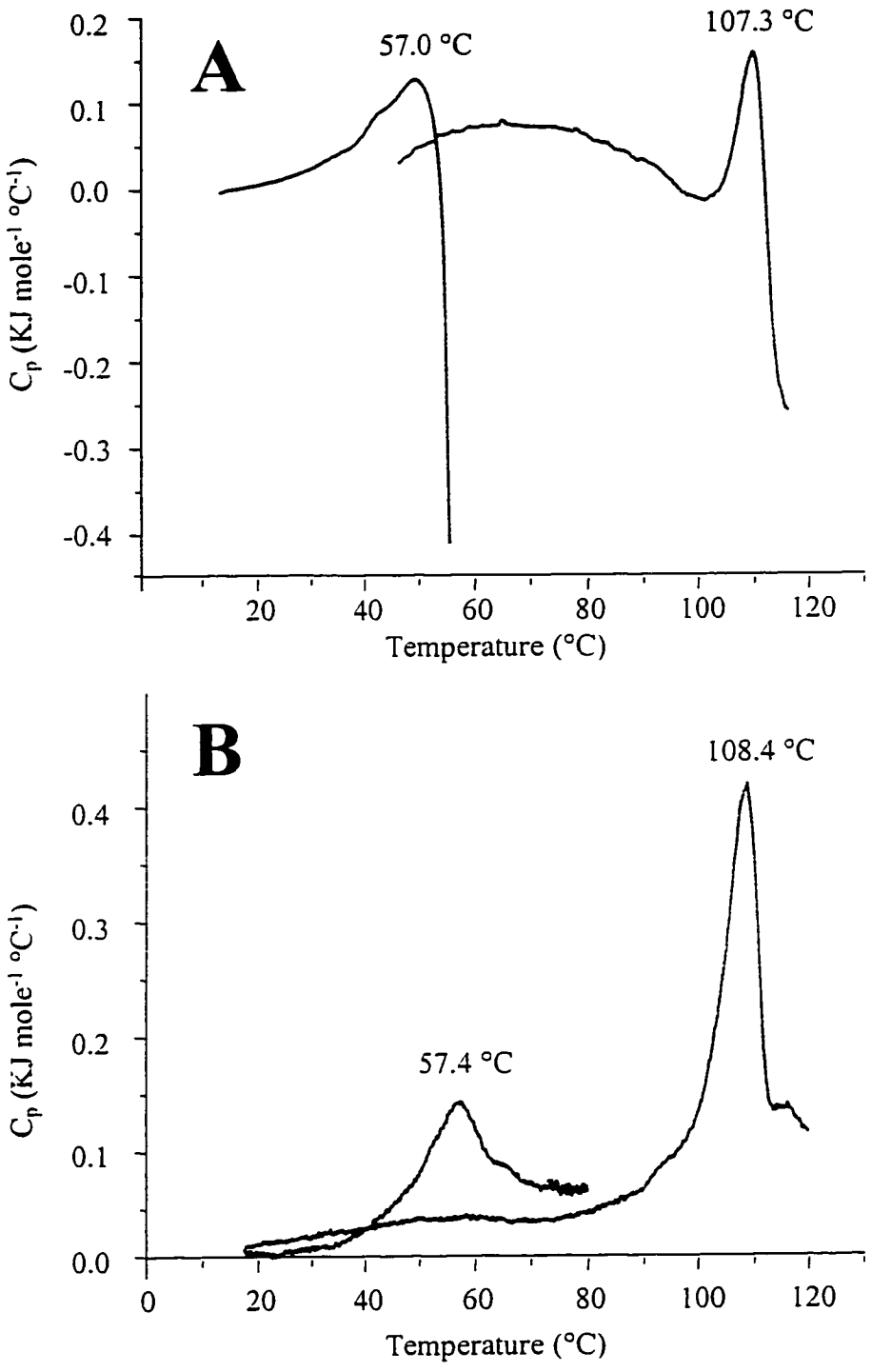
A
57.0 °C
107.3 °C
0.2
0.1
0.0
-0.1
-0.2
-0.3
-0.4
C_p (KJ mole^{-1} °C^{-1})
20
40
60
80
100
120
Temperature (°C)
B
108.4 °C
57.4 °C
0.4
0.3
0.2
0.1
0.0
C_p (KJ mole^{-1} °C^{-1})
0
20
40
60
80
100
120
Temperature (°C)

noteworthy that the T_m obtained for CM-PD is in excellent agreement with values of 57 °C and 60 °C previously determined using VT-FTIR and VT far-UV CD, respectively, (unpublished, K. Mekhssian and R. Aponte).

4.2.5 Chemical-Induced Denaturation by Gdn-HCl

Unfolding of *A. aeolicus* PD mediated by the chaotropic reagent Gdn-HCl was monitored at room temperature following changes in ellipticity by far-UV CD. The change in the α-helical signal at 222 nm was used to estimate the extent of denaturation. However, in order to confidently monitor the unfolding of the protein, it was necessary to determine the length of time required for the unfolding reaction to reach thermodynamic equilibrium. Towards this end, far-UV CD spectra were recorded after incubating PD for 1, 12, 24 and 36 h with 4 M Gdn-HCl at room temperature (see section 4.1.5). The degree of ellipticity at 222 nm decreased between the 1 h and 24 h incubations but remained constant above 24 h (data not shown). This suggested that equilibrium had been established somewhere between 12 h and 24 h. Hence, samples were incubated for 24 h before spectra were recorded. Unfolding was also reversible as the sample recovered 91% of its original activity and 89% of its original ellipticity at 222 nm upon removal of the denaturant by dialysis (see section 4.1.6). Therefore, calculations of the thermodynamic parameters associated with the unfolding reaction are permitted.

Table 2: Change in Enthalpy and Thermal Unfolding Temperature for a Two-Transition Fit

	$T_{m,1}$ (°C)	$T_{m,2}$ (°C)	ΔH_1 (kcal/mol)	ΔH_2 (kcal/mol)
E. coli CM-PD	50.1 ± 0.3	56.5 ± 0.1	32.9 ± 0.4	67.6 ± 0.3
A. aeolicus PD[a]	101.4 ± 0.4	107.4 ± 0.1	72.9 ± 1.7	180.2 ± 1.2

[a]Homodimer PD resulting from thrombin cleavage

Figure 8 shows an unusual profile for the unfolding of PD with increasing concentrations of Gdn-HCl, revealing at least two defined transitions. The protein retains helical structure from 1.0 to 3.0 M Gdn-HCl then there is a minor transition from 3.0 to 3.2 M denaturant yielding protein that now possesses 85% of its relative helical content. This species appears stable from 3.2 to 4.8 M Gdn-HCl. A major transition then occurs between 4.8 M and 6.0 M Gdn-HCl resulting in a complete loss of helical structure. with 50% unfolding ($D_{1/2}$) occuring by ~ 5.5 M denaturant. The remarkably high $D_{1/2}$ value suggests that *A. aeolicus* PD is very resistant to chemical denaturation by this reagent. A value of this magnitude also has been reported for other proteins originating from hyperthermophiles and extremophiles (8, 13). Intriguingly, the protein in the absence of denaturant possesses 15% less helical content than in the presence of 1.0 M Gdn-HCl. While the observation must be verified by collecting more data points between these two concentrations, this trend has been documented in studies following the Gdn-HCl-induced unfolding of other (hyper)thermophilic protein (14) suggesting that it is real. The complexity of the pattern and an inability at this time to confidently assign a model for the unfolding precluded an accurate calculation of the conformational stability (ΔG_{fold}^{H2O}) of *A. aeolicus* PD. In contrast, *E. coli* CM-PD has been reported to unfold via a simple two-state model and the thermodynamic parameters for the unfolding reaction have been calculated (15).

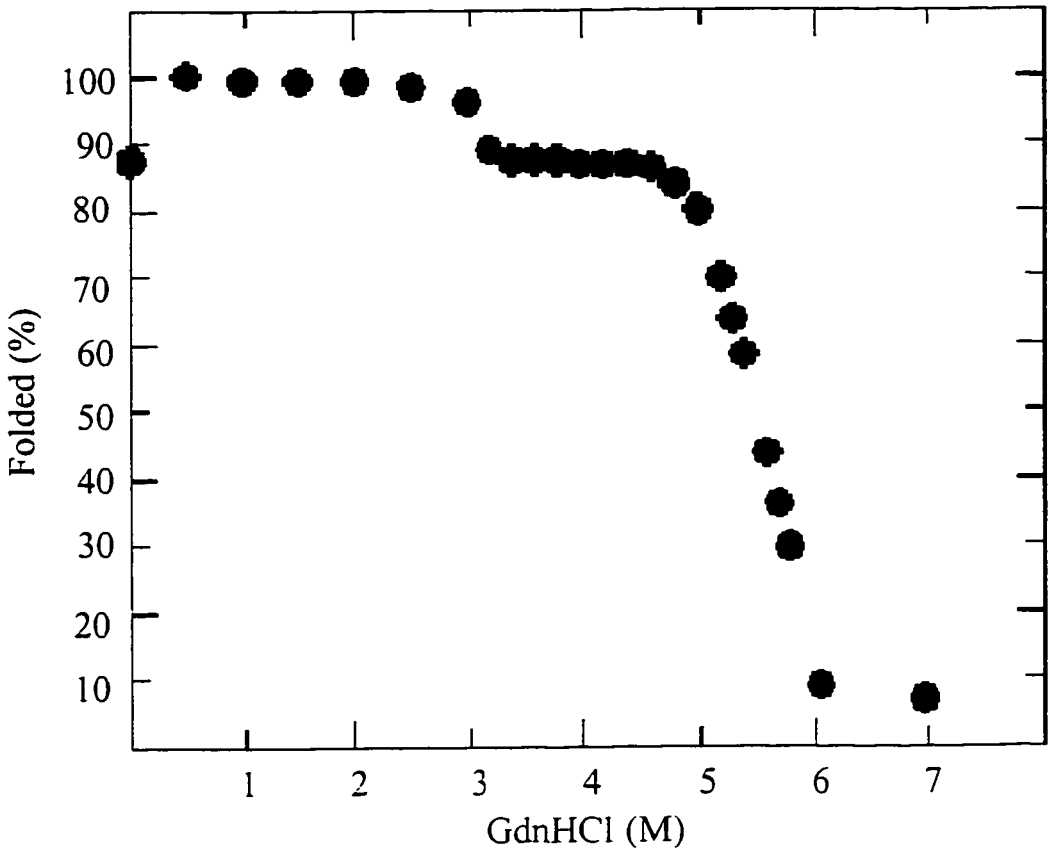

Figure 8. Gdn-HCl denaturation of *A. aeolicus* PD monitored by circular dichroism. The % folded is plotted as a function of signal change at 222 nm in response to increasing Gnd-HCl concentration for *A. aeolicus* PD.

4.3 DISCUSSION

The aim of the studies presented in this chapter was to gain information regarding the secondary structure of *A. aeolicus* PD and to characterize the enzyme's resistance to thermal and chemical denaturation.

Together, far-UV CD and FTIR spectroscopies demonstrated the predominance of α-helical structure in *A. aeolicus* PD (Figure 1 and 5B, respectively). In addition, FTIR spectra enabled the elucidation of β-sheet structure and reverse turns (Figure 5B). The experimental findings agreed qualitatively with the results of secondary structure predicted from the primary sequence of the protein using the programs PepTool™ and PROF predictions (16, 17) where values of 55-60% α-helical structure, 15-20% β-sheet, and 20-30% loop structure were estimated. Both programs also predicted a rare extended helix of 33-37 residues at the C-terminal end also found in calmodulin and troponin C (11). The predictive and spectroscopic studies tentatively classify PD as an (α/β) protein. The (α/β) proteins typically have one β-sheet of primarily parallel strands interspersed with α-helices. Helices also pack on both sides, surrounding the sheet (11).

Far-UV CD and FTIR were also used to monitor changes in secondary structure resulting from temperature changes (Figures 2-4 and 6A-D). The results clearly indicate that *A. aeolicus* PD is highly thermally stable and possesses substantial secondary structure at 95°C. In addition, both VT far-UV CD and VT-FTIR show secondary structural changes upon heating (Figures 2 and 6A) which presumably lead to the functionally active form

of the enzyme. This premise is supported by activity studies at high temperature (section 3.2.1), where a 33-fold increase in specific activity was observed between 30 °C and 95 °C. Moreover, the temperature range for optimum growth for *A. aeolicus* is reported to be between 85 °C to 95 °C (18).

It is difficult to acertain if the secondary structural changes associated with the unfolding of *A. aeolicus* PD by the chemical denaturant Gdn-HCl bear any functional consequences as seen with increasing temperature. The unfolding of *A. aeolicus* appears to undergo an unusual multi-state transition yielding a stable "intermediate" between 3.2 to 4.6 M denaturant (Figure 8) . However, both two-state and multi-state transitions have been reported for other thermophilic proteins such as pyrophosphatase from *Thermus thermophilus* (13) and the α-subunit of luciferase from *Vibrio harveyi* (19). It would be of interest to conduct activity assays at the various concentrations of denaturant to correlate the subtle changes in secondary structure with catalytic function as we have done for the effects of temperature.

The common conclusion from model studies is that the stability of proteins from (hyper)thermophiles is optimized to maintain corresponding functional states under increased temperatures (8). For the standard state at 25 °C, enhanced thermal stability of (hyper)thermophilic proteins would then incur enhanced conformational rigidity in the their folded native state (14). Based on structural and thermodynamic data, the view is now widely accepted that the anomalous stability of (hyper)thermophile proteins correlates with strong local interactions and/or improved packing of the polypeptide

chain (8). Improved packing of *A. aeolicus* PD is suggested by the continued H/D exchange observed in both the amide I region and amide II regions of FTIR spectra even at high temperatures. The amide I H/D exchange was observed as a broadening of the α-helix band as temperature increased, while the amide II H/D exchange was seen as a decrease at 1543 cm^{-1} as temperature increased (Figure 6A). Similar absorbance patterns due to H/D exchange were reported for the thermally stable α-amylase from the mesophile *Bacilllus lichenifomis* using FTIR (23). In many but not all studies, a decrease in exchange rates for slowly exchanging amide protons is reported to be correlated inversely with T_m values (24-27).

Additional evidence for improved packing in thermostable proteins is illustrated by the fact that unfolding *A. aeolicus* PD at room temperature requires high concentrations of Gdn-HCl. This reflects the inability of Gdn-HCl to access nonpolar hydrophobic surfaces in the interior of the protein (11). A $D_{1/2}^{25°C}$ of 5.5 M was estimated from Figure 8, a value that is more than twice that of 2.6 M reported for *E. coli* CM-PD (15). Similar differences in $D_{1/2}$ values between hyperthermophiles and their mesophilic counterparts have also been reported by Jaenicke (8).

Due to instrument limitations, CD and FTIR spectroscopies could not provide a good estimate of the melting temperature of *A. aeolicus* PD. In contrast, DSC supplied a T_m value of ~108 °C which was 51 °C higher than that recorded for *E. coli* CM-PD (Figures 7A and 7B). The higher enthalpy changes associated with the transitions for *A. aeolicus* PD compared to *E. coli* CM-PD implies that PD may contain more stabilizing

interactions and require more heat to unfold it. Yip *et al.* (20) reported the presence of extensive ion-pair networks in glutamate dehydrogenase (GluDH) from the hyperthermophile *Pyrococcus furiosus* that were absent in the mesophilic counterparts from *E. coli* and *Clostridium symbiosum*. Not only was there a smaller overall number of ion-pairs in the enzymes from the mesophilic organisms, but the larger ion-pair clusters seemed to disappear rapidly as enzyme thermal stability fell below 100 °C with the networks becoming less extensive and more fragmented (20). Structural and genomic correlations using an extensive database of proteins from hyperthermophilic and mesophilic organisms showed that the larger proportion of charged *versus* polar (uncharged) amino acids is a signature of all hyperthermophilic organisms (21). In addition, the proportion of solvent accessible charged residues at the protein surface markedly increased at the expense of polar residues (21). The calculated pI of *A. aeolicus* PD is 7.73 compared to 5.68 for *E. coli* CM-PD suggests that the thermophilic PD houses a higher number of basic residues capable of participating in ion-pair or H-bonding networks.

Finally, our studies also provide some insight into the protein dynamics of *A. aeolicus* PD. VT-FTIR and VT-far-UV CD shows that PD can lose and regain ~10% of its secondary structure upon heating and cooling, respectively (Figures 3 and 6). At ambient temperature PD contains some aggregated protein which dissipates upon heating the protein but reappears upon cooling (Figures 6B and 6D). It should be noted that these temperature-induced conformational changes observed for *A. aeolicus* PD are reversible only because they occur *prior* to denaturation of the protein. The temperature range used

in these studies results in unfolding transitions which are irreversible for most mesophilic proteins (7, 12). However, an increase of ~15 °C above the temperature for optimal activity for both *A. aeolicus* (section 3.2.1) and *E. coli* CM-PD (22) results in the unfolding of both proteins (Figures 7A and 7B).

In summary, *A. aeolicus* PD functions at temperatures requiring structural adaptation. The enzyme appears to "relax" and adopt a more flexible conformation as temperature increases towards the optimal activity temperature of ~ 95 °C. Similar structural changes appear to occur in the presence of Gdn-HCl at room temperature but they have yet to be correlated with biological function.

4.4 REFERENCES

1. Schmid, F. X. (1997). *In Protein Structure a Practical Approach* (ed. T.E. Creighton). Chapter 11. IRL Press, New York
2. Mantsch, H. H., and Chapman, D. (1995). *Infrared Spectroscopy of Biomolecules*. Wiley, New York.
3. Susi, H., Timasheff, S. N. and Stevens, L. (1967). *J. Biol. Chem.* **242**, 5460-5466.
4. Susi, H. (1972). *Methods Enzymol.* **26**, 455-472.
5. Jackson, M. and Mantsch, H. (1995). *Crit. Rev. Biochem. and Mol. Biol.* **30**, 95-120.
6. Johnson, W. C. Jr. (1992). *Methods Enzymol.* **210**, 426-447.
7. Jaenicke, R. (1997). *BioProt Network*. Institut für Biophysik und Physikalische Biochemie, Universität Regensburg, Regensburg, Germany. (http://www.protein.bio.msu.su/biokhimiya/contents/v63/full/63030370.htm)
8. Jaenicke, R. (2000). *Proc. Natl. Acad. Sci.* **97**, 2962-2964.
9. Leuschner, C. and Antranikian, G. (1995). *World J. Microbiol. Biotechnol.* **11**, 95-114.
10. Makhatadze, G. I. (1998). *Curr. Protocols Prot. Sci.* 7.9.1-7.9.14.
11. Creighton, E. T. (1993). *Proteins: Structure and Molecular Properties (2nd edition)*. W. H. Freeman and Company, New York. pp. 191-192, 224-227.
12. Cooper, A., (1999). *Protein: A Comprehensive Treatise*. JAI Press Inc. pp.217-270.
13. Hansen, T., Urbanke, C., Leppanen, V. M., Goldman, A., Brandenburg, K. and Schafer, G. (1999). *Arch. Biochem. Biophys.* **363**, 135-147.
14. Jaenicke, R. and Böhm, G. (1998). *Curr. Opin. Struct. Biol.* **8**, 738-748.

15. Christendat, D. and Turnbull, J. (1999). *Biochemistry* **38**, 4782-4793.

16. Rost, B. and Sander, C. (1993). *J. Mol. Biol.* **232**, 584-599.

17. Rost, B. and Sander, C. (1994). *Proteins* **19**, 55-72.

18. Deckert, G., Warren, P. V., Gaasterland, T., Young, W. G., Lenox, A. L., Graham, D. E., Overbeek, R., Snead, M. A., Keller, M., Aujay, M., Huber, R., Feldman, R. A., Short, J. M., Olsen, G. J. and Swanson, R. V. (1998). *Nature 392*, 353-358.

19. Noland, B. W., Dangott, L. J. and Baldwin, T. O. (1999). *Biochemistry* **38**, 16136-16145.

20. Yip, K. S., Britton, K. L., Stillman, T. J., Lebbink, J., de Vos, W. M., Robb, F. T., Vetriani, C., Maeder, D. and Rice, D. W. (1998). *Eur. J. Biochem.* **255**, 336-346.

21. Cambillau, C. and Claverie, J-M. (2000). *J. Biol. Chem.* **275**, 32383-32386.

22. Turnbull, J. (1988). *Mechanistic Studies on a Bifunctional Enzyme*, Ph. D. Australian National University.

23. Heberle, J. and Fitter, J. (2000). *Biophysical Journal*. **79**, 1629-1636.

24. de Jongh, H. H., Goormaghtigh, E. and Ruysschaert, J. M. (1995). *Biochemistry*. **34**, 172-179.

25. Roder, H. (1989). *Methods Enzymol.* **176**, 446-473.

26. Wagner, G. and Wulthrich, K. (1979). *J. Mol. Biol.* **130**, 31-37.

27. Zavodszky, P., Kardos, J. and Petsko, G. A. (1998). *Proc. Natl. Acad. Sci.* **95**, 7406-7411.

5.0 Ongoing Work

Site-directed mutagenesis (SDM) studies have been initiated on *A. aeolicus* PD by S. MacNamara under the supervision of R. Aponte. Residues were targeted on the basis of primary sequence alignment between the PD domain of *E. coli* CM-PD and *A. aeolicus* PD (refer to section 1.3), and from functional studies on the *E. coli* protein. These residues have been identified to play key roles in catalysis, prephenate or tyrosine binding, or in maintaining the structural integrity of the active site. From the many conserved residues, five (Lys129, His147, His 205, His 217, Arg250), were selected from *A. aeolicus* PD for SDM (refer to Table 1 in section 1.2).

The SDM protocol presently being used is adapted from the QuickChange™ XL mutagenesis protocol by Stratagene. This method uses complementary oligonucleotides which incorporates mutations that codes for the desired residue change, and a silent mutation to facilitate screening of the mutants at the genetic level.

To date, 3 of the 5 desired mutants have been successfully screened, and will be sequenced to ensure that no other changes have been incorporated into the *tryA* gene during the mutagenesis process. Small-scale expression of the potential mutants has also been initiated, as described section 2.1.4, to determine if the mutations have caused the expected functional changes. Protein variants will be overexpressed, purified, characterized and subjected to crystallization trials.

Crystallization trials have been initiated in collaboration with D. Cristendat at the University of Toronto, Department of Botany. Recently, crystals were obtained in the presence and absence of ligands, and they are presently being assessed by X-ray diffraction. If successful, this study will produce the first crystal structure of this enzyme family and the first view of the PD active site. Crystal structures of the wild-type and the variants will be invaluable to the understanding of the dehydrogenase reaction mechanism and the global effects these substitions have on PD.